CONTEXTUAL MODULATION OF NEURAL RESPONSES IN THE MOUSE VISUAL SYSTEM

by

Alexandr Pak

A Dissertation

Submitted to the Faculty of Purdue University

In Partial Fulfillment of the Requirements for the degree of

Doctor of Philosophy

Department of Biological Sciences

West Lafayette, Indiana

May 2021

THE PURDUE UNIVERSITY GRADUATE SCHOOL
STATEMENT OF COMMITTEE APPROVAL

Dr. Alexander Chubykin, Chair

Department of Biological Sciences

Dr. Edward Bartlett

Department of Biomedical Engineering

Dr. Estuardo Robles

Department of Biological Sciences

Dr. Scott Pluta

Department of Biological Sciences

Approved by:

Dr. Janice Evans

To my parents Kim Inna Alexandrovna and Pak Moisey Nikiphorovich.

ACKNOWLEDGMENTS

Flying across the ocean from Kazakhstan to pursue PhD studies in the US, I know very well the importance of the community that shares your cultural background, personal, and professional goals. This work would not be possible without all the people who helped me to grow as a person and scientist during my stay at Purdue.

I would like to thank everyone who supported me on this journey starting from Kazakh-Turkish High School for gifted children where I first learned about science. If my mother did not force me to attend that school, I might have been on a different path right now. I appreciate the time and effort my teachers put into educating and guiding students like me.

I thank my professors at Nazarbayev University who introduced me to the idea of an academic career and provided opportunities to do research. I also thank VISRA program for allowing me to have summer research experience in the US.

I thank my PhD supervisor Dr. Alex Chubykin for providing the opportunity to pursue interesting and challenging questions for my graduate work and his confidence in my abilities to do high-quality science.

I thank my committee members Dr. Scott Pluta, Dr. Edward Bartlett, and Dr. Estuardo Robles for guiding me during graduate school by providing insightful comments on my work and advice regarding my future career.

I thank the first cohort of graduate and undergraduate students of Chubukin lab, Sam, Qiuyu, Mang, and Yu for promoting a supportive lab culture, where we could freely exchange ideas and discuss science.

I thank the Purdue Kazakh community for creating a supportive and warm environment.

Lastly, I am thankful for the PULSe program that allowed me to pursue graduate studies at Purdue. I thank staff members, faculty, and fellow PULSe students for their work to support and improve the program.

TABLE OF CONTENTS

LIST OF TABLES

LIST OF FIGURES

LIST OF ABBREVIATIONS

µm: micrometers

Ach: acetylcholine

ACSF: artificial cerebral spinal fluid

AL: anterolateral

AM: anteromedial area

ANOVA: analysis of variance

AP: anterior/posterior

BNC: Bayonet Neill-Concelman

CDF: cumulative distribution function

CGG: Cytosine Guanine Guanine

Ch: channel

ChR2: channelrhodopsin 2

cm: centimeter

cpd: cycles per degree of visual angle

CSD: current source density

CTR: control stimulus

dB: decibel

deg: degrees

DEV: deviant stimulus

DHPG: 3,5-Dihydroxyphenylglycine

dLGN: dorsal lateral geniculate nucleus DNA: deoxyribonucleic acid

DSGC: direction selective retinal ganglion cell

DV: dorsal/ventral

EPSC: excitatory postsynaptic current

FBI: feedback inhibition

FFI: feed forward inhibition

FGM: figure-ground modulation

FMR1 fragile X mental retardation 1 gene

FMRP: Fragile X mental retardation protein

FR: firing rate

FS: fast spiking

FX: Fragile X Syndrome

GABA: gamma-Aminobutyric acid

GLM: generalized linear model

GUI: graphical user interface

hrs: hours

Hz: Hertz

IR: infrared

kg: kilograms

kHz: kilohertz

KO: knockout

KS: Kolmogorov-Smirnov

L: length

L1: cortical layer 1

L2/3: cortical layers 2 and 3

L4: cortical layer 4

L5: cortical layer 5

L6: cortical layer 6

LED: light-emitting diode

LFP: local field potential

LI: laterointermediate

LM: lateral medial area

LP: lateral posterior nucleus of the thalamus

LTD: long term depression

LTP: Long term potentiation

m: meters

mg: milligrams

mGluR: metabotropic glutamate receptor

min: minute

ML: medial/lateral

mm: millimeter

MMN: mismatch negativity

mRNA: messenger RNA

ms: milliseconds

NE: noradrenaline

NMDA: N-methyl-D-aspartate

ns: not significant

PACUC: Purdue University animal care and use committee

PCA: principal components analysis

PCs: pyramidal cells

PFA: paraformaldehyde

PM: posteromedial

PSTH: peristimulus time histogram

PV: parvalbumin

RGC: retinal ganglion cells

RL: rostrolateral area

RNA: ribonucleic acid

ROI: region of interest

RS: regular spiking

RSC: retrosplenial cortex

s: seconds

S1: primary somatosensory cortex

SC: superior colliculus

SD: standard deviation

SEM: standard error of the mean

SERT: serotonin transporter

SF: spatial frequency

SRP: stimulus selective response potentiation

SST: somatostatin

STD: Short term depression

STD: standard stimulus

STP: Short term plasticity

t: test statistic

TF: temporal frequency

TRN: thalamic reticular nucleus

TTL: transistor-transistor logic

V1: primary visual cortex

V2: secondary visual cortex

VEP: visually evoked potential

W: width

WT: wild type

z: z-score

ABSTRACT

The visual system is responsible for processing visual input, inferring its environmental causes, and assessing its behavioral significance that eventually relates to visual perception and guides animal behavior. There is emerging evidence that visual perception does not simply mirror the outside world but is heavily influenced by contextual information. Specifically, context might refer to the sensory, cognitive, and/or behavioral cues that help to assess the behavioral relevance of image features. One of the most famous examples of such behavior is visual or optical illusions. These illusions contain sensory cues that induce a subjective percept that is not aligned with the physical nature of the stimulation, which, in turn, suggests that a visual system is not a passive filter of the outside world but rather an active inference machine.

Such robust behavior of the visual system is achieved through intricate neural computations spanning several brain regions that allow dynamic visual processing. Despite the numerous attempts to gain insight into those computations, it has been challenging to decipher the circuit-level implementation of contextual processing due to technological limitations. These questions are of great importance not only for basic research purposes but also for gaining deeper insight into neurodevelopmental disorders that are characterized by altered sensory experiences. Recent advances in genetic engineering and neurotechnology made the mouse an attractive model to study the visual system and enabled other researchers and us to gain unprecedented cellular and circuit-level insights into neural mechanisms underlying contextual processing.

We first investigated how familiarity modifies the neural representation of stimuli in the mouse primary visual cortex (V1). Using silicon probe recordings and pupillometry, we probed neural activity in naive mice and after animals were exposed to the same stimulus over the course of several days. We have discovered that familiar stimuli evoke low-frequency oscillations in V1. Importantly, those oscillations were specific to the spatial frequency content of the familiar stimulus. To further validate our findings, we investigated how this novel form of visual learning is represented in serotonin-transporter (SERT) deficient mice. These transgenic animals have been previously found to have various neurophysiological alterations. We found that SERT-deficient animals showed longer oscillatory spiking activity and impaired cortical tuning after visual learning. Taken together, we discovered a novel phenomenon of familiarity-evoked oscillations in V1 and utilized it to reveal altered perceptual learning in SERT-deficient mice.

Next, we investigated how spatial context influences sensory processing. Visual illusions provide a great opportunity to investigate spatial contextual modulation in early visual areas. Leveraging behavioral training, high-density silicon probe recordings, and optogenetics, we provided evidence for an interplay of feedforward and feedback pathways during illusory processing in V1. We first designed an operant behavioral task to investigate illusory perception in mice. Kanizsa illusory contours paradigm was then adapted from primate studies to mouse V1 to elucidate neural correlates of illusory responses in V1. These experiments provided behavioral and neurophysiological evidence for illusory perception in mice. Using optogenetics, we then showed that suppression of the lateromedial area inhibits illusory responses in mouse V1. Taken together, we demonstrated illusory responses in mice and their dependence on the top-down feedback from higher-order visual areas.

Finally, we investigated how temporal context modulates neural responses by combining silicon probe recordings and a novel visual oddball paradigm that utilizes spatial frequency filtered stimuli. Our work extended prior oddball studies by investigating how adaptation and novelty processing depends on the tuning properties of neurons and their laminar position. Furthermore, given that reduced adaptation and sensory hypersensitivity are one of the hallmarks of altered sensory experiences in autism, we investigated the effects of temporal context on visual processing in V1 of a mouse model of fragile X syndrome (FX), a leading monogenetic cause of autism. We first showed that adaptation was modulated by tuning properties of neurons in both genotypes, however, it was more confined to neurons preferring the adapted feature in FX mice. Oddball responses, on the other hand, were modulated by the laminar position of the neurons in WT with the strongest novelty responses in superficial layers, however, they were uniformly distributed across the cortical column in FX animals. Lastly, we observed differential processing of omission responses in FX vs. WT mice. Overall, our findings suggest that reduced adaptation and increased oddball processing might contribute to altered perceptual experiences in FX and autism.

CHAPTER 1. INTRODUCTION

1.1 Ascending pathway to the visual cortex

Vision is one of the core senses that we use to explore, interpret, and interact with the outside world. One of the major goals of modern neuroscience is to gain mechanistic insight into vertebrate visual processing. Our interest stems not only from mere scientific curiosity but also because the acquired knowledge might guide research to improve the lives of individuals with neurophysiological disorders that are characterized by altered sensory experiences. Historically, the primate and cat visual systems have been major experimental models for neuroscientists that provided a lot of insight into visual processing. However, in the past decade, there has been a big surge of research using the mouse visual system as a platform to dissect the neural circuitry of visual processing. What makes a mouse such a powerful experimental model to study vision? Despite numerous disadvantages like a lower visual acuity, a smaller binocular zone, and a smaller brain size, genetic tools available in mice, along with logistics and ethical considerations, made it a great model to study visual circuits (Baker, 2013). Specifically, the investigation of genetically defined cell populations allowed researchers to gain unprecedented cellular and circuit-level insight into mammalian visual processing (Seabrook, Burbridge, Crair, & Huberman, 2017). It remains unknown how much of what we learn from mice can be translated to humans but having easy access and control over large neural ensembles is a unique feature of the mouse model.

The general image forming visual processing pathway of the mammals is conserved across species. It starts from the light entering the eye, where it is phototransduced and processed by retinal circuits. The retinal information output leaves via the optic nerve and passes optic chiasm (midline), so that it represents a given visual field in the contralateral visual thalamus and cortex. The retinal output directly projects to several subcortical regions, including the dorsal lateral geniculate nucleus (dLGN), superior colliculus (SC), and suprachiasmatic nucleus (SCN). dLGN relays information to the primary visual cortex (V1) via thalamocortical (TC) projections. From there, visual information is sent to both higher-order visual areas (HVA) and to subcortical regions. Overall, the retinal-geniculo-cortical pathway represents a direct route of the visual input to the visual cortex in both mice and primates (**Figure 1**).

In addition to neural circuits directly involved in image processing, modulatory mechanisms control the non-visual aspects of vision, including pupil reflexes, eye movements, and the circadian clock. They are important to regulate light intensity entering the eye, image stabilization, and effective sampling of the visual environment. Furthermore, eye and pupil tracking are often used in experimental set-ups to monitor the animal's engagement and brain state (Dhande et al., 2013; Hattar et al., 2003).

1.1.1 Retina

Visual processing begins once light enters the eye and reaches the retinal surface. The retina consists of three nuclear and two synaptic (inner and outer plexiform) layers. Light detection is mediated by photoreceptors in the outer plexiform layer (OPL) by rods (low-light conditions) and cones (during daylight). Rods significantly outnumber cones. Furthermore, mice have dichromatic vision, their cones contain pigments that are most sensitive to ultraviolet and green light (Peirson, Brown, Pothecary, Benson, & Fisk, 2018). After light is converted to the electrical signal, it is then transmitted to dendrites of horizontal and bipolar neurons. Horizontal cells possess lateral connections to mediate feedforward and feedback modulation of both photoreceptors and bipolar cells, whereas the latter sends signals to the inner plexiform latter (IPL). There, bipolar cells target dendrites of both amacrine and retinal ganglion cells (RGCs). Amacrine cells send lateral and vertical projections to provide inhibitory feedforward and feedback signals. RGCs integrate inputs along the dendrites and send signals to the brain down the optic nerve. Given the complex architecture and connectivity patterns in the retina, it is not surprising that more than 30 different RGC subpopulations have been described to date with diverse morphologies and response profiles (Baden et al., 2016).

The output from the retina represents an initial step of visual processing. What kind of information is sent to the brain? To gain insight into the function of RGCs, a classical study by Kuffler investigated neural responses of anesthetized cats in response to various light patterns presented on a restricted space of the TV screen (Kuffler, 1953). Given that the retinal surface represents a topographical map of the outside world (retinotopic map), one can find a direct correspondence between single-neuron activity and spatially restricted space in the visual scene. The receptive field (RF) of the neuron in the visual system refers to the small region of the retina

that upon light stimulation drives neural responses. This concept has been proven to be very useful in describing and investigating visual processing across different stages. The study demonstrated the presence of concentric RF with a "center-surround" organization in the retina. Specifically, two main types of fields were described: 1) cells with the "on"-center field that are excited by the light inside the RF and inhibited if the surrounding of the RF was activated, and 2) "off"-center fields that were activated when the light was shone onto the surround of the RF. This was an important discovery illustrating one of the first steps of feature coding in the visual system. Moreover, recent studies employing mouse retina revealed direction-selective RGCs (DS-RGCs), suggesting that retinal circuits are capable of more complex computations (Mauss, Vlasits, Borst, & Feller, 2017).

1.1.2 Superior Colliculus

Despite the overall similarity of the early visual processing pathway across different mammals, there are a couple of major differences that should be mentioned. First, the lateral placement of eyes in the mouse leads to a smaller overlap between left and right visual fields (smaller binocular zone), which is about 40° of a visual angle compared to 140° observed in nonhuman primates (Heesy, 2004; Scholl, Burge, & Priebe, 2013). Therefore, most neurons in the mouse visual system are driven by inputs from the contralateral eye. Second, more than 80% of the retinal output projects to superficial SC in mice, whereas only ~10% in monkeys (Ellis, Gauvain, Sivyer, & Murphy, 2016). What is the functional significance of SC in the mouse visual system? SC receives multisensory information from different sensory modalities and is important for sensorimotor integration. It also receives retinotopically mapped inputs from the retina and contains different visual feature maps (Dhande & Huberman, 2014). The mouse SC was found to be important for innate defensive behaviors, in which vision is important to detect avian predators and motor commands to promote escape. Those conclusions were derived from experiments showing freezing or flight behaviors in mice in response to looming visual stimuli mimicking predators. Apart from that, SC is also involved in orienting behaviors and eye movements (De Franceschi, Vivattanasarn, Saleem, & Solomon, 2016; Wallace et al., 2013; Yilmaz & Meister, 2013).

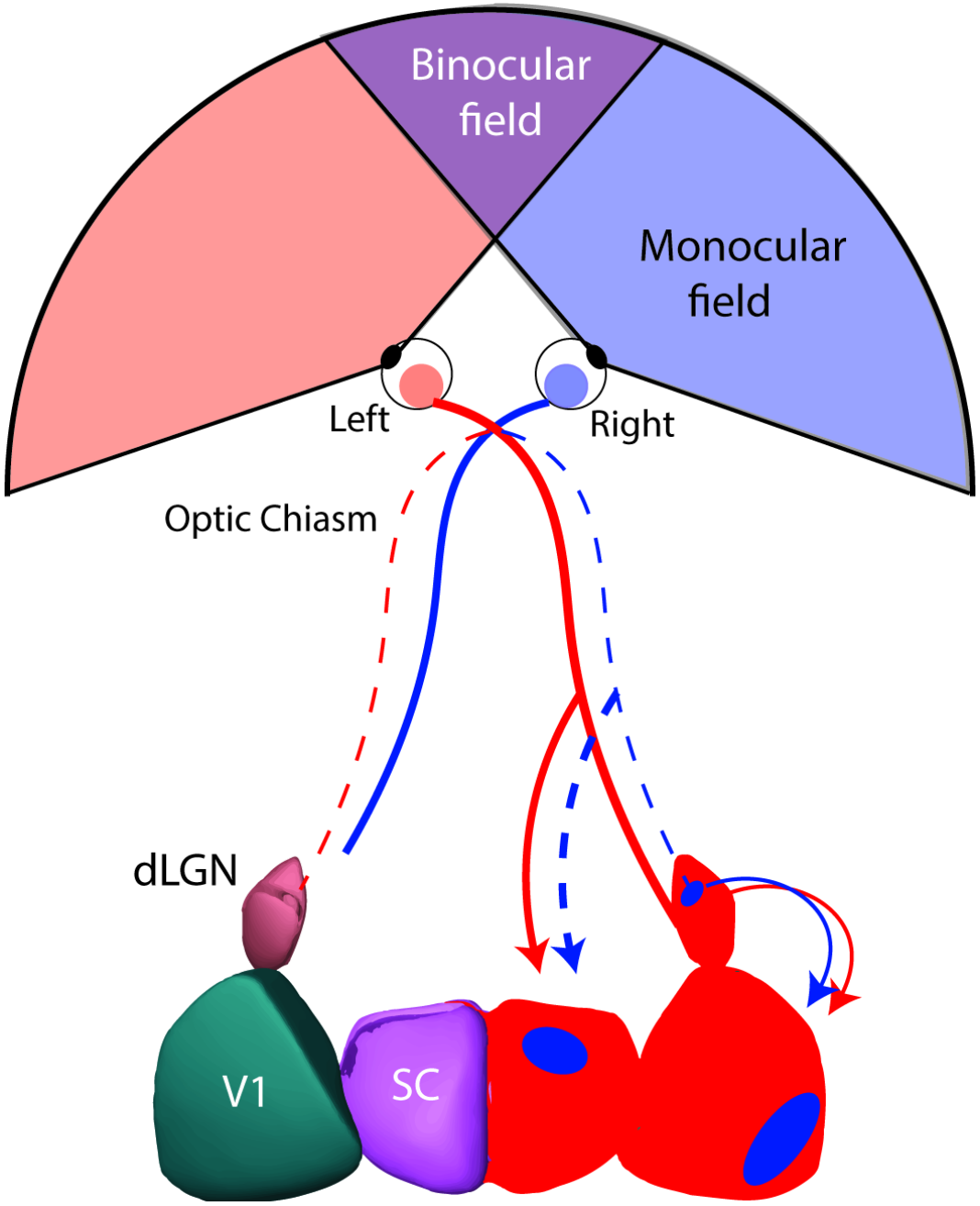

Figure 1. Ascending pathway to the visual cortex

1.1.3 Visual thalamus

dLGN of the thalamus is a major relay station of the retinal output to the visual cortex. The RGCs project to dLGN to establish a retinotopic map of the world (topographic map of the retinal surface). Visual information from the given retina is mostly represented in the contralateral visual thalamus with a smaller binocular zone that receives input from both eyes. After passing a midline, the left retina strongly innervates the right dLGN, but ~3% of RGCs also project to the ipsilateral side (Kerschensteiner & Guido, 2017). dLGN of the mouse can be subdivided into a "core" that projects to the cortical layer 4 and "shell" that target layers 1-3 of V1 (Usrey & Alitto, 2015). Those subregions are differentially targeted by different RGC populations, with classical RGCs projecting to the core and nonclassical "On-Off" DS- RGCs projecting to the shell (Huberman et al., 2009). Overall, dLGN neurons have similar RF configurations as RGCs.

Visual thalamus contains two major types of neurons: 1) excitatory thalamocortical (TC) that represent ~80% of cells and 2) GABAergic interneurons that make dendrodendritic and axodendritic connections with TC cells and other interneurons. It has been recently shown that dLGN cells receive diverse excitatory inputs from the RGCs so that some cells might receive retinotopically matched inputs from a few cells of a single type of RGCs, whereas others receive converging inputs from dozens of cells of various types (Hammer, Monavarfeshani, Lemon, Su, & Fox, 2015; Rompani et al., 2017). Moreover, dLGN is also modulated by corticothalamic (CT) inputs and inhibitory signals from thalamic reticular nuclei (TRN). One of the important questions is whether dLGN simply relays retinal output to the cortex or performs additional processing. In contrast to cats and primates, a significant portion of the mouse dLGN cells is orientation- and direction-selective (Marshel, Kaye, Nauhaus, & Callaway, 2012; Piscopo, El-Danaf, Huberman, & Niell, 2013). It is unclear how much DS-RGCs contribute to the orientation selectivity in dLGN and whether it emerges from the local circuit computations. However, given that dLGN receives inputs not only from the retina but also from superficial SC, TRN, and feedback connections from layer 6 of V1, it is likely that retinal output undergoes additional processing in dLGN before reaching the V1.

There is extensive recurrent connectivity present among retina, dLGN, SC, and V1. Functional segregation of different pathways might be important for specific visual functions. The retinal-genico-cortical pathway is important for high-level image processing and learning new

visual behaviors, whereas retinal-collicular pathways might be more important for innate visual behaviors that require multisensory integration and quick motor responses.

1.2 Cortical processing

1.2.1 Primary visual cortex

dLGN neurons relay information to V1, a first step along the visual cortical pathway. One of the first insights into visual cortical processing that influenced the course of development of modern neuroscience was the discovery of orientation-selective cells in cat V1 by David Hubel and Torsten Wiesel. In their seminal study, they recorded single-neuron activity while presenting spots or oriented slits of light on the screen to the anesthetized cats (Hubel & Wiesel, 1959, 1962). They were first to characterize the RF of V1 neurons and discover preferential firing to specific orientations and directions of visual stimuli. Furthermore, they described two types of neurons in V1: 1) RF of "simple" cells contained excitatory and inhibitory subregions and were thought to emerge from converging inputs from dLGN neurons with concentric RF that were organized in such a way to best respond to a particular orientation, 2) RFs of "complex" cells did not have the inhibitory subregion and were thought to integrate information from several simple cells that have similar orientation preferences so that their responses did not depend on the specific location of the stimulus within the RF (**Figure 2**). In addition, it has been shown that the magnitude of the neural response depends on the size of the oriented bar within the RF so that larger bars within or exceeding the RF might elicit stronger responses, the phenomenon termed length summation. Interestingly, some neurons in the cat secondary visual area were shown to exhibit end-stopping, where a bar extending beyond the RF suppresses neural response (Hubel & Wiesel, 1965). Those were among the first examples of how surround might influence computations inside the "classical" RF and will be discussed in further detail in later sections of the dissertation.

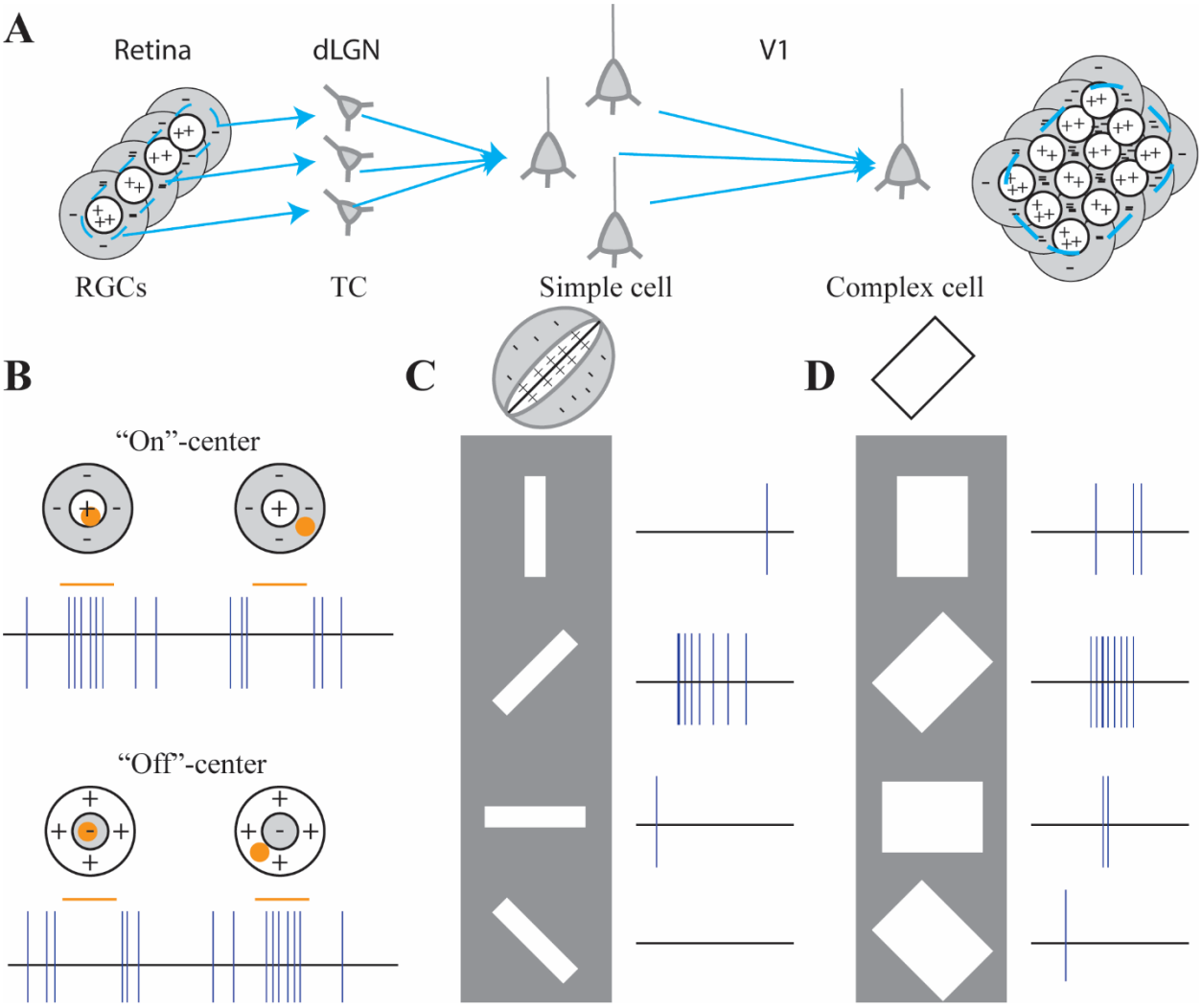

Figure 2. Emergence and properties of simple and complex RFs

A. Converging inputs from RGCs on dLGN and V1 cells. **B.** RF properties of RGCs. **C.** Orientation selectivity of simple cells. **D.** Orientation selectivity of complex cells

Neurons in V1 are organized to form a retinotopic map. However, in contrast to cats and primates, rodents lack organizational units like orientation and ocular dominance columns (Dräger, 1975; Ohki, Chung, Ch'ng, Kara, & Reid, 2005; Van Hooser, Heimel, Chung, Nelson, & Toth, 2005). Orientation columns contain neurons with similar orientation preferences, while neurons in the ocular dominance columns form stripes that are mostly innervated by one eye or the other (Hubel & Wiesel, 1965, 1968). The lack of clear clustering of neurons according to their orientation, known as the "salt-and-pepper" organization, raises the question: Do mouse neurons have similar tuning properties to primate ones? Functional studies of tuning properties of neurons in mouse V1 revealed highly selective neural responses to the orientation, direction, spatial frequency, temporal frequency, and contrast of the visual stimuli (Niell & Stryker, 2008). Furthermore, extra classical RF properties similar to the ones in monkeys were also described. But how are these tuning properties achieved without the classical columnar organization? Recent evidence suggests that there are "mini-columns" in the mouse V1 formed by neurons with similar tuning properties (Ringach et al., 2016). Consistent with this finding, pyramidal neurons have a higher probability of connecting to similarly tuned neurons in the local circuit, suggesting that they form functional ensembles (Hofer et al., 2011).

Cortex has six defined layers that have unique architecture, composition, and possibly functions. All layers but layer 1 of V1 are densely populated by excitatory and inhibitory neurons. Layer 1 contains apical dendrites of layer 5 pyramidal cells (PC) and integrates information from diverse sources, including inputs from the shell of dLGN and feedback connection from HVA. Layer 4 (L4) is a thalamorecipient layer and targeted by the core of the dLGN. According to the "canonical microcircuit" theory of primary sensory areas, the information from L4 is first routed to superficial layers (L2/3) and then to the deeper layer (L5 and L6) of V1 (**Figure 3A**) (Douglas & Martin, 1991). Despite being an oversimplification of cortical processing, this concept was useful to reveal general patterns of connectivity and aligned with early experimental data. How do different layers contribute to sensory processing? One of the examples of successfully utilizing genetic tools available in mice was the investigation of how different cortical layers interact during sensory processing. Several recent studies have revealed additional information that has corrected the original understanding of the circuit organization and information processing in mouse V1. First, all cortical layers were shown to receive thalamic inputs to some extent (Seabrook et al., 2017). Second, it has been shown that suppression of L4 does not impair L2/3 responses, while

inactivation of L2/3 does not impair deep cortical response (Constantinople & Bruno, 2013). Leveraging layer-specific markers, it has also been shown that while L4 strongly drives L2/3 while inhibiting L5 via local interneurons to sharpen the stimuli representations (Pluta et al., 2015). Layer 6 is capable of indirectly modulating V1 responses via CT projections to dLGN and directly inhibiting the whole cortical column via translaminar interneurons (Bortone, Olsen, & Scanziani, 2014; Olsen, Bortone, Adesnik, & Scanziani, 2012). Overall, there is a growing body of literature supporting the functional specialization of different cortical layers and the importance of laminar communication to support normal visual functions.

Most cortical neurons are excitatory (glutamatergic) principal cells (PC), whereas GABA (γ-aminobutyric acid)-ergic inhibitory neurons (IN) comprise only 15-25% of the neural population (Rudy, Fishell, Lee, & Hjerling-Leffler, 2011). Although small in number, INs exhibit a strong effect on circuit processing and neural plasticity. INs are very diverse in morphology, connectivity patterns, and spatial localization, which influences their functional grouping as well. Three major non-overlapping IN subtypes: parvalbumin (PV, or PVAL), somatostatin (SOM, or SST), and serotonin receptor 5HT3a expressing INs can be reliably targeted by genetic tools (Gonchar, Wang, & Burkhalter, 2008). They comprise 85% of all cortical INs and have recently been targets of extensive research to elucidate their role in learning, memory, and disease state (Isaacson & Scanziani, 2011; Wood, Blackwell, & Geffen, 2017). PV INs mostly target perisomatic regions and mediate feedforward inhibition that closely follows the excitation, thereby controlling the output of principal cells (Hofer et al., 2011). SOM INs mainly target distal dendrites of PC, affecting dendritic computations and influencing input to PC (Urban-Ciecko & Barth, 2016). VIP INs, on the other hand, mainly target other INs providing an additional level of control over inhibition in the brain (**Figure 3B**) (Guet-McCreight, Skinner, & Topolnik, 2020). Both VIP and SOM INs are targets of neuromodulation and top-down control from higher brain areas. Various computational motifs and di-tri-synaptic connections were described in literature mediating various functions ranging from gain modulation to the expression of behavior.

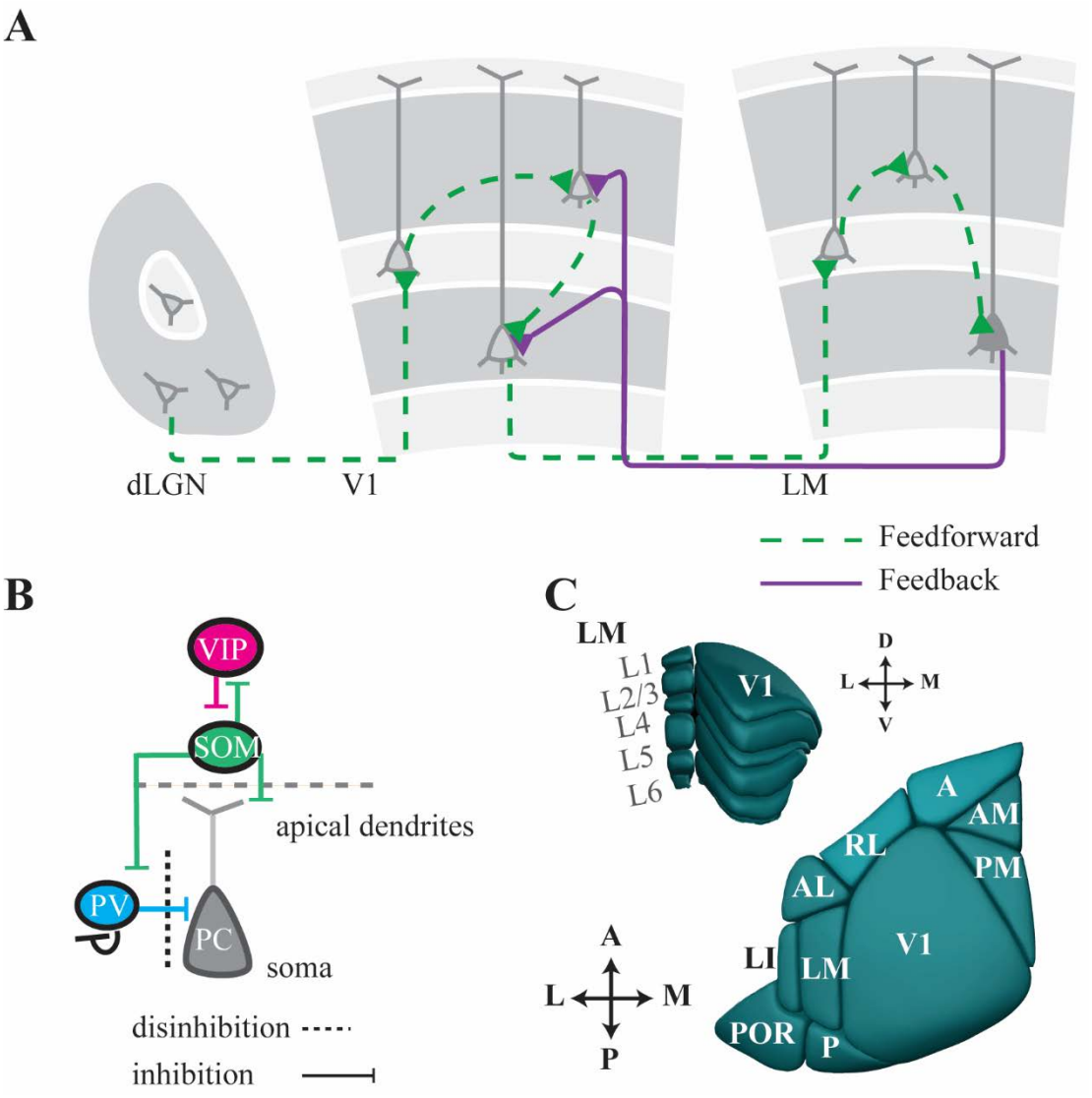

Figure 3. Cortical circuits

A. Canonical feedforward and feedback pathways. **B.** Connectivity patterns of IN subpopulations. **C.** Cortical layers and HVAs

One of the major roles of INs is to maintain cortical excitatory and inhibitory (EI) balance, which prevents runaway excitation and maintains equilibrium in local networks. Alterations in EI balance are implicated in various neurodegenerative and psychiatric disorders like autism and schizophrenia, highlighting the importance of keeping excitation under control (Selten, van Bokhoven, & Nadif Kasri, 2018). The tight alignment of excitation and inhibition provides a very small window for integration and information transfer, such that temporal modulation and interplay of INs and PCs dictate what and when input will be propagated to projection neurons (Isaacson & Scanziani, 2011). The activity of INs, but not PC, was also shown to be strongly modulated by context and brain state. Overall, INs regulate the input/output of PCs and perform a major role in circuit information processing and remodeling.

1.2.2 Higher-order visual areas

After visual information is processed and transformed in V1, it is then further directed to hierarchically higher-order visual areas (HVAs). Ultimately, intracortical interactions between V1 and HVAs are where complex representations emerge that compose visual perception. One of the hallmarks of visual cortical processing in primates is the anatomical and functional segregation of various HVAs to support various complex visual behaviors (Glickfeld & Olsen, 2017). Given the general notion of the hierarchical bottom-up building of representation in the visual system, these HVAs were shown to integrate information from cortical and subcortical regions and contain neurons that code for more complex representations. Do mice possess similar anatomical and functional segregations of HVAs? A study by Wang and Burkhalter was among the first to show that the mouse visual system contains retinotopically organized distinct HVAs (Wang & Burkhalter, 2007). They used tri-color anterograde tracers to investigate the major projections of V1 feedforward connections. This technique revealed that V1 targets nine distinct HVAs and several non-visual regions like somatosensory, cingulate, and entorhinal cortices. The results from anatomical tracing methods were then replicated and further refined by using functional approaches like intrinsic and calcium imaging (Garrett, Nauhaus, Marshel, & Callaway, 2014; Zhuang et al., 2017). To standardize the names and coordinates of HVAs, the Allen Mouse Common Coordinate Framework (CCF) was released by the Allen Institute for Brain Science. The list of names of HVAs commonly used in literature and corresponding names in the CCF are following: anterior (A/VISa), anterolateral (AL/VISal), anteromedial (AM/VISam),

laterointermediate (LI/VISli), lateromedial (LM/VISl), posterior (P/VISpl), posterior medial (PM/Vispm), rostrolateral (RL/VISrl), and primary visual cortex (V1/VISp) (**Figure 3C**).

To establish the hierarchy among HVAs, researchers investigated various properties of feedforward and feedback inputs, including laminar terminations, recruitment of excitation/inhibition, and latency of neural responses. First, the FF output from V1 mostly targets superficial and L4 of LM, whereas feedback inputs from LM strongly innervate L1 (Coogan & Burkhalter, 1993; Yamashita, Valkova, Gonchar, & Burkhalter, 2003). Second, FF inputs were found to evoke stronger inhibition compared to FB projections by recruiting local PV INs (Dong, Wang, Valkova, Gonchar, & Burkhalter, 2004; Yang, Carrasquillo, Hooks, Nerbonne, & Burkhalter, 2013). Third, the latency of visual stimulus-evoked neural response can be used to infer the relative position of the given area in the hierarchy (Fehérvári & Yagi, 2016; Polack & Contreras, 2012). There are two major parallel processing streams in the primate visual system: ventral one, which encodes objects ("what"), and dorsal one, which encodes the location ("where"). After defining anatomical borders of HVAs, a growing body of literature emerged, suggesting that similar parallel pathways exist in mice. Analogous to the ventral stream, LI, LM, P, and POR areas were discovered to be the target areas involved in object recognition and memory. The dorsal stream includes AL, RL, PM, A, and AM areas and strongly innervates regions responsible for spatial learning and motor control (Wang, Sporns, & Burkhalter, 2012). Furthermore, these modules provide output to and integrate information from subcortical regions, including SC and mouse pulvinar.

As visual information propagates through primate visual hierarchy, there is a progressive specialization of HVAs to extract specific patterns from the visual scene. The mouse visual system displays similar features; the size of the RF is larger in HVAs compared to V1, which results in higher magnification since the same retinotopic map needs to be represented in a smaller area. Lateromedial area (LM) is the most strongly interconnected with and shares similar topology as V1 and is considered to be analogous to primate V2 (Wang et al., 2012). Tuning properties in V1 and LM neurons were found to be comparable, but LM prefers higher spatial frequencies (Andermann, Kerlin, Roumis, Glickfeld, & Reid, 2011). A recent study from the Allen Institute investigated tuning properties of different HVAs across cortical layers. The strongest direction selectivity was found in L4 of V1. Neurons in superficial layers of LM and AL were found to have

higher direction selectivity than PM and AM. Neurons in AL and RL were found to prefer higher temporal frequencies and lower spatial frequencies, whereas AM was found to prefer higher spatial frequencies (de Vries et al., 2020). It is currently an active area of research, and there is growing evidence that different HVAs might be important for diverse visual-guided behaviors. Interestingly, functional specialization seems to develop not only from cortical interactions but also from subcortical circuits involving SC and LP (Tohmi, Meguro, Tsukano, Hishida, & Shibuki, 2014).

1.3 Contextual visual processing

Is there a direct mapping from image features to perception, or does the visual system perform additional computations before the percept is formed? There is emerging evidence that contextual information plays an important role in visual perception and is crucial for extracting behaviorally relevant information. Context refers to sensory, behavioral, and/or cognitive cues that might influence the processing of visual information. Visual illusions provide compelling evidence of spatial contextual modulation, in which part of the image might influence the processing of another region. Furthermore, the temporal context or stimulus history heavily influences visual processing. The same visual stimuli might be processed differently based on the observer's prior experiences with the object e.g., familiar vs. a novel or rewarded vs. neutral stimuli.

1.3.1 Spatial context

Early neurophysiology studies of classical RF properties were the basis for prominent theories of a representational framework, where the visual cortex was considered as a feature detector that encodes simple features in V1 and increasingly complex representations along the cortical hierarchy (Hubel & Wiesel, 1962; Riesenhuber & Poggio, 1999). While it is true that complex representations emerge in HVAs, recent evidence suggests that they also exist in lower-order regions and might arise from FB inputs. Spatial contextual modulation has been investigated in the primate visual cortex (Zipser, Lamme, & Schiller, 1996), but recent studies leveraging genetic tools available in mice provided circuit-level insights into contextual processing (Kato, Gillet, & Isaacson, 2015; Makino & Komiyama, 2015; Pak, Ryu, Li, & Chubykin, 2020; Ross & Hamm, 2020). One example of spatial contextual modulation is the segregation of salient features from the background. Figure-ground modulation (FGM) is a process in which neural responses are

differentially upregulated by the same visual features when they are part of the figure (object) vs background (**Figure 4A**) (Qiu & von der Heydt, 2005). Enhancement is evident in the latter part of neural responses suggesting the importance of recurrent processing. It has been recently shown that there are neural correlates of FGM in mice and their dependence on top-down feedback from HVAs. Furthermore, VIP INs are recruited by the figure to disinhibit local activity via SOM INs, and their inhibition leads to the decreased FGM (Kirchberger et al., 2020; Schnabel et al., 2018). Another example of spatial contextual processing is visual illusions. Kanizsa illusory triangle is formed by a specific configuration of three different inducers (pacmen) that leads to the perceptual completion of the triangle without the real contours. The triangle is made of illusory (subjective) contours (IC) and can be vividly perceived despite breaks in continuity (**Figure 4B**) (Kanizsa, 1955). A classical study by von der Heydt was the first to show neural correlates of illusory perception in the early visual cortex (von der Heydt & Peterhans, 1989). They demonstrated that spatial context that induces illusory contours evoked neural responses despite the lack of direct activation of the classical RF of neurons. These results were validated and further extended in both cats and primates by numerous groups (Grosof, Shapley, & Hawken, 1993; Nieder, 2002; Peterhans & von der Heydt, 1989). Lee et al. explored neural responses to Kanizsa illusion in primate V1 and V2 and found that IC responses emerged earlier in V2 compared to V1, suggesting that recurrent connectivity might be important for illusory perception (Lee & Nguyen, 2001).

1.3.2 Temporal context

Similar to how the visual system segregates important visual features from the background of the scene, it also needs to identify salient visual patterns across time. To achieve this, most of the incoming visual information is suppressed due to the redundancy (behavioral unimportance), and only unexpected or novel stimuli that are potentially behaviorally relevant are amplified in the sensory areas. At the neuronal level, it is implemented by a decrease in firing rate or stimulus-specific adaptation (SSA) to redundant and repetitive stimuli. On the other hand, neural responses are amplified when a deviant or novel stimulus is encountered which is called a mismatch response or deviance-detection (DD). The effects of recent stimulus history on sensory processing have been extensively studied using an "oddball" paradigm in both human individuals and animal models (Pazo-Alvarez, Cadaveira, & Amenedo, 2003; Ross & Hamm, 2020; Ulanovsky, Las, & Nelken, 2003). The oddball paradigm involves the presentation of two different stimuli: "standard"

(redundant) and "deviant" (oddball). The standard stimulus is presented with a high probability to build a statistical context, whereas the deviant stimulus is a rare stimulus that violates the expectations of the standard stimulus (**Figure 4C**). Enhanced response to the deviant stimuli was termed mismatch negativity (MMN) and was first reported in human studies employing electroencephalography (EEG) (R. Näätänen, 1995; Tiitinen, May, & Näätänen, 1997). It appears ~150ms after stimulus onset and represents the combination of SSA and DD. This phenomenon was replicated and investigated in different sensory modalities and species (Chen, Helmchen, & Lütcke, 2015; Musall, Haiss, Weber, & von der Behrens, 2015; Parras et al., 2017). Importantly, MMN was found to be impaired in various neurodevelopmental disorders, including schizophrenia and autism, which makes the oddball paradigm a powerful method to investigate both temporal contextual processing and neurophysiological deficits of neurodevelopmental disorders (Lavoie, Polari, Goldstone, Nelson, & McGorry, 2019; Risto Näätänen et al., 2011; Tada et al., 2019).

By leveraging the oddball paradigm and genetic tools available in mice, recent studies advanced our understanding of the cellular and circuit-level mechanisms of SSA and DD (Ross & Hamm, 2020). In contrast to early MMN experiments, recent animal studies employed a control sequence that allowed them to decompose the MMN into SSA and DD. Specifically, they investigated the stimulus representation in different contexts, in which the same stimulus acted as redundant, deviant, and neutral to control for physical attributes of the stimulus. By recording both subthreshold and suprathreshold responses SSA and MMN were found to occur in the early and late parts of neural responses, respectively. Furthermore, they found that oddball responses are also present in PV and SOM INs (Chen et al., 2015). To investigate how different INs contribute to the oddball responses, several studies employed opto- and chemogenetic approaches to selectively modulate different IN subpopulations. Suppression of PV INs in the auditory cortex resulted in a uniform decrease in both SSA and deviant stimuli, whereas inhibition of SST INs only reduced SSA but not mismatch responses (Natan et al., 2015). Interestingly, another study showed that suppression of SOM abolishes DD in PC in the V1 (Hamm & Yuste, 2016).

1.3.3 Perceptual learning and reward processing

While recent sensory experience shapes neural responses on short timescales, long-term changes in the local circuit can be induced by perceptual training. In recent years we have

witnessed a paradigm shift in the canonical feedforward theory of brain functioning, in which primary sensory areas are only responsible for feeding information to higher-order brain areas (Fiser et al., 2016; Gavornik & Bear, 2014; B.-H. Liu, Huberman, & Scanziani, 2016; Shuler & Bear, 2006). It has been recognized that feedback connections and top-down modulation are of significant importance for learning and memory. Numerous studies reported that rodent primary visual cortex is capable of encoding reward timing, familiarity, and spatiotemporal sequences (Chubykin, Roach, Bear, & Shuler, 2013; Gavornik & Bear, 2014). Shuler and Bear were the first to show that V1 is capable of encoding reward timing, a feature mainly attributed to higher brain areas (Shuler & Bear, 2006). They trained rats to associate visual stimulation with the reward given at a delay and observed the emergence of neural responses reporting the time reward was provided. Three different types of responses were observed: 1) a sustained increase in firing rate 2) a sustained decrease in firing rate, and 3) peak firing at the time of reward. Almost a decade after this discovery, Chubykin et al. reported that reward timing in V1 requires cholinergic input (Chubykin et al., 2013). It was also shown in slice experiments that pairing white matter stimulation with the neuromodulator release in V1 increases the duration of neural responses, offering a potential mechanism for encoding reward timing (**Figure 4E**). This observation was verified by disrupting cholinergic projections *in vivo*, which resulted in the abolishment of reward timing in behaving rats. It was later confirmed by the Shuler group that basal forebrain cholinergic projections are required for reward encoding and behavior (reward consumption) by using optogenetics (C. H. Liu, Coleman, Davoudi, Zhang, & Hussain Shuler, 2015).

Further evidence that V1 is more than a simple feature detector came from several studies reporting various visual experience-dependent changes occurring in V1 (**Figure 4D**). One of the first studies employing perceptual training described stimulus-response potentiation (SRP), which occurs upon entrainment of V1 to a particular orientation grating and manifests as an increase in visually evoked potential (VEP) amplitude (VEPs are visually induced changes in the local field potentials (LFPs), the low-frequency part of electrophysiological data) (Sam F. Cooke & Bear, 2010; Frenkel et al., 2006). Cooke et al. showed that SRP shares similar molecular mechanisms with the NMDA receptor-dependent long-term potentiation (LTP) and could be blocked by ZIP peptide, which erases LTP (Serrano, Yao, & Sacktor, 2005). Furthermore, it was also shown that blocking ACh muscarinic receptors reduces SRP. They also described orientation-selective habituation (OSH), which happens after mice become familiar with the trained stimuli and can be

observed on both a circuit level (SRP) and through a behavioral paradigm of exploratory behavior in an open arena (S. F. Cooke, Komorowski, Kaplan, Gavornik, & Bear, 2015). It was later shown by Gavornik et al. that V1 is also capable of learning spatiotemporal sequences and demonstrates VEPs even when some of the elements of the sequence are omitted. This type of sequential plasticity is specific to the temporal and spatial characteristics of the stimuli and can be blocked by local infusion of scopolamine, a non-specific muscarinic receptor antagonist (Gavornik & Bear, 2014). Overall, there is extensive evidence for spatial and temporal contextual modulation of visual responses over the short and long timescales.

1.4 Mouse models of neurodevelopmental disorders

One of the major benefits brought by the mouse experimental model was the ability to generate transgenic animals that recapitulate neurophysiological phenotypes of human neurodevelopmental disorders. This offers a unique opportunity to gain insight into the molecular, cellular, and circuit-level impairments underlying neurophysiological deficits. While it is challenging to investigate complex social and cognitive alterations in mice, sensory processing offers a window into discovering impairments in general neural mechanisms and possible intervention strategies to address them. In this work, we investigated two different mouse models: Fmr1 KO mouse model of fragile X syndrome (FX) and serotonin-transporter KO (SERT KO) mice.

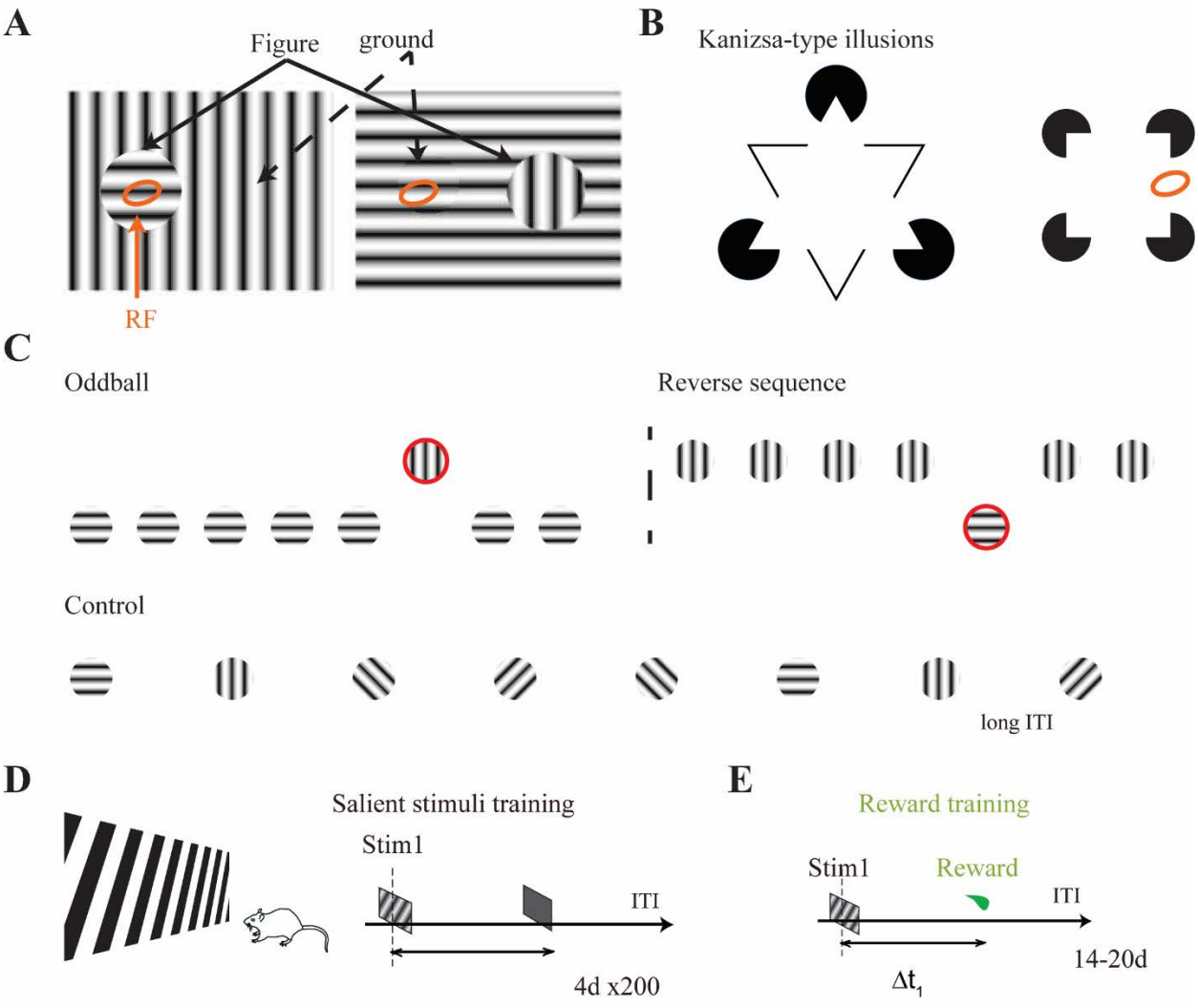

Figure 4. Spatiotemporal modulation of visual responses

A. Figure-ground modulation. B. Kanizsa-type illusionss. C. Oddball paradigm. D. Perceptual experience. E. Reward training

1.4.1 Fmr1 KO

Fragile X syndrome (FX) is the leading cause of intellectual disability and ASD (autism spectrum disorders), affecting approximately 1 in 5000 males in the United States (CDC, 2016). The complex nature of the disorder and variability marked by unrelated symptoms including hyperactivity, anxiety, social deficits, and Intellectual disability makes it difficult to find a "one-fits-all" treatment strategy to improve the lives of affected people (Bear, Huber, & Warren, 2004; Gross, Berry-Kravis, & Bassell, 2012). Furthermore, there is a huge social and economic burden for the families of affected individuals. Therefore, there is a critical need to understand the underlying causes of the disorder to design effective interventions. Currently, there is no treatment to combat FX despite the prevalence of research programs dedicated to unraveling the molecular and genetic pathophysiology of the disease. Although potential therapeutics have been identified in the last 10 years from animal studies, these drugs have failed to meet behavioral endpoints in human clinical trials of FX. These recent failures have raised questions of whether different approaches are needed to complement existing knowledge and gain novel insights into the complex nature of FX. Although there is extensive variability in FX symptomology, robust hallmarks of this condition include altered neuronal excitability, abnormal functional connectivity, and abnormal architecture of local circuitry (Contractor, Klyachko, & Portera-Cailliau, 2015; Haberl et al., 2015; Hoffman et al., 2012). It has been shown that local circuits exhibit hyperconnectivity while long-range connections are impaired in *Fmr1* KO mice (Contractor et al., 2015).

FX is caused by the expansion of the CGG repeats in the 5’ untranslated region of the *FMR1* gene that leads to its transcriptional silencing and the loss of fragile X mental retardation protein (FMRP). The FMRP is an mRNA-binding protein that negatively regulates ~4% of protein expression and is highly abundant in neurons (Brown et al., 2001; Darnell, 2011). The loss of such a global regulator of translation might lead to diverse alterations due to the increased protein synthesis. Using FX mice, several studies reported altered dendritic spine morphology and development, with an increased number of immature spines (Grossman, Elisseou, McKinney, & Greenough, 2006; Hinton, Brown, Wisniewski, & Rudelli, 1991). Those alterations might be linked to increased excitability and persistent neural activity that ultimately may be related to sensory hypersensitivity, and predisposition to epilepsy observed in FX. A major advancement in the FX field was the discovery of enhanced long-term depression (LTD) in the hippocampus of

FX mice, which was mediated through the group 1 G-protein-coupled metabotropic glutamate receptor (mGluR) and was protein synthesis-independent (Carroll, Lissin, von Zastrow, Nicoll, & Malenka, 1999; Huber, Gallagher, Warren, & Bear, 2002; Snyder et al., 2001). The discovery was exciting because FMRP may inhibit the group 1 mGluRs signaling downstream of the mGluRs. Consequently, the loss of FMRP leads to exaggerated group 1 mGluR signaling. The ideas and experimental evidence in support of this hypothesis were described in the "mGluR theory of fragile X" (Bear et al., 2004). A large body of experimental evidence has been generated in support of this theory; the blockade of mGluR5 was shown to rescue numerous cognitive and behavioral alterations observed in FX mice, including dendritic spine density, exaggerated protein synthesis, anxiety, and audiogenic seizures (Bear et al., 2004; Dölen et al., 2007; Nakamoto et al., 2007). However, recent human clinical trials in FX individuals utilizing mGluR5 antagonists failed to reach behavioral endpoints suggesting that further research is needed to decipher not only molecular pathways but also the circuit and systems-level impairments observed in FX (Berry-Kravis et al., 2016).

1.4.2 SERT KO

There is compelling evidence of the involvement of 5-hydroxytryptamine (serotonin, 5-HT) in plasticity and modulation of the visual cortex. 5-HT signaling is important both during the prenatal period for maturation of cortical architecture and later in life for experience mediated plasticity. Early studies report that electrical activation of raphe nucleus, the major site of serotonergic neurons, altered the excitability of the visual cortex (Gasanov, Mamedov, & Samedova, 1989; Lidov, Grzanna, & Molliver, 1980). More direct evidence came from *in vivo* studies, in which direct application of 5-HT was shown to both facilitate and inhibit neuronal responses in the visual cortex (Krnjević & Phillis, 1963; Waterhouse, Ausim Azizi, Burne, & Woodward, 1990). Such variability might arise from the experimental design, model organisms, or the visual cortex itself, given different receptor distributions in cortical layers, synapse composition, and interactions with other neurotransmitters (Gu, 2007).

The variable effects of 5-HT on cortical neurons in part arise from the differential spatial and functional distribution of 5-HT receptors (Yoshikuni Edagawa, Hiroshi Saito, & Kazuho Abe, 1998a). There are seven major types (5-HT1-7) and 15 variants of serotonin receptors identified

so far; most of them are G-protein coupled receptors (GPCRs), while only one is a ligand-gated ionic channel (5-HT3) (Bradley et al., 1986). Depending on the activation pathway, 5-HT receptors can be grouped into three groups: 1) 5-HT1 activate Gi/o pathway; 2) 5-HT2 couple to the Gq/11; 3) the remaining 5-HT4-7 work through Gs pathway. 5-HT1 receptor activation decreases cell excitability by increasing potassium ion conductance (Li, 1999, 2004; McCormick, Wang, & Huguenard, 1993). On the other hand, 5-HT2 and 5-HT4 activation lead to increased neuronal excitability due to decreased potassium conductance (Bockaert, Fozard, Dumuis, & Clarke, 1992; Edagawa, Saito, & Abe, 2000). 5-HT3 receptors were found to be expressed in a subpopulation of GABAergic neurons in the cortex, which is aligned with the previous observations that 5-HT3 activation leads to decreased excitation in the visual cortex of the ferret (Roerig & Katz, 1997; Tecott, Maricq, & Julius, 1993). It also provided anatomical evidence that serotonergic projections directly innervate cortical GABAergic neurons. Previous research suggests that 5-HT5 receptors modulate serotonergic neurons, whereas 5-HT6/7 play a role in learning and memory (Tassone, Madeo, Sciamanna, Pisani, & Bonsi, 2010; West, Marcy, Marino, & Schaffhauser, 2009; Xiang et al., 2016).

Alterations in serotonin signaling have been implicated in various psychiatric disorders and depression (Lesch, 1996). To further unravel the role of the serotonergic system in the body, Bengel et al. generated a serotonin transporter (5-HTT, SERT) knockout mouse model (SLC6A4 knockout mice) (Bengel, 1998). SERT is a major regulator of serotonin homeostasis. Thus its inhibition has a profound effect on 5-HT signaling (Ansorge, Zhou, Lira, Hen, & Gingrich, 2004; Persico, 2001; Salichon, 2001). It has been confirmed that these mice lack functional SERT, and an abnormal 5-HT concentration has been observed. This mouse line represents a constitutive knockout of the SERT and thus exhibits various physiological, anatomical, and behavioral abnormalities, including altered neuronal density in visual/somatosensory cortices, anxiety, higher body weight, and decreased sensitivity to drugs like MDMA. This is a valuable model that has helped researchers relate structural and physiological brain abnormalities to the serotonergic system (Gobbi, Murphy, Lesch, & Blier, 2001; Montanez, Owens, Gould, Murphy, & Daws, 2003; Murphy & Lesch, 2008). Yet, very little electrophysiological data is available to reflect underlying circuit/neuronal level changes.

Interestingly, chronic treatment with the antidepressant fluoxetine (inhibits SERT) reopened the critical period in adult rats, which allowed ocular dominance plasticity to take place during adulthood (Vetencourt et al., 2008). The same research group has also reported that fluoxetine treatment helps to restore binocularity ("lazy eye," decreased visual capacity in one eye) in amblyopic rats. They found that the effect they observed was mediated through decreased GABAergic transmission, which is consistent with previous studies suggesting a direct effect of serotonergic projections on GABAergic neurons. In addition, stronger LTP was observed after theta-burst stimulation, suggesting increased capability for plasticity in treated adult rats. This study was consistent with the idea that the serotonergic system might gate cortical plasticity through modulation of the activity of inhibitory interneurons and suggested potential candidates for the treatment of amblyopia during adulthood. This idea was later validated by numerous studies, and clinical trials were performed to test the potential use of antidepressants for treating amblyopia (Bachatene, Bharmauria, Cattan, & Molotchnikoff, 2013; Guirado, Perez-Rando, Sanchez-Matarredona, Castrén, & Nacher, 2014; Quinlan, 2008).

In vitro brain slice studies found that serotonin can induce both LTP and LTD in visual cortical slices depending on the site of recording, stimulation protocol, the animal model used, and age (Kojic, Gu, Douglas, & Cynader, 1997). Despite these variations; it can be concluded from the literature that 5-HT can induce LTP and LTD in brain slices from kittens (Kojic et al., 2000), while an increase or decrease in LTP can be observed in rats depending on the experimental design (Edagawa et al., 1998a; Yoshikuni Edagawa, Hikoshi Saito, & Kazuho Abe, 1998b; Kim et al., 2006). A recent study in mouse visual cortex suggested that 5-HT application combined with the spike-timing-dependent plasticity (STDP)-inducing conditioning protocol transforms "eligibility traces" (synaptic weights that can be updated) to LTD in layer two of V1. It is hypothesized that activity-dependent changes in synapses form eligibility traces, which can be later transformed by neurotransmitters into long-term changes in the cortex. This study was motivated by the fact that unlike the classical Hebbian plasticity, not only glutamate receptors but also neuromodulators acting through Gs and Gq pathway are necessary for LTP/D in the visual cortex (Choi et al., 2005). Furthermore, the authors propose a computational model based on their observations that 5-HT transforms eligibility traces into LTD and noradrenaline (NA) into LTP. This model may also explain the underlying mechanism of reward timing in V1. Importantly, inhibition of 5-HT2c

receptor blocks the consolidation of eligibility traces by 5-HT, suggesting the underlying mechanism of action (He et al., 2015).

SERT null mice lack a functional serotonin transporter and have an abnormal concentration of 5-HT throughout their life, from the prenatal period to adulthood. This mouse line has recently been proposed to serve as one of the models recapitulating some autism phenotypes since 5-HT alterations are described in many autistic patients. Overall, 5-HTT KO mice have proven to be a valid model for studying the serotonergic system (Murphy & Lesch, 2008). Although many studies characterized physiological and behavioral abnormalities, there is very little electrophysiological data available, and it is not known whether visual cortical circuitry is altered in this mouse line.

1.5 References

Andermann, Mark L., Kerlin, Aaron M., Roumis, Demetris K., Glickfeld, Lindsey L., & Reid, R. C. (2011). Functional Specialization of Mouse Higher Visual Cortical Areas. *Neuron, 72*(6), 1025-1039. doi:https://doi.org/10.1016/j.neuron.2011.11.013

Ansorge, M. S., Zhou, M., Lira, A., Hen, R., & Gingrich, J. A. (2004). Early-life blockade of the 5-HT transporter alters emotional behavior in adult mice. *Science, 306*.

Bachatene, L., Bharmauria, V., Cattan, S., & Molotchnikoff, S. (2013). Fluoxetine and serotonin facilitate attractive-adaptation-induced orientation plasticity in adult cat visual cortex. *European Journal of Neuroscience, 38*(1), 2065-2077. doi:10.1111/ejn.12206

Baden, T., Berens, P., Franke, K., Rosón, M. R., Bethge, M., & Euler, T. (2016). The functional diversity of retinal ganglion cells in the mouse. *Nature, 529*(7586), 345-350.

Baker, M. (2013). Neuroscience: through the eyes of a mouse. *Nature News, 502*(7470), 156.

Bear, M. F., Huber, K. M., & Warren, S. T. (2004). The mGluR theory of fragile X mental retardation. *Trends Neurosci, 27*(7), 370-377. doi:10.1016/j.tins.2004.04.009

Bengel, D. (1998). Altered brain serotonin homeostasis and locomotor insensitivity to 3,4-methylenedioxymethamphetamine ("Ecstasy") in serotonin transporter-deficient mice. *Mol. Pharmacol., 53*.

Berry-Kravis, E., Des Portes, V., Hagerman, R., Jacquemont, S., Charles, P., Visootsak, J., . . . von Raison, F. (2016). Mavoglurant in fragile X syndrome: Results of two randomized, double-blind, placebo-controlled trials. *Sci Transl Med, 8*(321), 321ra325. doi:10.1126/scitranslmed.aab4109

Bockaert, J., Fozard, J. R., Dumuis, A., & Clarke, D. E. (1992). The 5-HT4 receptor: a place in the sun. *Trends in Pharmacological Sciences, 13*, 141-145. doi:http://dx.doi.org/10.1016/0165-6147(92)90051-7

Bortone, D. S., Olsen, S. R., & Scanziani, M. (2014). Translaminar inhibitory cells recruited by layer 6 corticothalamic neurons suppress visual cortex. *Neuron, 82*(2), 474-485. doi:10.1016/j.neuron.2014.02.021

Bradley, P. B., Engel, G., Feniuk, W., Fozard, J. R., Humphrey, P. P. A., Middlemiss, D. N., . . . Saxena, P. R. (1986). Proposals for the classification and nomenclature of functional receptors for 5-hydroxytryptamine. *Neuropharmacology, 25*(6), 563-576. doi:http://dx.doi.org/10.1016/0028-3908(86)90207-8

Brown, V., Jin, P., Ceman, S., Darnell, J. C., O'Donnell, W. T., Tenenbaum, S. A., . . . Warren, S. T. (2001). Microarray identification of FMRP-associated brain mRNAs and altered mRNA translational profiles in fragile X syndrome. *Cell, 107*(4), 477-487. doi:10.1016/s0092-8674(01)00568-2

Carroll, R. C., Lissin, D. V., von Zastrow, M., Nicoll, R. A., & Malenka, R. C. (1999). Rapid redistribution of glutamate receptors contributes to long-term depression in hippocampal cultures. *Nat Neurosci, 2*(5), 454-460. doi:10.1038/8123

Chen, I.-W., Helmchen, F., & Lütcke, H. (2015). Specific early and late oddball-evoked responses in excitatory and inhibitory neurons of mouse auditory cortex. *Journal of Neuroscience, 35*(36), 12560-12573.

Choi, S. Y., Chang, J., Jiang, B., Seol, G. H., Min, S. S., Han, J. S., . . . Kirkwood, A. (2005). Multiple receptors coupled to phospholipase C gate long-term depression in visual cortex. *The Journal of neuroscience : the official journal of the Society for Neuroscience, 25*(49), 11433-11443. doi:10.1523/jneurosci.4084-05.2005

Chubykin, A. A., Roach, E. B., Bear, M. F., & Shuler, M. G. (2013). A cholinergic mechanism for reward timing within primary visual cortex. *Neuron, 77*(4), 723-735. doi:10.1016/j.neuron.2012.12.039

Constantinople, C. M., & Bruno, R. M. (2013). Deep Cortical Layers Are Activated Directly by Thalamus. *Science, 340*(6140), 1591-1594. doi:10.1126/science.1236425

Contractor, A., Klyachko, V. A., & Portera-Cailliau, C. (2015). Altered Neuronal and Circuit Excitability in Fragile X Syndrome. *Neuron, 87*(4), 699-715. doi:10.1016/j.neuron.2015.06.017

Coogan, T., & Burkhalter, A. (1993). Hierarchical organization of areas in rat visual cortex. *The Journal of Neuroscience, 13*(9), 3749-3772. doi:10.1523/jneurosci.13-09-03749.1993

Cooke, S. F., & Bear, M. F. (2010). Visual Experience Induces Long-Term Potentiation in the Primary Visual Cortex. *The Journal of Neuroscience, 30*(48), 16304-16313. doi:10.1523/jneurosci.4333-10.2010

Cooke, S. F., Komorowski, R. W., Kaplan, E. S., Gavornik, J. P., & Bear, M. F. (2015). Visual recognition memory, manifested as long-term habituation, requires synaptic plasticity in V1. *Nat Neurosci, 18*(2), 262-271. doi:10.1038/nn.3920

Darnell, J. C. (2011). Defects in translational regulation contributing to human cognitive and behavioral disease. *Current opinion in genetics & development, 21*(4), 465-473. doi:10.1016/j.gde.2011.05.002

De Franceschi, G., Vivattanasarn, T., Saleem, A. B., & Solomon, S. G. (2016). Vision guides selection of freeze or flight defense strategies in mice. *Current biology, 26*(16), 2150-2154.

de Vries, S. E. J., Lecoq, J. A., Buice, M. A., Groblewski, P. A., Ocker, G. K., Oliver, M., . . . Koch, C. (2020). A large-scale standardized physiological survey reveals functional organization of the mouse visual cortex. *Nature Neuroscience, 23*(1), 138-151. doi:10.1038/s41593-019-0550-9

Dhande, O. S., Estevez, M. E., Quattrochi, L. E., El-Danaf, R. N., Nguyen, P. L., Berson, D. M., & Huberman, A. D. (2013). Genetic dissection of retinal inputs to brainstem nuclei controlling image stabilization. *Journal of Neuroscience, 33*(45), 17797-17813.

Dhande, O. S., & Huberman, A. D. (2014). Retinal ganglion cell maps in the brain: implications for visual processing. *Current opinion in neurobiology, 24*, 133-142.

Dölen, G., Osterweil, E., Rao, B. S. S., Smith, G. B., Auerbach, B. D., Chattarji, S., & Bear, M. F. (2007). Correction of Fragile X Syndrome in Mice. *Neuron, 56*(6), 955-962. doi:https://doi.org/10.1016/j.neuron.2007.12.001

Dong, H., Wang, Q., Valkova, K., Gonchar, Y., & Burkhalter, A. (2004). Experience-dependent development of feedforward and feedback circuits between lower and higher areas of mouse visual cortex. *Vision Research, 44*(28), 3389-3400. doi:https://doi.org/10.1016/j.visres.2004.09.007

Douglas, R. J., & Martin, K. A. (1991). A functional microcircuit for cat visual cortex. *The Journal of physiology, 440*, 735-769. doi:10.1113/jphysiol.1991.sp018733

Dräger, U. C. (1975). Receptive fields of single cells and topography in mouse visual cortex. *Journal of Comparative Neurology, 160*(3), 269-289.

Edagawa, Y., Saito, H., & Abe, K. (1998a). 5-HT1A receptor-mediated inhibition of long-term potentiation in rat visual cortex. *European Journal of Pharmacology, 349*(2–3), 221-224. doi:http://dx.doi.org/10.1016/S0014-2999(98)00286-6

Edagawa, Y., Saito, H., & Abe, K. (1998b). Serotonin inhibits the induction of long-term potentiation in rat primary visual cortex. *Progress in Neuro-Psychopharmacology and Biological Psychiatry, 22*(6), 983-997. doi:http://dx.doi.org/10.1016/S0278-5846(98)00055-4

Edagawa, Y., Saito, H., & Abe, K. (2000). The serotonin 5-HT2 receptor–phospholipase C system inhibits the induction of long-term potentiation in the rat visual cortex. *European Journal of Neuroscience, 12*(4), 1391-1396. doi:10.1046/j.1460-9568.2000.00007.x

Ellis, E. M., Gauvain, G., Sivyer, B., & Murphy, G. J. (2016). Shared and distinct retinal input to the mouse superior colliculus and dorsal lateral geniculate nucleus. *Journal of Neurophysiology, 116*(2), 602-610.

Fehérvári, T. D., & Yagi, T. (2016). Population Response Propagation to Extrastriate Areas Evoked by Intracortical Electrical Stimulation in V1. *Frontiers in Neural Circuits, 10*(6). doi:10.3389/fncir.2016.00006

Fiser, A., Mahringer, D., Oyibo, H. K., Petersen, A. V., Leinweber, M., & Keller, G. B. (2016). Experience-dependent spatial expectations in mouse visual cortex. *Nature Neuroscience, 19*(12), 1658-1664. doi:10.1038/nn.4385

Frenkel, M. Y., Sawtell, N. B., Diogo, A. C., Yoon, B., Neve, R. L., & Bear, M. F. (2006). Instructive effect of visual experience in mouse visual cortex. *Neuron, 51*(3), 339-349. doi:10.1016/j.neuron.2006.06.026

Garrett, M. E., Nauhaus, I., Marshel, J. H., & Callaway, E. M. (2014). Topography and Areal Organization of Mouse Visual Cortex. *The Journal of Neuroscience, 34*(37), 12587-12600. doi:10.1523/jneurosci.1124-14.2014

Gasanov, G. G., Mamedov, Z. G., & Samedova, N. F. (1989). Changes in reactivity of neurons of the visual cortex under influence of the posterolateral hypothalamus and the nuclei of the midbrain raphe. *Neuroscience and Behavioral Physiology, 19*(2), 169-175. doi:10.1007/bf01190464

Gavornik, J. P., & Bear, M. F. (2014). Learned spatiotemporal sequence recognition and prediction in primary visual cortex. *Nat Neurosci, 17*(5), 732-737. doi:10.1038/nn.3683

Glickfeld, L. L., & Olsen, S. R. (2017). Higher-Order Areas of the Mouse Visual Cortex. *Annual review of vision science, 3*(1), 251-273. doi:10.1146/annurev-vision-102016-061331

Gobbi, G., Murphy, D. L., Lesch, K. P., & Blier, P. (2001). Modifications of the serotoninergic system in mice lacking serotonin transporters. An in vivo electrophysiological study. *J. Pharmacol. Exp. Ther., 296*.

Gonchar, Y., Wang, Q., & Burkhalter, A. (2008). Multiple distinct subtypes of GABAergic neurons in mouse visual cortex identified by triple immunostaining. *Frontiers in Neuroanatomy, 2*(3). doi:10.3389/neuro.05.003.2007

Grosof, D. H., Shapley, R. M., & Hawken, M. J. (1993). Macaque VI neurons can signal 'illusory'contours. *Nature, 365*(6446), 550.

Gross, C., Berry-Kravis, E. M., & Bassell, G. J. (2012). Therapeutic strategies in fragile X syndrome: dysregulated mGluR signaling and beyond. *Neuropsychopharmacology, 37*(1), 178-195. doi:10.1038/npp.2011.137

Grossman, A. W., Elisseou, N. M., McKinney, B. C., & Greenough, W. T. (2006). Hippocampal pyramidal cells in adult Fmr1 knockout mice exhibit an immature-appearing profile of dendritic spines. *Brain Res, 1084*(1), 158-164. doi:10.1016/j.brainres.2006.02.044

Gu, Q. (2007). Serotonin Involvement in Plasticity of the Visual Cortex. In K.-Y. Tseng & M. Atzori (Eds.), *Monoaminergic Modulation of Cortical Excitability* (pp. 113-124). Boston, MA: Springer US.

Guet-McCreight, A., Skinner, F. K., & Topolnik, L. (2020). Common Principles in Functional Organization of VIP/Calretinin Cell-Driven Disinhibitory Circuits Across Cortical Areas. *Frontiers in Neural Circuits, 14*(32). doi:10.3389/fncir.2020.00032

Guirado, R., Perez-Rando, M., Sanchez-Matarredona, D., Castrén, E., & Nacher, J. (2014). Chronic fluoxetine treatment alters the structure, connectivity and plasticity of cortical interneurons. *International Journal of Neuropsychopharmacology, 17*(10), 1635-1646. doi:10.1017/S1461145714000406

Haberl, M. G., Zerbi, V., Veltien, A., Ginger, M., Heerschap, A., & Frick, A. (2015). Structural-functional connectivity deficits of neocortical circuits in the Fmr1 (-/y) mouse model of autism. *Science advances, 1*(10), e1500775-e1500775. doi:10.1126/sciadv.1500775

Hamm, J. P., & Yuste, R. (2016). Somatostatin interneurons control a key component of mismatch negativity in mouse visual cortex. *Cell reports, 16*(3), 597-604.

Hammer, S., Monavarfeshani, A., Lemon, T., Su, J., & Fox, M. A. (2015). Multiple retinal axons converge onto relay cells in the adult mouse thalamus. *Cell reports, 12*(10), 1575-1583.

Hattar, S., Lucas, R. J., Mrosovsky, N., Thompson, S., Douglas, R., Hankins, M. W., . . . Foster, R. G. (2003). Melanopsin and rod–cone photoreceptive systems account for all major accessory visual functions in mice. *Nature, 424*(6944), 75-81.

He, K., Huertas, M., Hong, Su Z., Tie, X., Hell, Johannes W., Shouval, H., & Kirkwood, A. (2015). Distinct Eligibility Traces for LTP and LTD in Cortical Synapses. *Neuron, 88*(3), 528-538. doi:10.1016/j.neuron.2015.09.037

Heesy, C. P. (2004). On the relationship between orbit orientation and binocular visual field overlap in mammals. *The Anatomical Record Part A: Discoveries in Molecular, Cellular, and Evolutionary Biology, 281A*(1), 1104-1110. doi:10.1002/ar.a.20116

Hinton, V. J., Brown, W. T., Wisniewski, K., & Rudelli, R. D. (1991). Analysis of neocortex in three males with the fragile X syndrome. *Am J Med Genet, 41*(3), 289-294. doi:10.1002/ajmg.1320410306

Hofer, S. B., Ko, H., Pichler, B., Vogelstein, J., Ros, H., Zeng, H., . . . Mrsic-Flogel, T. D. (2011). Differential connectivity and response dynamics of excitatory and inhibitory neurons in visual cortex. *Nature Neuroscience, 14*(8), 1045-1052. doi:10.1038/nn.2876

Hoffman, G. E., Le, W. W., Entezam, A., Otsuka, N., Tong, Z. B., Nelson, L., . . . Usdin, K. (2012). Ovarian abnormalities in a mouse model of fragile X primary ovarian insufficiency. *J Histochem Cytochem, 60*(6), 439-456. doi:10.1369/0022155412441002

Hubel, D. H., & Wiesel, T. N. (1959). Receptive fields of single neurones in the cat's striate cortex. *The Journal of physiology, 148*(3), 574.

Hubel, D. H., & Wiesel, T. N. (1962). Receptive fields, binocular interaction and functional architecture in the cat's visual cortex. *The Journal of physiology, 160*(1), 106.

Hubel, D. H., & Wiesel, T. N. (1965). Receptive fields and functional architecture in two nonstriate visual areas (18 and 19) of the cat. *Journal of Neurophysiology, 28*(2), 229-289.

Hubel, D. H., & Wiesel, T. N. (1968). Receptive fields and functional architecture of monkey striate cortex. *The Journal of physiology, 195*(1), 215-243.

Huber, K. M., Gallagher, S. M., Warren, S. T., & Bear, M. F. (2002). Altered synaptic plasticity in a mouse model of fragile X mental retardation. *Proceedings of the National Academy of Sciences, 99*(11), 7746-7750. doi:10.1073/pnas.122205699

Huberman, A. D., Wei, W., Elstrott, J., Stafford, B. K., Feller, M. B., & Barres, B. A. (2009). Genetic identification of an On-Off direction-selective retinal ganglion cell subtype reveals a layer-specific subcortical map of posterior motion. *Neuron, 62*(3), 327-334.

Isaacson, J. S., & Scanziani, M. (2011). How inhibition shapes cortical activity. *Neuron, 72*(2), 231-243. doi:10.1016/j.neuron.2011.09.027

Kanizsa, G. (1955). Margini quasi-percettivi in campi con stimolazione omogenea. *Rivista di Psicologia, 49*(1), 7-30.

Kato, H. K., Gillet, S. N., & Isaacson, J. S. (2015). Flexible Sensory Representations in Auditory Cortex Driven by Behavioral Relevance. *Neuron, 88*(5), 1027-1039. doi:10.1016/j.neuron.2015.10.024

Kerschensteiner, D., & Guido, W. (2017). Organization of the dorsal lateral geniculate nucleus in the mouse. *Visual neuroscience, 34*, E008-E008. doi:10.1017/S0952523817000062

Kim, H.-S., Jang, H.-J., Cho, K.-H., June Hahn, S., Kim, M.-J., Hee Yoon, S., . . . Rhie, D.-J. (2006). Serotonin inhibits the induction of NMDA receptor-dependent long-term potentiation in the rat primary visual cortex. *Brain Research, 1103*(1), 49-55. doi:http://dx.doi.org/10.1016/j.brainres.2006.05.046

Kirchberger, L., Mukherjee, S., Schnabel, U. H., van Beest, E. H., Barsegyan, A., Levelt, C. N., . . . Roelfsema, P. R. (2020). The essential role of feedback processing for figure-ground perception in mice. *bioRxiv*, 456459. doi:10.1101/456459

Kojic, L., Dyck, R. H., Gu, Q., Douglas, R. M., Matsubara, J., & Cynader, M. S. (2000). Columnar distribution of serotonin-dependent plasticity within kitten striate cortex. *Proceedings of the National Academy of Sciences, 97*(4), 1841-1844. doi:10.1073/pnas.97.4.1841

Kojic, L., Gu, Q., Douglas, R. M., & Cynader, M. S. (1997). Serotonin facilitates synaptic plasticity in kitten visual cortex: an in vitro study. *Developmental Brain Research, 101*(1–2), 299-304. doi:http://dx.doi.org/10.1016/S0165-3806(97)00083-7

Krnjević, K., & Phillis, J. W. (1963). Iontophoretic studies of neurones in the mammalian cerebral cortex. *The Journal of physiology, 165*(2), 274-304.

Kuffler, S. W. (1953). DISCHARGE PATTERNS AND FUNCTIONAL ORGANIZATION OF MAMMALIAN RETINA. *Journal of Neurophysiology, 16*(1), 37-68. doi:10.1152/jn.1953.16.1.37

Lavoie, S., Polari, A. R., Goldstone, S., Nelson, B., & McGorry, P. D. (2019). Staging model in psychiatry: Review of the evolution of electroencephalography abnormalities in major psychiatric disorders. *Early Intervention in Psychiatry, 13*(6), 1319-1328. doi:10.1111/eip.12792

Lee, T. S., & Nguyen, M. (2001). Dynamics of subjective contour formation in the early visual cortex. *Proceedings of the National Academy of Sciences, 98*(4), 1907-1911. doi:10.1073/pnas.98.4.1907

Lesch, K. P. (1996). Association of anxiety-related traits with a polymorphism in the serotonin transporter gene regulatory region. *Science, 274*.

Li, Q. (1999). Reduction of 5-hydroxytryptamine (5-HT)1A-mediated temperature and neuroendocrine responses and 5-HT1A binding sites in 5-HT transporter knockout mice. *J. Pharmacol. Exp. Ther., 291*.

Li, Q. (2004). Medial hypothalamic 5-hydroxytryptamine (5-HT)1A receptors regulate neuroendocrine responses to stress and exploratory locomotor activity: application of recombinant adenovirus containing 5-HT1A sequences. *J. Neurosci., 24*.

Lidov, H. G. W., Grzanna, R., & Molliver, M. E. (1980). The serotonin innervation of the cerebral cortex in the rat—an immunohistochemical analysis. *Neuroscience, 5*(2), 207-227. doi:http://dx.doi.org/10.1016/0306-4522(80)90099-8

Liu, B.-H., Huberman, A. D., & Scanziani, M. (2016). Cortico-fugal output from visual cortex promotes plasticity of innate motor behaviour. *Nature, 538*(7625), 383-387. doi:10.1038/nature19818

Liu, C. H., Coleman, J. E., Davoudi, H., Zhang, K., & Hussain Shuler, M. G. (2015). Selective activation of a putative reinforcement signal conditions cued interval timing in primary visual cortex. *Curr Biol, 25*(12), 1551-1561. doi:10.1016/j.cub.2015.04.028

Makino, H., & Komiyama, T. (2015). Learning enhances the relative impact of top-down processing in the visual cortex. *Nature Neuroscience, 18*(8), 1116-1122. doi:10.1038/nn.4061

Marshel, J. H., Kaye, A. P., Nauhaus, I., & Callaway, E. M. (2012). Anterior-posterior direction opponency in the superficial mouse lateral geniculate nucleus. *Neuron, 76*(4), 713-720.

Mauss, A. S., Vlasits, A., Borst, A., & Feller, M. (2017). Visual Circuits for Direction Selectivity. *Annual Review of Neuroscience, 40*(1), 211-230. doi:10.1146/annurev-neuro-072116-031335

McCormick, D. A., Wang, Z., & Huguenard, J. (1993). Neurotransmitter Control of Neocortical Neuronal Activity and Excitability. *Cerebral Cortex, 3*(5), 387-398. doi:10.1093/cercor/3.5.387

Montanez, S., Owens, W. A., Gould, G. G., Murphy, D. L., & Daws, L. C. (2003). Exaggerated effect of fluvoxamine in heterozygote serotonin transporter knockout mice. *J. Neurochem., 86*.

Murphy, D. L., & Lesch, K.-P. (2008). Targeting the murine serotonin transporter: insights into human neurobiology. *Nature reviews. Neuroscience, 9*(2), 85-96. doi:10.1038/nrn2284

Musall, S., Haiss, F., Weber, B., & von der Behrens, W. (2015). Deviant processing in the primary somatosensory cortex. *Cerebral Cortex, 27*(1), 863-876.

Näätänen, R. (1995). The mismatch negativity: a powerful tool for cognitive neuroscience. *Ear Hear, 16*(1), 6-18.

Näätänen, R., Kujala, T., Kreegipuu, K., Carlson, S., Escera, C., Baldeweg, T., & Ponton, C. (2011). The mismatch negativity: an index of cognitive decline in neuropsychiatric and neurological diseases and in ageing. *Brain, 134*(12), 3435-3453. doi:10.1093/brain/awr064

Nakamoto, M., Nalavadi, V., Epstein, M. P., Narayanan, U., Bassell, G. J., & Warren, S. T. (2007). Fragile X mental retardation protein deficiency leads to excessive mGluR5-dependent internalization of AMPA receptors. *Proc Natl Acad Sci U S A, 104*(39), 15537-15542. doi:10.1073/pnas.0707484104

Natan, R. G., Briguglio, J. J., Mwilambwe-Tshilobo, L., Jones, S. I., Aizenberg, M., Goldberg, E. M., & Geffen, M. N. (2015). Complementary control of sensory adaptation by two types of cortical interneurons. *eLife, 4*, e09868.

Nieder, A. (2002). Seeing more than meets the eye: processing of illusory contours in animals. *Journal of Comparative Physiology A, 188*(4), 249-260. doi:10.1007/s00359-002-0306-x

Niell, C. M., & Stryker, M. P. (2008). Highly Selective Receptive Fields in Mouse Visual Cortex. *The Journal of Neuroscience, 28*(30), 7520-7536. doi:10.1523/jneurosci.0623-08.2008

Ohki, K., Chung, S., Ch'ng, Y. H., Kara, P., & Reid, R. C. (2005). Functional imaging with cellular resolution reveals precise micro-architecture in visual cortex. *Nature, 433*(7026), 597-603. doi:10.1038/nature03274

Olsen, S. R., Bortone, D. S., Adesnik, H., & Scanziani, M. (2012). Gain control by layer six in cortical circuits of vision. *Nature, 483*(7387), 47-52. doi:10.1038/nature10835

Pak, A., Ryu, E., Li, C., & Chubykin, A. A. (2020). Top-Down Feedback Controls the Cortical Representation of Illusory Contours in Mouse Primary Visual Cortex. *The Journal of Neuroscience, 40*(3), 648-660. doi:10.1523/jneurosci.1998-19.2019

Parras, G. G., Nieto-Diego, J., Carbajal, G. V., Valdés-Baizabal, C., Escera, C., & Malmierca, M. S. (2017). Neurons along the auditory pathway exhibit a hierarchical organization of prediction error. *Nature Communications, 8*(1), 2148.

Pazo-Alvarez, P., Cadaveira, F., & Amenedo, E. (2003). MMN in the visual modality: a review. *Biol Psychol, 63*(3), 199-236.

Peirson, S. N., Brown, L. A., Pothecary, C. A., Benson, L. A., & Fisk, A. S. (2018). Light and the laboratory mouse. *Journal of neuroscience methods, 300*, 26-36. doi:10.1016/j.jneumeth.2017.04.007

Persico, A. M. (2001). Barrel pattern formation requires serotonin uptake by thalamocortical afferents, and not vesicular monoamine release. *J. Neurosci., 21*.

Peterhans, E., & von der Heydt, R. (1989). Mechanisms of contour perception in monkey visual cortex. II. Contours bridging gaps. *Journal of Neuroscience, 9*(5), 1749-1763.

Piscopo, D. M., El-Danaf, R. N., Huberman, A. D., & Niell, C. M. (2013). Diverse visual features encoded in mouse lateral geniculate nucleus. *Journal of Neuroscience, 33*(11), 4642-4656.

Pluta, S., Naka, A., Veit, J., Telian, G., Yao, L., Hakim, R., . . . Adesnik, H. (2015). A direct translaminar inhibitory circuit tunes cortical output. *Nature Neuroscience, 18*(11), 1631-1640. doi:10.1038/nn.4123

Polack, P.-O., & Contreras, D. (2012). Long-Range Parallel Processing and Local Recurrent Activity in the Visual Cortex of the Mouse. *The Journal of Neuroscience, 32*(32), 11120-11131. doi:10.1523/jneurosci.6304-11.2012

Qiu, F. T., & von der Heydt, R. (2005). Figure and ground in the visual cortex: v2 combines stereoscopic cues with gestalt rules. *Neuron, 47*(1), 155-166. doi:10.1016/j.neuron.2005.05.028

Quinlan, E. M. (2008). Is the selective serotonin reuptake inhibitor fluoxetine a fountain of youth? *Future Neurology, 3*(4), 385-389. doi:10.2217/14796708.3.4.385

Riesenhuber, M., & Poggio, T. (1999). Hierarchical models of object recognition in cortex. *Nature Neuroscience, 2*(11), 1019-1025. doi:10.1038/14819

Ringach, D. L., Mineault, P. J., Tring, E., Olivas, N. D., Garcia-Junco-Clemente, P., & Trachtenberg, J. T. (2016). Spatial clustering of tuning in mouse primary visual cortex. *Nature Communications, 7*(1), 12270. doi:10.1038/ncomms12270

Roerig, B., & Katz, L. C. (1997). Modulation of Intrinsic Circuits by Serotonin 5-HT₃Receptors in Developing Ferret Visual Cortex. *The Journal of Neuroscience, 17*(21), 8324-8338.

Rompani, S. B., Muellner, F. E., Wanner, A., Zhang, C., Roth, C. N., Yonehara, K., & Roska, B. (2017). Different modes of visual integration in the lateral geniculate nucleus revealed by single-cell-initiated transsynaptic tracing. *Neuron, 93*(4), 767-776. e766.

Ross, J. M., & Hamm, J. P. (2020). Cortical Microcircuit Mechanisms of Mismatch Negativity and Its Underlying Subcomponents. *Frontiers in Neural Circuits, 14*(13). doi:10.3389/fncir.2020.00013

Rudy, B., Fishell, G., Lee, S., & Hjerling-Leffler, J. (2011). Three groups of interneurons account for nearly 100% of neocortical GABAergic neurons. *Dev Neurobiol, 71*(1), 45-61. doi:10.1002/dneu.20853

Salichon, N. (2001). Excessive activation of serotonin (5-HT) 1B receptors disrupts the formation of sensory maps in monoamine oxidase A and 5-HT transporter knock-out mice. *J. Neurosci., 21*.

Schnabel, U. H., Bossens, C., Lorteije, J. A. M., Self, M. W., Op de Beeck, H., & Roelfsema, P. R. (2018). Figure-ground perception in the awake mouse and neuronal activity elicited by figure-ground stimuli in primary visual cortex. *Scientific Reports, 8*(1), 17800. doi:10.1038/s41598-018-36087-8

Scholl, B., Burge, J., & Priebe, N. J. (2013). Binocular integration and disparity selectivity in mouse primary visual cortex. *J Neurophysiol, 109*(12), 3013-3024. doi:10.1152/jn.01021.2012

Seabrook, T. A., Burbridge, T. J., Crair, M. C., & Huberman, A. D. (2017). Architecture, Function, and Assembly of the Mouse Visual System. *Annual Review of Neuroscience, 40*(1), 499-538. doi:10.1146/annurev-neuro-071714-033842

Selten, M., van Bokhoven, H., & Nadif Kasri, N. (2018). Inhibitory control of the excitatory/inhibitory balance in psychiatric disorders. *F1000Research, 7*, 23-23. doi:10.12688/f1000research.12155.1

Serrano, P., Yao, Y., & Sacktor, T. C. (2005). Persistent Phosphorylation by Protein Kinase Mζ Maintains Late-Phase Long-Term Potentiation. *The Journal of Neuroscience, 25*(8), 1979-1984. doi:10.1523/jneurosci.5132-04.2005

Shuler, M. G., & Bear, M. F. (2006). Reward timing in the primary visual cortex. *Science, 311*(5767), 1606-1609. doi:10.1126/science.1123513

Snyder, E. M., Philpot, B. D., Huber, K. M., Dong, X., Fallon, J. R., & Bear, M. F. (2001). Internalization of ionotropic glutamate receptors in response to mGluR activation. *Nature Neuroscience, 4*(11), 1079-1085. doi:10.1038/nn746

Tada, M., Kirihara, K., Mizutani, S., Uka, T., Kunii, N., Koshiyama, D., . . . Kasai, K. (2019). Mismatch negativity (MMN) as a tool for translational investigations into early psychosis: A review. *International Journal of Psychophysiology, 145*, 5-14. doi:https://doi.org/10.1016/j.ijpsycho.2019.02.009

Tassone, A., Madeo, G., Sciamanna, G., Pisani, A., & Bonsi, P. (2010) Electrophysiology of 5-HT6 Receptors. *Vol. 94. International Review of Neurobiology* (pp. 111-128).

Tecott, L. H., Maricq, A. V., & Julius, D. (1993). Nervous system distribution of the serotonin 5-HT3 receptor mRNA. *Proc Natl Acad Sci U S A, 90*(4), 1430-1434.

Tiitinen, H., May, P., & Näätänen, R. (1997). The transient 40-Hz response, mismatch negativity, and attentional processes in humans. *Prog Neuropsychopharmacol Biol Psychiatry, 21*(5), 751-771. doi:10.1016/s0278-5846(97)00077-8

Tohmi, M., Meguro, R., Tsukano, H., Hishida, R., & Shibuki, K. (2014). The Extrageniculate Visual Pathway Generates Distinct Response Properties in the Higher Visual Areas of Mice. *Current biology, 24*(6), 587-597. doi:https://doi.org/10.1016/j.cub.2014.01.061

Ulanovsky, N., Las, L., & Nelken, I. (2003). Processing of low-probability sounds by cortical neurons. *Nature Neuroscience, 6*(4), 391-398. doi:10.1038/nn1032

Urban-Ciecko, J., & Barth, A. L. (2016). Somatostatin-expressing neurons in cortical networks. *Nature reviews. Neuroscience, 17*(7), 401-409. doi:10.1038/nrn.2016.53

Usrey, W. M., & Alitto, H. J. (2015). Visual functions of the thalamus. *Annual review of vision science, 1*, 351-371.

Van Hooser, S. D., Heimel, J. A. F., Chung, S., Nelson, S. B., & Toth, L. J. (2005). Orientation Selectivity without Orientation Maps in Visual Cortex of a Highly Visual Mammal. *The Journal of Neuroscience, 25*(1), 19-28. doi:10.1523/jneurosci.4042-04.2005

Vetencourt, J. F. M., Sale, A., Viegi, A., Baroncelli, L., De Pasquale, R., F. O'Leary, O., . . . Maffei, L. (2008). The Antidepressant Fluoxetine Restores Plasticity in the Adult Visual Cortex. *Science, 320*(5874), 385-388. doi:10.1126/science.1150516

von der Heydt, R., & Peterhans, E. (1989). Mechanisms of contour perception in monkey visual cortex. I. Lines of pattern discontinuity. *Journal of Neuroscience, 9*(5), 1731-1748.

Wallace, D. J., Greenberg, D. S., Sawinski, J., Rulla, S., Notaro, G., & Kerr, J. N. (2013). Rats maintain an overhead binocular field at the expense of constant fusion. *Nature, 498*(7452), 65-69.

Wang, Q., & Burkhalter, A. (2007). Area map of mouse visual cortex. *Journal of Comparative Neurology, 502*(3), 339-357. doi:10.1002/cne.21286

Wang, Q., Sporns, O., & Burkhalter, A. (2012). Network Analysis of Corticocortical Connections Reveals Ventral and Dorsal Processing Streams in Mouse Visual Cortex. *The Journal of Neuroscience, 32*(13), 4386-4399. doi:10.1523/jneurosci.6063-11.2012

Waterhouse, B. D., Ausim Azizi, S., Burne, R. A., & Woodward, D. J. (1990). Modulation of rat cortical area 17 neuronal responses to moving visual stimuli during norepinephrine and serotonin microiontophoresis. *Brain Research, 514*(2), 276-292. doi:http://dx.doi.org/10.1016/0006-8993(90)91422-D

West, P. J., Marcy, V. R., Marino, M. J., & Schaffhauser, H. (2009). Activation of the 5-HT6 receptor attenuates long-term potentiation and facilitates GABAergic neurotransmission in rat hippocampus. *Neuroscience, 164*(2), 692-701. doi:10.1016/j.neuroscience.2009.07.061

Wood, K. C., Blackwell, J. M., & Geffen, M. N. (2017). Cortical inhibitory interneurons control sensory processing. *Current opinion in neurobiology, 46*, 200-207. doi:10.1016/j.conb.2017.08.018

Xiang, K., Zhao, X., Li, Y., Zheng, L., Wang, J., & Li, Y. H. (2016). Selective 5-HT7 receptor activation may enhance synaptic plasticity through N-methyl-D-aspartate (NMDA) receptor activity in the visual cortex. *Current Neurovascular Research, 13*(4), 321-328. doi:10.2174/1567202613666160823164136

Yamashita, A., Valkova, K., Gonchar, Y., & Burkhalter, A. (2003). Rearrangement of synaptic connections with inhibitory neurons in developing mouse visual cortex. *Journal of Comparative Neurology, 464*(4), 426-437. doi:10.1002/cne.10810

Yang, W., Carrasquillo, Y., Hooks, B. M., Nerbonne, J. M., & Burkhalter, A. (2013). Distinct Balance of Excitation and Inhibition in an Interareal Feedforward and Feedback Circuit of Mouse Visual Cortex. *The Journal of Neuroscience, 33*(44), 17373-17384. doi:10.1523/jneurosci.2515-13.2013

Yilmaz, M., & Meister, M. (2013). Rapid innate defensive responses of mice to looming visual stimuli. *Current biology, 23*(20), 2011-2015.

Zhuang, J., Ng, L., Williams, D., Valley, M., Li, Y., Garrett, M., & Waters, J. (2017). An extended retinotopic map of mouse cortex. *eLife, 6*, e18372. doi:10.7554/eLife.18372

Zipser, K., Lamme, V. A., & Schiller, P. H. (1996). Contextual modulation in primary visual cortex. *The Journal of neuroscience : the official journal of the Society for Neuroscience, 16*(22), 7376-7389. doi:10.1523/JNEUROSCI.16-22-07376.1996

CHAPTER 2. CORTICAL TUNING IS IMPAIRED AFTER PERCEPTUAL EXPERIENCE IN V1 OF SEROTONIN TRANSPORTER DEFICIENT MICE

Adopted from: Pak, A., & Chubykin, A. A. (2020). Cortical Tuning is Impaired After Perceptual Experience in Primary Visual Cortex of Serotonin Transporter-Deficient Mice. Cerebral cortex communications, 1(1), tgaa066. https://doi.org/10.1093/texcom/tgaa066

2.1 Abstract

Serotonin (5-hydroxytryptamine, 5-HT) is crucial for the proper development of neuronal circuits early in life and their refinement throughout adulthood. Its signaling is tightly regulated by the serotonin transporter (SERT), alterations of which were implicated in various neurological and psychiatric disorders. Animal models lacking a functional SERT variant display diverse phenotypes, including increased anxiety, social communication deficits, and altered cortical development. However, it remains unclear how SERT disruption affects sensory processing and experience-dependent learning in adulthood. It has been previously shown that perceptual experience leads to the development of visual familiarity evoked theta oscillations in mouse V1. Here, we discovered that familiarity evoked theta oscillations were longer and less stimulus-specific in SERT knockout (KO) compared to wild-type (WT) mice. Interestingly, while the overall visual response properties were similar in naive mice, orientation and spatial frequency processing were significantly impaired in SERT KO compared to WT or SERT heterozygous mice following perceptual experience. Our findings shed more light on the mechanism of familiarity evoked oscillations and highlight the importance of serotonin signaling in perceptual learning.

2.2 Introduction

The serotonergic system is involved in reward/punishment processing, behavioral inhibition, mood, depression, cognitive flexibility, learning, and memory (Ansorge, Zhou, Lira, Hen, & Gingrich, 2004; J. Y. Cohen, Amoroso, & Uchida, 2015; Lanfumey, La Cour, Froger, & Hamon, 2000; Lottem et al., 2018; Matias, Lottem, Dugué, & Mainen, 2017; Sora et al., 1998). Mutations in serotonin transporter (SERT) are implicated in various neurological and neuropsychiatric disorders. Mouse models with partial or full loss of SERT functionality displayed a plethora of

phenotypes ranging from anxiety to altered cortical development (Bengel et al., 1998; Lira et al., 2003; Murphy & Lesch, 2008).

Previous research suggests that 5-HT plays a vital role in the sensory cortex. 5-HT is important for the remodeling of cortical circuits during development and adulthood. Visual cortex requires both sensory and neuromodulatory inputs, especially during early life, for proper development (Gu, 2002; Kojic et al., 2000). Neuromodulators have been shown to regulate cortical plasticity and sensory processing during the critical period of development and adulthood (Wang, Gu, & Cynader, 1997). Consistent with these observations, a SERT inhibitor, fluoxetine, can reopen the critical period in the adult visual cortex allowing for plasticity to reoccur. This effect was mediated through reduced intercortical inhibition and increased brain-derived neurotrophic factor levels (Maya Vetencourt et al., 2008).

5-HT can also directly modulate cortical circuits during adulthood (Celada, Puig, & Artigas, 2013; Puig, Artigas, & Celada, 2004). Recent evidence suggests that activation of dorsal raphe serotonergic neurons inhibits baseline activity but not odor-evoked responses in the olfactory cortex (Lottem, Lörincz, & Mainen, 2016). Furthermore, another study in SERT-deficient rats described altered sensory processing in the somatosensory cortex mediated by the reduced feed-forward inhibition in layer IV of the barrel cortex, which subsequently altered sensory integration (Miceli et al., 2017). These findings suggest that 5-HT alterations might lead to altered sensory processing. Previous studies demonstrated the direct effects of 5-HT receptor agonists in rodent visual cortex. Fast spiking and low threshold interneurons were shown to be modulated by $5HT_3$ and $5HT_{1A}$ receptor agonists in rat visual cortex slices (Xiang & Prince, 2003). Another recent study showed that $5\text{-}HT_{2A}$ receptor agonist decreased visual processing and altered surround suppression in mouse V1 (Michaiel, Parker, & Niell, 2019).

Previous experience has also been shown to alter the information processing in the primary visual cortex (V1). Presentations of phase reversing gratings over several days lead to the increase in the amplitude of visually evoked potentials (VEPs), the phenomenon known as stimulus response potentiation (SRP) (S. F. Cooke, Komorowski, Kaplan, Gavornik, & Bear, 2015; Frenkel et al., 2006). Similarly, presentations of a sequence of sinusoidal gratings also lead to the potentiation of VEPs specific for the familiar sequence (Gavornik & Bear, 2014). Repetitive pairings of a visual stimulus to a water reward delivered at a temporal delay lead to the development of a persistent neuronal activity, which can encode the time of the reward (Shuler &

Bear, 2006). This reward timing was dependent on the cholinergic muscarinic receptors (Chubykin, Roach, Bear, & Shuler, 2013). Interestingly, the persistent activity encoding reward timing has been shown to be in the form of persistent theta oscillation lasting to the time of reward (Zold & Hussain Shuler, 2015). We have recently demonstrated that persistent theta oscillations could encode general visual stimulus familiarity without any reward presentation (Kissinger, Pak, Tang, Masmanidis, & Chubykin, 2018). These familiarity-evoked theta oscillations were also dependent on the muscarinic receptors. They were also impaired in Fmr1 KO mice, a model of Fragile X syndrome, the most common inherited form of intellectual disability and autism (Kissinger et al., 2020). In addition to induction of the persistent activity, perceptual learning has been demonstrated to improve stimulus selectivity in the adult visual cortex (Sam F. Cooke & Bear, 2010; Gilbert & Li, 2012; Hua et al., 2010; Makino & Komiyama, 2015; Poort et al., 2015). Such improvements are mediated through increased selectivity and sharper tuning to a trained stimulus, but not at the expense of overall cortical tuning (Jurjut, Georgieva, Busse, & Katzner, 2017). However, it remains unclear how perceptual learning can modify cortical tuning in the case of altered 5-HT signaling.

Using silicon probe recordings, we investigated the role of the serotonergic neuromodulation in the familiarity-evoked theta oscillations and in the experience-dependent changes in cortical tuning using serotonin transporter (SERT) heterozygotes (HET) and knockout (KO) mice (Bengel et al., 1998). We found that orientation, spatial frequency tuning, and contrast sensitivity are not altered in naive mutant mice. The perceptual experience did, however, impair cortical tuning in SERT-deficient mice, especially in KO mice, in a multitude of ways. First, familiarity evoked theta oscillations were longer and less specific in SERT KO mice. Second, we observed decreased orientation selectivity and broadened tuning width in SERT KO after the perceptual experience. Third, low spatial frequency (SF) responses were increased in SERT KO. Fourth, both SERT KO and HET showed altered contrast sensitivity after perceptual learning. Overall, we found intact visual processing in naive mice but impaired cortical tuning after perceptual experience in SERT-deficient mice.

2.3 Materials and Methods

2.3.1 Mice

All procedures involving animal use were approved by the Purdue University Animal Care and Use Committee. Serotonin transporter knockout mice, B6.129(Cg)-Slc6a4^{tm1Kpl}/J, were acquired from the Jackson Laboratory (stock # 008355). We bred SERT HET and HET mice to generate SERT KO, HET, and WT littermate controls. In total, 26 mice were used: 4 SERT littermate control WT (2M and 2F), 8 HET (4M and 4F), 10 KO (5M and 5F), and four male age-matched control WT C57BL/6 mice. Mice were group-housed on a 12 hr light/dark cycle with ad libitum water and food access.

2.3.2 Surgical protocol

Animal surgical procedures were performed as previously described (Kissinger et al., 2018). Briefly, about 2-month-old mice were induced with 5% isoflurane and head-fixed to a motorized stereotaxic apparatus (Neurostar). Their body temperature was maintained using a heating pad, and they were kept at 1.5-2% isoflurane anesthesia. The ophthalmic ointment was applied to prevent eye drying. Next, we shaved and sterilized the skin above the skull. The skull was exposed to install a small head post and a reference pin. Neurostar software with an integrated mouse brain atlas was used to label V1 coordinates (from lambda AP 0.8 mm, LM: ±3.2 mm) with a black marker. To fix the head post and seal all exposed areas, we used Medical grade Metabond™. After surgery, mice were monitored for at least three days for any signs of distress or infection. Animals were then habituated to a head-fixation apparatus for at least four days and a minimum of 90 min per day, while sitting in front of the computer monitor and viewing gray screen. On the recording day, a small craniotomy was made above V1 in one of the hemispheres under 1.5% isoflurane anesthesia. Mice were then transferred to the recording room and head-fixed to the apparatus for electrophysiological recordings.

2.3.3 *In vivo* electrophysiology

All experiments were performed in awake head-fixed mice. After animals were moved to the recording room, 30 min was allowed for them to recover from anesthesia. A 64-channel silicon probe (Shobe, Claar, Parhami, Bakhurin, & Masmanidis, 2015) (channel separation: vertical 25

µm, horizontal 20 µm, 3 columns, 1.05 mm in length) was inserted to perform acute extracellular electrophysiology. Each animal underwent a maximum of two recording sessions (one per hemisphere). Data were acquired at 30 kHz using OpenEphys hardware and software. An Arduino board was used to synchronize data acquisition and visual stimulus presentations using TTL communication. We used custom-written Python scripts in PsychoPy (Peirce, 2009) to present visual stimuli and send the TTL signals. After each recording session, silicon probes were cleaned in trypsin (2.5%) solution.

2.3.4 Histology

After electrophysiological recordings, 100 mg/kg ketamine and 16 mg/kg xylazine solution was used to anesthetize animals. Mice were then perfused transcardially with 1x PBS solution followed by 4% paraformaldehyde (PFA). After decapitation, the brain was extracted and stored in PFA in a refrigerator. The brain was sliced the following day in 0.1 mm sections in PBS using a vibratome. Coronal slices were mounted on slides using n-propyl-gallate media and sealed with transparent nail polish. A light microscope (VWR) was used to image slices for the electrode track verification in V1.

2.3.5 Visual stimulation

All visual stimulations were designed and presented using an open-source Python software, PsychoPy (Peirce, 2009). Visual stimuli were binocularly presented on a gamma calibrated LCD monitor (22' ViewSonic VX2252, 60 Hz), which was placed 17 cm in front of the mouse. The mean luminance of the monitor was 30 cd/m^2. For perceptual experience, mice were presented with the same visual stimulus (30º drifting grating, contrast = 100%, temporal frequency = 2 Hz, spatial frequency = 0.04 cpd, duration = 0.4s) for four days, 200 presentations a day with an Inter-stimulus-interval of 3-5s. For orientation tuning experiments, we presented sinusoidal drifting gratings of 12 different directions. Stimuli were created with the following parameters; contrast = 100%, spatial frequency = 0.04 cpd, temporal frequency = 2 Hz, and duration = 0.5s. There was a 3-5s inter-trial-interval. To generate visual stimulations for a spatial frequency tuning, we performed spatial filtering of white noise (Kissinger et al., 2018). Specifically, we band-pass filtered white noise in different non-overlapping SF bands. The procedure, and a Python code for

spatial frequency filtering, were adapted from http://www.djmannion.net/psych_programming/vision/sf_filt/sf_filt.html. Overall, six different spatial frequencies were generated for SF tuning: 7.5E-3, 0.015, 0.03, 0.06, 0.12, and 0.24 cycles/degrees. We chose these frequencies based on previous studies and known spatial frequency tuning of mouse V1 neurons (Niell & Stryker, 2008). The use of these stimuli for SF tuning has been verified in our previous study (Kissinger et al., 2018). The SF tuning sequence contained 6 different SF stimuli presented in a pseudorandom order, each with an equal probability of being presented. We used an inter-trial interval of at least 4s to prevent any adaptation. Furthermore, SF filtered stimuli were randomly generated on each trial to sample different receptive fields uniformly. This was mainly important for lower spatial frequencies. For contrast sensitivity experiments, we presented a 0º oriented (vertical) static grating at five different contrast levels: 6.25, 12.5, 25, 50, and 100%.

2.3.6 LFP analysis

Broadband electrophysiology traces were first downsampled to 1 kHz. Symmetric linear-phase FIR filter (default parameters) was then used to remove 60 Hz cable noise (mne Python library). Next, we identified layer 4 responses by finding a channel with the strongest negative deflection in the first 100 ms after stimulus onset. Complex wavelet convolution was used to perform time-frequency decomposition. We designed 40 different wavelets across a logarithmic range of 2-80 Hz, with cycles ranging from 3 to 10. This gave us an optimal time-frequency precision tradeoff. These wavelets were convolved with averaged LFP traces and then averaged to produce power spectra heatmaps that were dB baseline normalized. To quantify a mean power within a particular band, we averaged responses within 1s after the stimulus onset. 6 different frequency bands were used: theta (4-8Hz), alpha (8-12 Hz), beta (12-30 Hz), low gamma (30-50Hz), and high gamma (50-80Hz). We also extracted phases of the signal and then quantified an inter-trial phase-coherence (ITPC) by averaging complex vectors defined by those angles within 0.5s after the stimulus onset.

$$ITPC_{tf} = \left| \frac{1}{N} \sum_{r=1}^{N} e^{ik_{tf}} \right|$$

where N is the number of trials, e^{ik} indicates a complex polar representation of the phase angle k at specific frequency (f) and time point (t) (M. X. Cohen, 2014). We did not quantify ITPC for frequencies above 40 Hz as it will require larger number of trials and can be limited by the monitor refresh rate.

2.3.7 Single unit analysis

Spike detection and sorting along with manual curation of units were performed as previously described (Kissinger et al., 2018). Briefly, Kilosort was used for spike detection and sorting (Pachitariu, Steinmetz, Kadir, Carandini, & Harris, 2016). Default configuration parameters were used for clustering, but a threshold for spike detection was changed from -4 to -6 SD. Templates were initialized from the data. Kilosort was run using MATLAB (Mathworks) on a computer running Windows 10. For clustering purposes, all the different recording sessions were concatenated together. This allowed us to track single neurons across different recording sessions performed on the same day. After spike detection and sorting, we visualized and verified clustering results using the Klusta/Phy GUI, which was then used for manually removing, splitting, and merging units when necessary (Rossant et al., 2016). We only included high-quality single units that had a clear refractory period and a high amplitude waveform template. To merge and split units, we followed the guidelines available online (https://github.com/kwikteam/phy-contrib/blob/master/docs/template-gui.md). Peristimulus time histograms (PSTHs) of single units were constructed by binning spike times across trials with 10 ms bins and convolving the obtained histogram with a Gaussian Kernel (width = 100 ms). The Z-score was calculated using the following formula.

$$z = \frac{FR - mean(baseFR)}{sd\ (baseFR)}$$

FR is a firing rate at each time point, and base refers to the baseline activity over 0-0.3s for tuning experiments or 0-0.5 for all other recordings. To investigate the oscillatory activity, we focused on the neurons that upregulate their firing in response to visual stimuli. We used the Wilcoxon Signed rank test to identify these neurons by comparing baseline firing rate 0.05-0.5s versus stimulus window 0.5-0.95s. The oscillatory duration was quantified using a peak detection algorithm. The time of the last peak exceeding a 1.5 z-score firing rate was computed for each unit and stimulus condition. For orientation tuning experiments, the orientation selectivity index was

computed using the following formula (Ringach, Shapley, & Hawken, 2002; Scholl, Tan, Corey, & Priebe, 2013):

$$OSI = \frac{\sqrt{(\sum r_k \sin(2\theta_k))^2 + (\sum r_k \cos(2\theta_k))^2}}{\sum r_k}$$

where θ and k represent orientation (in radians) and stimulus index, respectively. This is a more robust measure of selectivity compared to a conventional measure. We also fitted a double Gaussian to find the tuning width sigma (σ).

$$R(\theta) = \mathrm{R}_0 + R_p e^{\frac{-(\theta - \theta_p)^2}{2\sigma^2}} + R_n e^{\frac{-(\theta - \theta_p + 180)^2}{2\sigma^2}}$$

The function has five parameters to fit: baseline firing rate R_0, preferred orientation θ_{pref}, the response at the preferred orientation R_p, the response at the null orientation R_n, and tuning width σ.

For spatial frequency analysis, we first defined a preferred SF as the one that induces the strongest response (peak in the tuning curve). Population tuning curves were then constructed using normalized firing rates across different neurons. We also quantified a low spatial frequency suppression (LSFS) by dividing the response to the lowest SF tested (7.5E-3 cpd) by the response at the preferred SF. To quantify tuning bandwidth, we fitted a difference of Gaussian function to SF tuning curves (Hawken & Parker, 1987):

$$R(SF) = \mathrm{R}_0 + K_e e^{\frac{-(SF - \mu_e)^2}{2\sigma_e^2}} - K_i e^{\frac{-(SF - \mu_i)^2}{2\sigma_i^2}}$$

This function has 7 free parameters: baseline firing rate R_0, amplitude K_e and K_i, center μ_e and μ_i, width σ_e and σ_i of the excitatory and inhibitory components, respectively.

For contrast sensitivity curves, we fitted a hyperbolic ratio function (Albrecht & Hamilton, 1982):

$$R(c) = \mathrm{R}_0 + R_{max} \frac{c^n}{c_{50}^n + c^n}$$

where c is the contrast of the stimulus. It has 4 parameters: baseline firing rate R_0, maximum response R_{max}, exponent n, and semisaturation point c_{50}.

All curve fitting procedures were performed using the least-squares method in Python (scipy.optimize.curve_fit). The fitting error was defined as:

$$fit\ error = \frac{\sum (y_i - f_i)^2}{\sum (y_i - \bar{y})^2}$$

where y_i is the observed value, $\bar{y}$ is mean of observed data, and f_i is the fitted value. For statistical analysis of parameters, we only included units with a fitting error < 0.7.

Population neural decoding for orientation, spatial frequency, and contrast responses were performed using Linear Discriminant Analysis (LDA) in Python's scikit-learn package (default parameters) (Virtanen et al., 2020). Population spike counts within 0.05-0.5s relative to the stimulus onset were used to train classifiers. 4-fold cross-validation with five repeats was performed. The number of folds was chosen so that the test size was not below 30 samples. The number of units used for training was comparable between pre and post perceptual experience and across different genotypes.

2.3.8 Pupillometry

The detailed procedure has been previously described (Kissinger et al., 2018). Briefly, video acquisition of the mouse pupil was performed under IR illumination. Videos were then analyzed post hoc using a Python computer vision library, OpenCV. We first performed a histogram equalization to enhance the contrast of the video frames. Manual thresholding was then used to detect putative pupil. Given a good preprocessing pipeline, we performed the pupil tracking by first detecting contours and then fitting a minimum enclosing circle. This ensured that whiskers and small local contrast variations did not affect the tracking. The x,y-coordinate, and radius were extracted based on the fitted circle. We analyzed both a raw diameter of the pupil and area % change from the baseline. A subset of videos was analyzed with a DeepLabCut (Mathis et al., 2018). We trained a convolutional neural network (ResNet50) on a GPU to detect pupil coordinates. In total, 250 frames from different mice and lighting conditions were used for training. The circle was fitted to four pupil coordinates using least-square optimization in Python. For validation purposes, we generated at least one labeled video for each mouse before including its data in the final analysis. Furthermore, we excluded outlier data points by thresholding pupil diameter to be in the range of 10-50 pixels.

2.3.9 Statistical Analysis

Python's scipy.stats library was used to perform all statistical analyses (Virtanen et al., 2020). We did not test the normality of residuals, and only non-parametric tests were used. Kruskal-Wallis

test was used as a non-parametric version of ANOVA when more than two groups were compared. A Mann-Whitney U test was used for pairwise comparisons. It was used to compare trial averaged LFPs, z-score firing rates, and pupil dynamics in different conditions and groups. It was also used to compare fitted parameters between genotypes.

2.4 Increased duration of visual experience-dependent oscillatory activity in neurons of SERT KO mice

To investigate the role of 5-HT signaling in visual processing and experience-dependent learning, we performed *in vivo* silicon probe recordings using 64 channel probes in awake head-fixed SERT mice (Shobe et al., 2015) **(Figure 5A)**. We have previously shown that the perceptual experience of a sinusoidal drifting grating for four days (200 presentations per day) leads to the emergence of the theta oscillations specific to the familiar stimulus in mouse V1 (Kissinger et al., 2018), while the presentation of a novel stimulus did not evoke these oscillations. Using a similar paradigm, we investigated visual experience-dependent learning in SERT-deficient mice. A sinusoidal drifting grating (direction: 30º, spatial frequency 0.04 cpd, temporal frequency: 2 Hz) was presented to mice 200 times a day for four days (**Figure 5B**). Both electrophysiological and pupillometry recordings were performed before (pre) and after (post) perceptual experience. In line with our LFP findings and previous study, we observed oscillatory activity in single units after perceptual experience in all three groups (**Figure 5C and 6**). There was no significant difference in power spectra across genotypes after perceptual experience, however, there was a significantly lower ITPC of low frequency bands in response to novel stimulus in SERT-deficient mice (**Figure 6 and 7**). There was a significantly stronger grating-evoked population z-score responses in naive SERT KO compared to other genotypes (**Figure 5D left**, z-score firing rate pre: genotype WT vs HET vs KO (P = 0.01), Kruskal-Wallis test, n = 158, 98, and 150 units; WT vs HET (P = 0.18), WT vs KO (P = 0.003), and HET vs KO (P = 0.03), post hoc Mann-Whitney U test). There was no difference in z-score firing rate between groups in experienced mice (**Figure 5D middle**, z-score firing rate post: genotype (P = 0.54), Kruskal-Wallis test, n = 110, 96, and 93 units). Responses to the novel checkerboard stimulus were significantly weaker in SERT KO mice compared to other genotypes (**Figure 5D right**, z-score firing rate novel: genotype (P = 0.004), Kruskal-Wallis test, n = 110, 96, and 93 units; WT vs HET (P = 0.39), WT vs KO (P = 0.001), and HET vs KO (P = 0.004), post hoc Mann-Whitney U test).

Figure 5. Longer visual experience dependent oscillatory activity in units of SERT-deficient mice.

A. *In vivo* extracellular electrophysiology with 64ch silicon probes in awake head-fixed mice. **B.** Animals were recorded pre and post perceptual experience. During pre recording, a block of drifting grating stimuli (pre) was presented (x20, 0.5 s in duration). It was followed by tuning experiments, which consisted of orientation, spatial frequency, and contrast tuning experiments. During perceptual experience, a sinusoidal drifting grating was presented to animals 200 times a day for four days. Post recording was similar to pre, but animals were also presented with a novel stimulus, a checkerboard pattern (x20, 0.5s). **C.** Heatmap of z-score firing rate of single units in pre (left), post familiar (middle), and post novel condition of SERT WT, HET, and KO mice. **D.** Line plots show the mean of z-score responses of three different groups. Inset bar plots show the mean ± s.e.m. of z-score within 0.05-0.5s after the stimulus onset. **E.** Cumulative distribution function of oscillatory duration across three different conditions. Inset point plots show the mean ± s.e.m. of oscillatory duration across three genotypes.

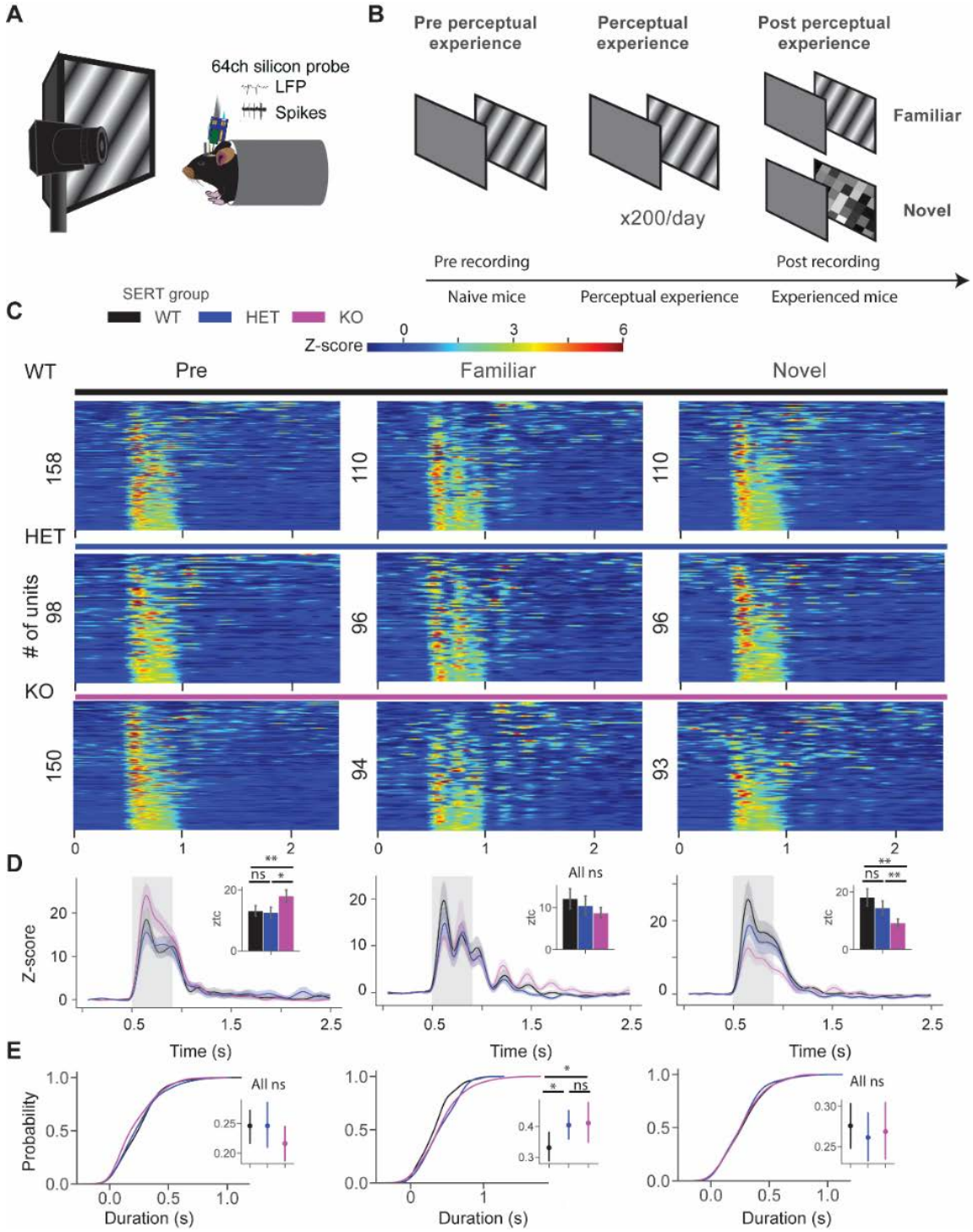
A
64ch silicon probe
LFP
Spikes
B
Pre perceptual experience
Perceptual experience
Post perceptual experience
Familiar
Novel
x200/day
Pre recording
Post recording
Naive mice
Perceptual experience
Experienced mice
C
SERT group
WT
HET
KO
Z-score
0
3
6
WT
Pre
Familiar
Novel
158
110
110
HET
# of units
98
96
96
KO
150
94
93
0
1
2
D
Z-score
20
10
0
0.5
1.5
2.5
ns
*
**
All ns
ztc
E
Time (s)
Probability
1.0
0.5
0.0
Duration (s)
All ns
ns

Our pupillometry results were in line with our previous study. There was a strong surprise response (pupil dilation) to the visual stimulus in pre condition (naive mice), however, after perceptual learning, mice showed surprise response in novel but not in familiar condition. Baseline pupil size was qualitatively larger in SERT-deficient mice compared to WT but it did not reach significance. However, a significantly weaker surprise response was observed in novel condition in SERT KO compared to other groups (**Figure 8**). To quantify the duration of the oscillatory activity, we used a peak detection algorithm. The time point of the last detected peak in the PSTH of the unit was used as a measure of the duration of oscillations. There was no oscillatory activity in pre and novel condition, hence, no significant differences were observed (**Figure 5E left and right**, duration pre: genotype (P = 0.21), Kruskal-Wallis test, n = 120, 80, and 125; novel: genotype (P = 0.82), Kruskal-Wallis test, n = 130, 128, and 81 units). We observed a significantly longer oscillatory activity in experienced SERT-deficient mice compared to WT (**Figure 5E middle,** duration post: genotype (P = 0.049), Kruskal-Wallis test, n = 102, 93, and 77 units; WT vs HET (P = 0.01), WT vs KO (P = 0.03), and HET vs KO (P = 0.36), post hoc Mann-Whitney U test). These results suggest that perceptual experience might have altered circuit-level changes in SERT mice.

2.5 Reduced orientation and oscillation selectivity in SERT KO mice after the perceptual experience

To gain a deeper insight into the effects of perceptual experience on visual processing in SERT deficient mice, we investigated cortical tuning properties. We first focused on orientation selectivity and tuning of V1 neurons. Sinusoidal drifting gratings of 12 different directions were presented to investigate orientation tuning properties. We first looked at population direction tuning curves of three different groups pre vs. post perceptual experience (**Figure 9A and D**). The polar plots were constructed by averaging direction tuning curves, which were aligned so that the preferred direction indicates 0º. We fitted a double Gaussian function to the direction tuning curves to quantify the tuning width, sigma (σ) (**Figure 9H**). We did not find a significant difference in both orientation selectivity index (OSI) and tuning width between groups before perceptual experience (**Figure 9B**, pre OSI: genotype (P = 0.82), Kruskal-Wallis test, n = 222, 106, and 110 units; sigma: genotype (P = 0.37), Kruskal-Wallis test, n = 196, 87, and 98 units). Tuning width was comparable to what has been reported previously (Niell & Stryker, 2008). We found an

overrepresentation of preference for cardinal orientations in WT but not in other groups (Kreile, Bonhoeffer, & Hübener, 2011) (**Figure 9C**). Strikingly, we found a significantly lower OSI and wider tuning width in SERT KO compared to other groups after perceptual experience (**Figure 9E**, post OSI: genotype (P = 0.0003), Kruskal-Wallis test, n = 172, 136, and 96 units, WT vs HET (P = 0.05), WT vs KO (P = 0.002), and HET vs KO (P = 4.01E-5); post hoc Mann-Whitney U test; sigma: genotype (P = 0.02), Kruskal-Wallis test, n = 154, 122, and 72 units, WT vs HET (P = 0.15), WT vs KO (P = 0.004), and HET vs KO (P = 0.02), post hoc Mann-Whitney U test). We also found that both WT and HET had an overrepresentation of neurons preferring cardinal orientations after perceptual experience (**Figure 9F**).

We next investigated the oscillatory dynamics in response to drifting gratings. It has been previously shown that oscillations are partly specific to the orientation of the grating. We qualitatively observed that oscillations in SERT KO mice were evoked by a broad range of different directions (**Figure 9G and I**). To compare oscillatory dynamics between groups, we averaged oscillatory duration across different stimuli for each unit. We found significantly longer oscillations in SERT KO mice compared to other groups (**Figure 9J**, duration post: genotype (P = 0.001), Kruskal-Wallis test, n = 202, 134, and 109 units, WT vs HET (P = 0.049), and WT vs KO (P = 0.0002), and HET vs KO (P = 0.023), post hoc Mann-Whitney U test). Neural decoding analysis was then used to investigate whether reduced selectivity would affect orientation decoding. Using population spike counts pre vs. post from different genotypes, we trained classifiers using Linear Discriminant Analysis (LDA) implemented in Python. We performed a 4-fold cross-validation with 5 repeats and found that orientation decoding accuracy dropped after perceptual experience only in SERT KO mice (**Figure 9K**, orientation decoding accuracy mean ± s.e.m. % WT vs HET vs KO pre: (98.6 ± 0.3 vs 99.4 ± 0.2 vs 99.4 ± 0.2), n = 241, 116, and 120 units; post: (97.5 ± 0.6 vs 94.9 ± 0.6 vs 59.4 ± 1.6), n = 204, 148, and 109 units). Together, our findings suggest that both orientation and oscillation selectivity were impaired in SERT KO but not in other groups following visual experience.

Figure 6. Altered oscillatory dynamics pre but not after visual experience in SERT deficient mice.

A. Averaged layer 4 LFP traces of SERT WT, HET, and KO in different conditions: pre (left), post familiar (middle), and post novel (right). Inset bar plots show the mean ± s.e.m. of the amplitude (pre: cycle1 (P = 0.49), cycle2 (P = 0.01), and cycle3 (P = 0.46), Kruskal-Wallis test, n = 7, 6, and 9 mice; post hoc cycle2: WT vs HET (P = 0.006), WT vs KO (P = 0.009), and HET vs KO (P = 0.46), Mann-Whitney U test; post: cycle1 (P = 0.35), cycle2 (P = 0.35), and cycle3 (P = 0.37), Kruskal-Wallis test, n = 7, 8, and 9 mice; novel: cycle1 (P = 0.27), cycle2 (P = 0.59), and cycle3 (P = 0.27), Kruskal-Wallis test, n = 7, 8, and 9 mice). **B.** Time frequency spectra of LFP traces of WT (top), HET (middle), and KO (bottom). **C.** Bar plots show the mean ± s.e.m. of normalized power across different frequency bands (pre: θ (P = 0.02), α (P = 0.66), β (P = 0.10), low γ (P = 0.02), and high γ (P = 0.47), Kruskal-Wallis test, n = 7, 6, and 9 mice, post hoc θ WT vs HET (P = 0.006), WT vs KO (P = 0.028), HET vs KO (P = 0.131), low γ WT vs HET (P = 0.004), WT vs KO (P =0.022), and HET vs KO (P = 0.476), Mann-Whitney U test; post: θ (P = 0.54), α (P = 0.68), β (P = 0.91), low γ (P = 0.96), and high γ (P = 0.49), Kruskal-Wallis test, n = 7, 8, and 9 mice; novel: θ (P = 0.84), α (P = 0.05), β (P = 0.31), low γ (P = 0.85), and high γ (P = 0.97), Kruskal-Wallis test, n = 7, 6, and 9 mice).

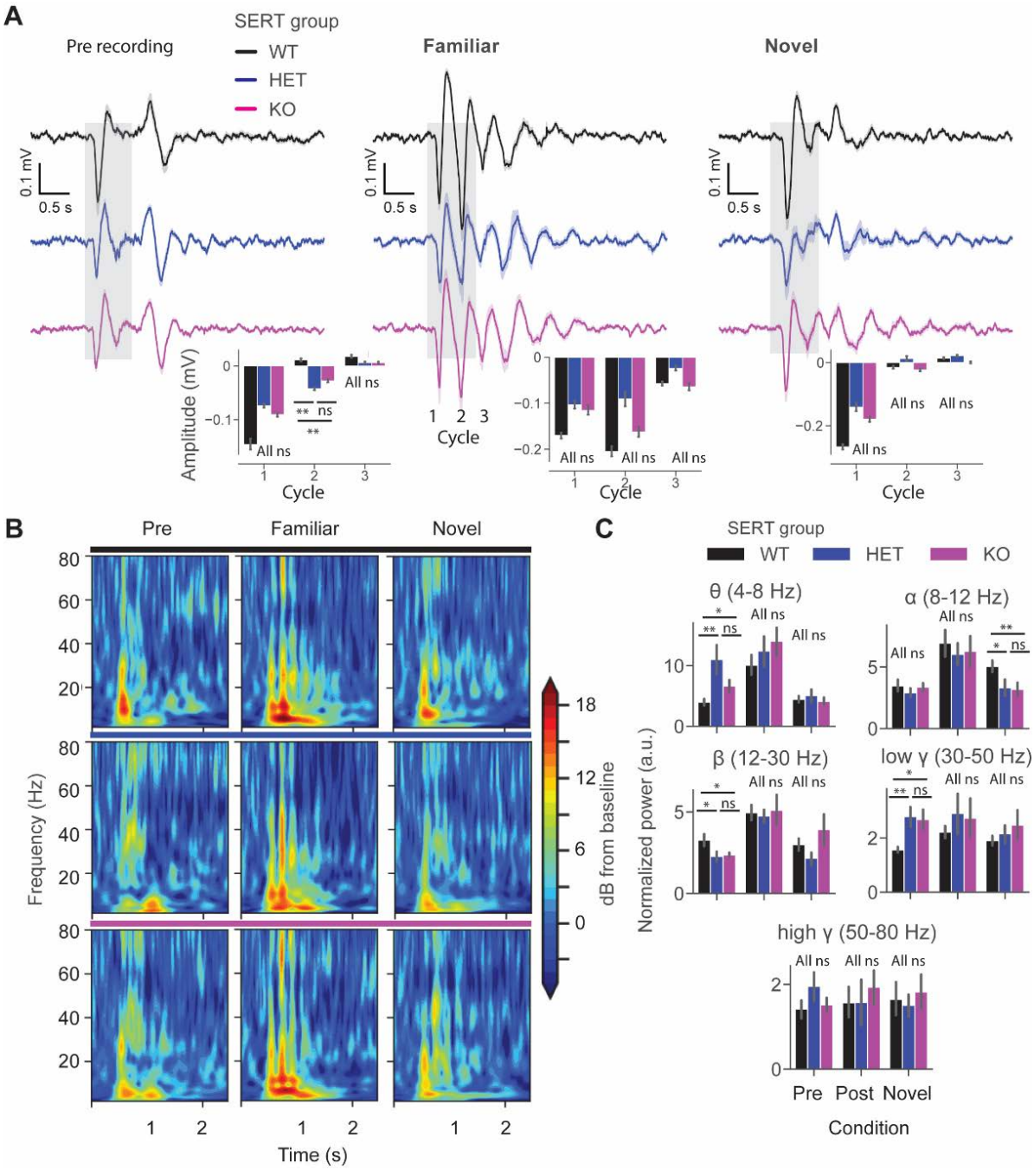
A
SERT group
WT
HET
KO
Pre recording
Familiar
Novel
0.1 mV
0.5 s
Amplitude (mV)
All ns
**
ns
Cycle
B
Pre
Familiar
Novel
Frequency (Hz)
Time (s)
dB from baseline
C
θ (4-8 Hz)
α (8-12 Hz)
β (12-30 Hz)
low γ (30-50 Hz)
high γ (50-80 Hz)
Normalized power (a.u.)
Pre
Post
Novel
Condition

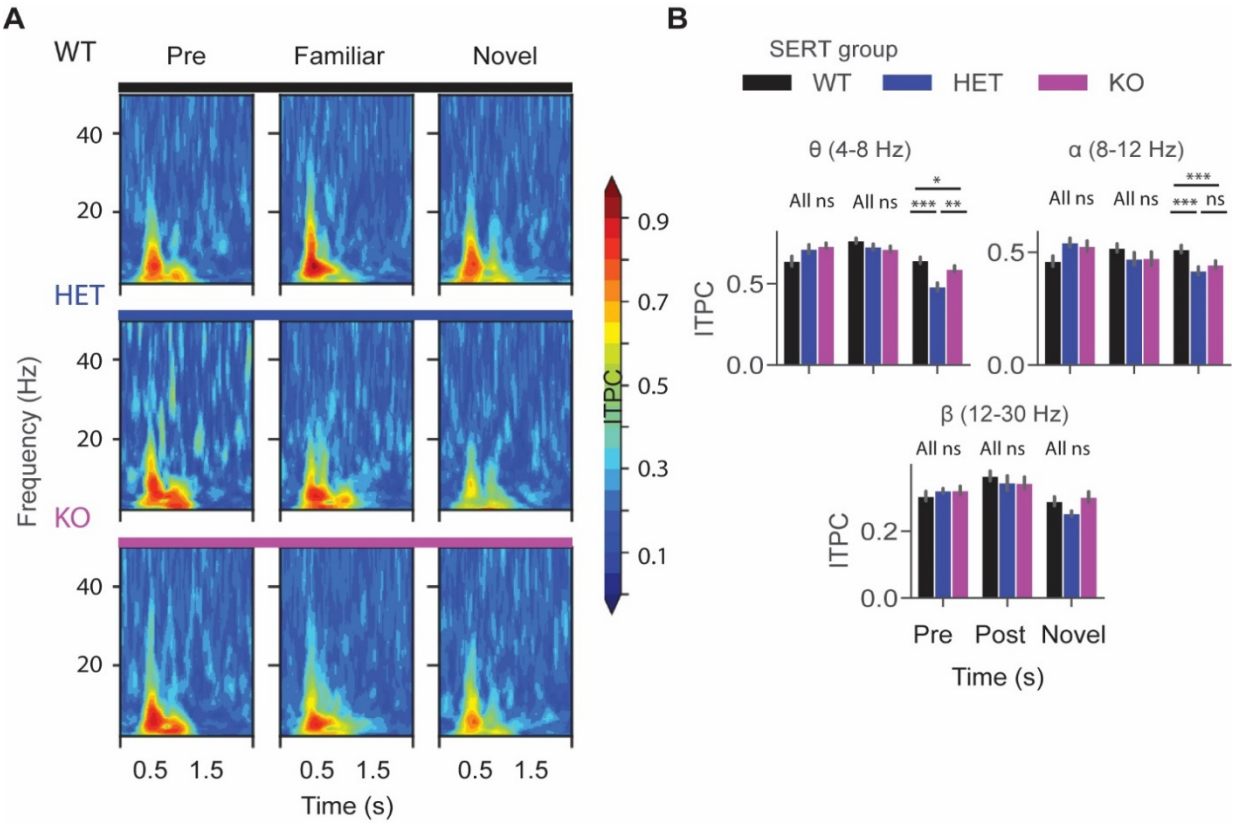

Figure 7. Inter-trial phase coherence (ITPC) is lower in response to the novel stimulus in SERT HET and KO vs WT mice in low frequency bands.

A. Heatmaps show ITPC of the LFP traces of WT (top), HET (middle), and KO (bottom) for pre (left), post visual experience (middle), and novel stimulus (right). **C.** Bar plots show the mean ± s.e.m. of mean ITPC within 0-0.5 s relative to the stimulus onset across different frequency bands (**pre**: θ (P = 0.302), α (P = 0.104), β (P = 0.521), Kruskal-Wallis test, n = 18, 6, and 18 channels; **post**: θ (P = 0.071), α (P = 0.387), β (P = 0.483), Kruskal-Wallis test, n = 21, 12, and 24 channels; **novel**: θ (P = 0.0001), α (P = 0.0001), β (P = 0.115),, Kruskal-Wallis test, n = 18, 12, and 19 channels; post hoc θ WT vs HET (P = 3.8e-5), WT vs KO (P = 0.048), and HET vs KO (P = 0.0016); α WT vs HET (P = 0.0001), WT vs KO (P = 0.0003), and HET vs KO (P = 0.150), Mann-Whitney U test).

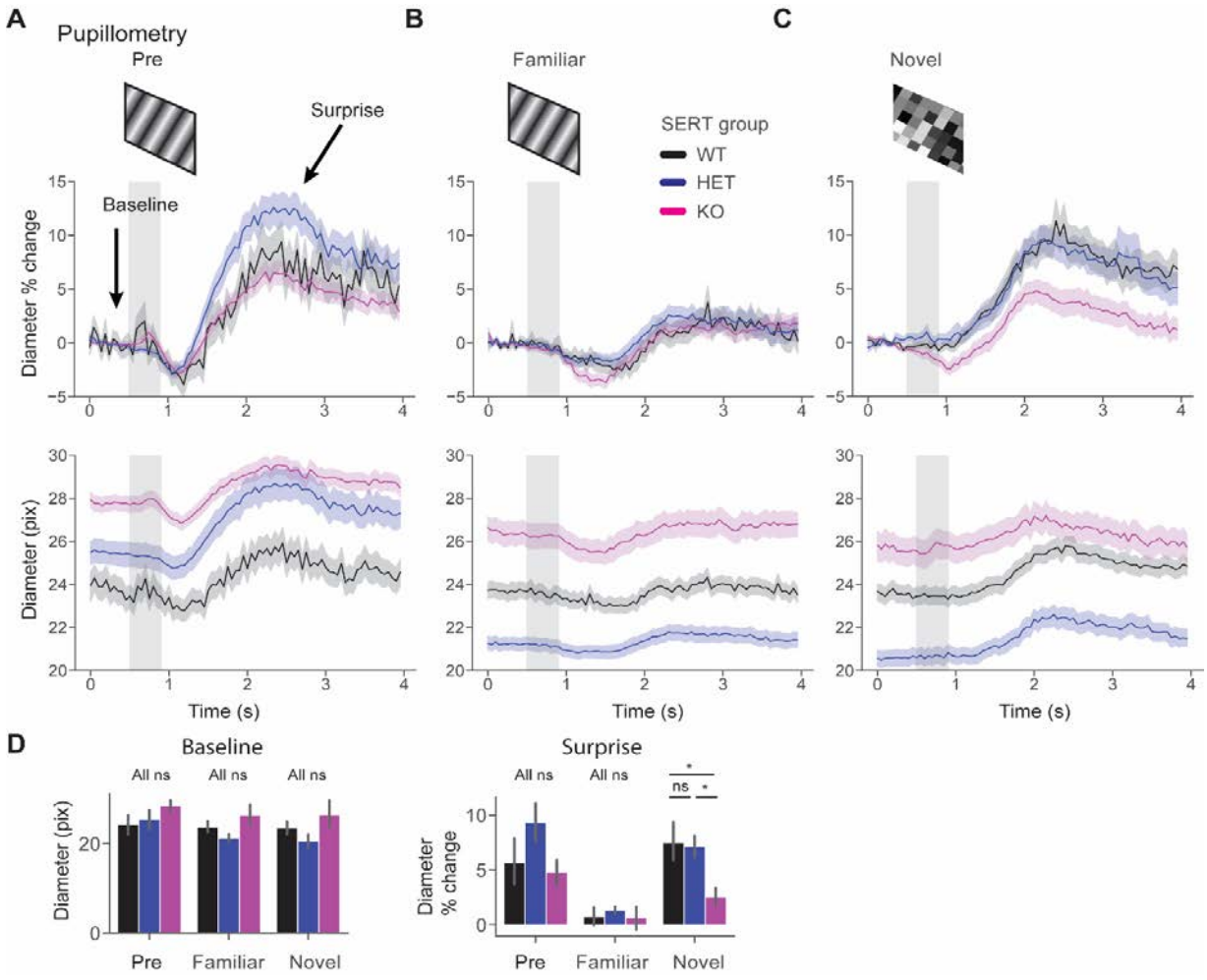

Figure 8. Surprise response in SERT KO mice.

A. Normalized (top) and raw (bottom) pupil diameter in response to drifting grating stimulus in naive mice. Note: strong surprise response due to the novelty of the stimulus. **B.** Same as in A, but after perceptual experience to the familiar stimulus. Note: surprise response is small due to the familiarity to the stimulus. **C.** Same as in B, but for the novel stimulus. Note: strong surprise response due to the novelty of the stimulus. **D.** Bar plots show the mean ± s.e.m. of raw diameter (left) for baseline pupil size or normalized diameter (right) for surprise response across different conditions. (Baseline pupil size: pre (P = 0.24), post (P = 0.21), and novel (P = 0.32), Kruskal-Wallis test, n = 7 WT, 6 HET, and 6 KO mice; surprise: pre (P = 0.15), post (P = 0.68), novel (P = 0.03), Kruskal-Wallis test, n = 7 WT, 6 HET, and 6 KO mice , post hoc novel WT vs HET (P = 0.47), WT vs KO (P = 0.02), and HET vs KO (P = 0.01), Mann-Whitney U test).

Figure 9. Reduced orientation and oscillation selectivity in SERT KO compared to WT and HET mice after perceptual experience.

A. Polar plots show mean ± s.e.m. of population direction tuning across three groups. **B.** OSI and tuning width before perceptual experience. **C.** Point plot shows the number of units preferring different orientations in naive mice. **D.** Same as in A, but after perceptual experience. **E.** Same as in B, but for experienced mice. **F.** Same as in C, but for experienced mice. **G.** Averaged unit z-score responses to 12 different directions of three different groups. The 30º drifting grating was a familiar stimulus (highlighted in yellow). **H.** Example direction tuning curves fitted with a double Gaussian (red) for the three different groups. **I.** Bar plots show the mean ± s.e.m. duration of oscillatory activity across different orientations. **J.** Cumulative distribution function of duration of oscillations across different groups. **K.** Orientation decoding accuracy of classifiers trained on population spike counts from different groups using LDA.

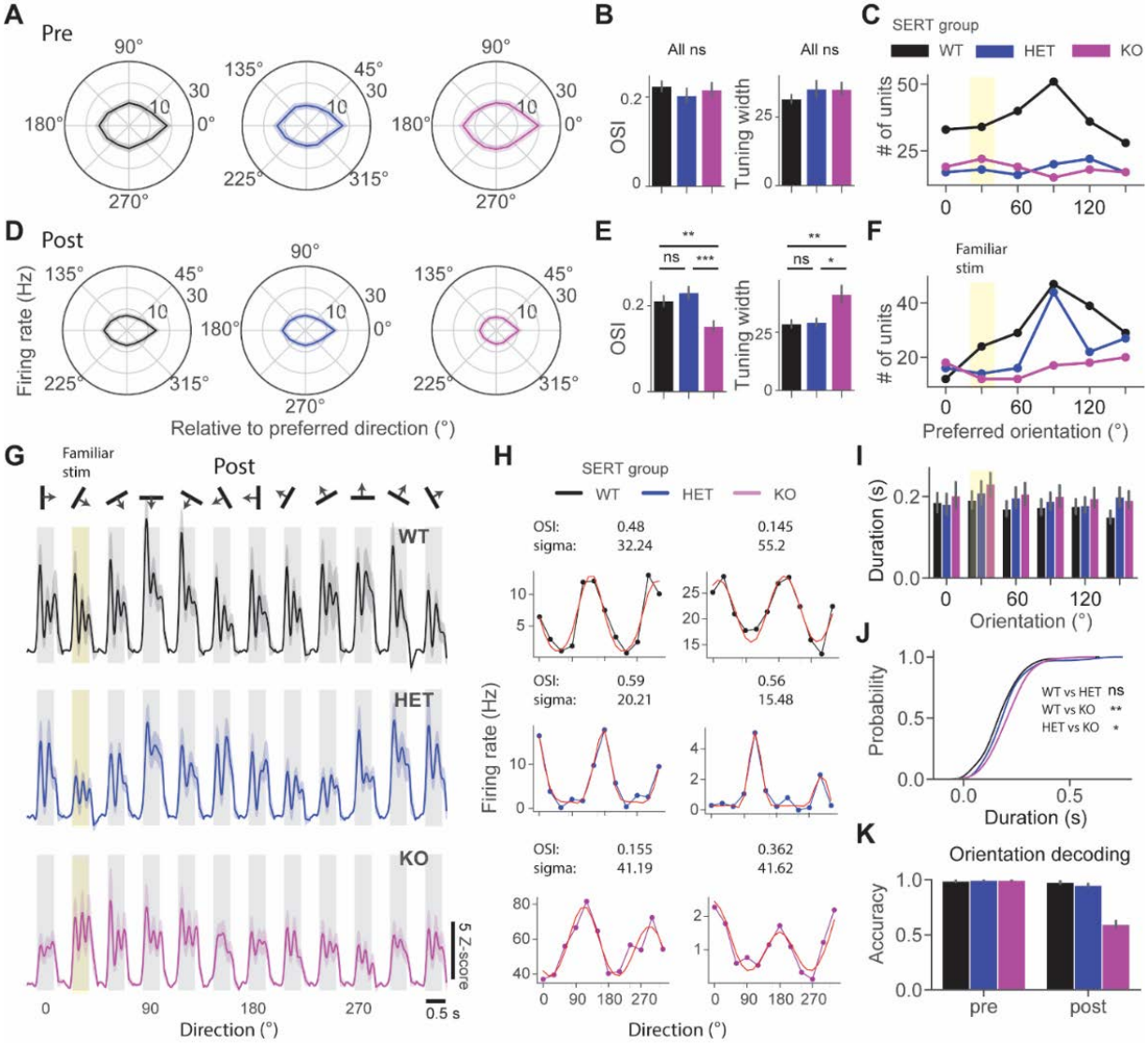
A
Pre
90°
135°
45°
180°
0°
225°
315°
270°
10
30
B
All ns
OSI
Tuning width
C
SERT group
WT
HET
KO
# of units
D
Post
Firing rate (Hz)
Relative to preferred direction (°)
E
ns
***
*
F
Familiar stim
Preferred orientation (°)
G
Familiar stim
Post
WT
HET
KO
5 Z-score
0.5 s
Direction (°)
H
SERT group
OSI: 0.48
sigma: 32.24
0.145
55.2
OSI: 0.59
sigma: 20.21
0.56
15.48
OSI: 0.155
sigma: 41.19
0.362
41.62
Firing rate (Hz)
Direction (°)
I
Duration (s)
Orientation (°)
J
Probability
WT vs HET ns
WT vs KO **
HET vs KO *
Duration (s)
K
Orientation decoding
Accuracy
pre
post

2.6 Perceptual experience alters spatial frequency processing in SERT KO mice

We next investigated spatial frequency tuning (SF) properties pre and post perceptual experience. Oscillations have been previously shown to be specific to the spatial frequency of the experienced stimulus. We designed visual stimuli of different spatial frequencies by performing spatial filtering of white noise in different frequency bands (**Figure 10A**) to probe SF tuning and specificity of oscillations to the grating pattern. It has been previously shown that these stimuli can be used to probe SF tuning. We fitted a difference-of-Gaussians (DOG) model to SF tuning curves to quantify tuning bandwidth (**Figure 10B**). We did not find any significant differences in the low spatial frequency suppression (LSFS) or the full width at half maximum (FWHM) of fitted SF tuning curves in naive mice (**Figure 11**). Inspection of average population responses revealed oscillatory activity at high SF only in SERT KO mice (**Figure 10A**). We did not find a significant difference in the FWHM of the SF tuning curves between groups in experienced mice (**Figure 10C**, FWHM post: genotype (P = 0.78), Kruskal-Wallis test, n = 145, 147, and 128 units), however, there was a significantly weaker suppression at low SF in SERT KO mice compared to other groups (**Figure 10D**, LSFS post: genotype (P = 0.01), Kruskal-Wallis test, n = 171, 175, and 151 units, WT vs HET (P = 0.21), WT vs KO (P = 0.01), and HET vs KO (0.002), post hoc Mann-Whitney U test). 0.71), SF = 0.03 (P = 0.76), SF = 0.06 (P = 0.33), SF = 0.12 (P = 0.005), SF = 0.24 (P = 0.79), Kruskal-Wallis test, n = 215, 205, and 173 units). Population responses were stronger at low and weaker at high SF in SERT KO (**Figure 10E**, normalized SF responses post: SF=7.5E-3: WT vs HET (P = 0.1), WT vs KO (P = 0.003), and HET vs KO (0.0003), SF = 0.12: WT vs HET (P = 0.44), WT vs KO (P = 0.002), HET vs KO (P = 0.002), post hoc Mann-Whitney U test, n = 215, 205, and 173 units). Units preferring higher than trained SF (0.06 and 0.12 cpd) were overrepresented in both WT and HET but not in SERT KO mice (**Figure 10F**).

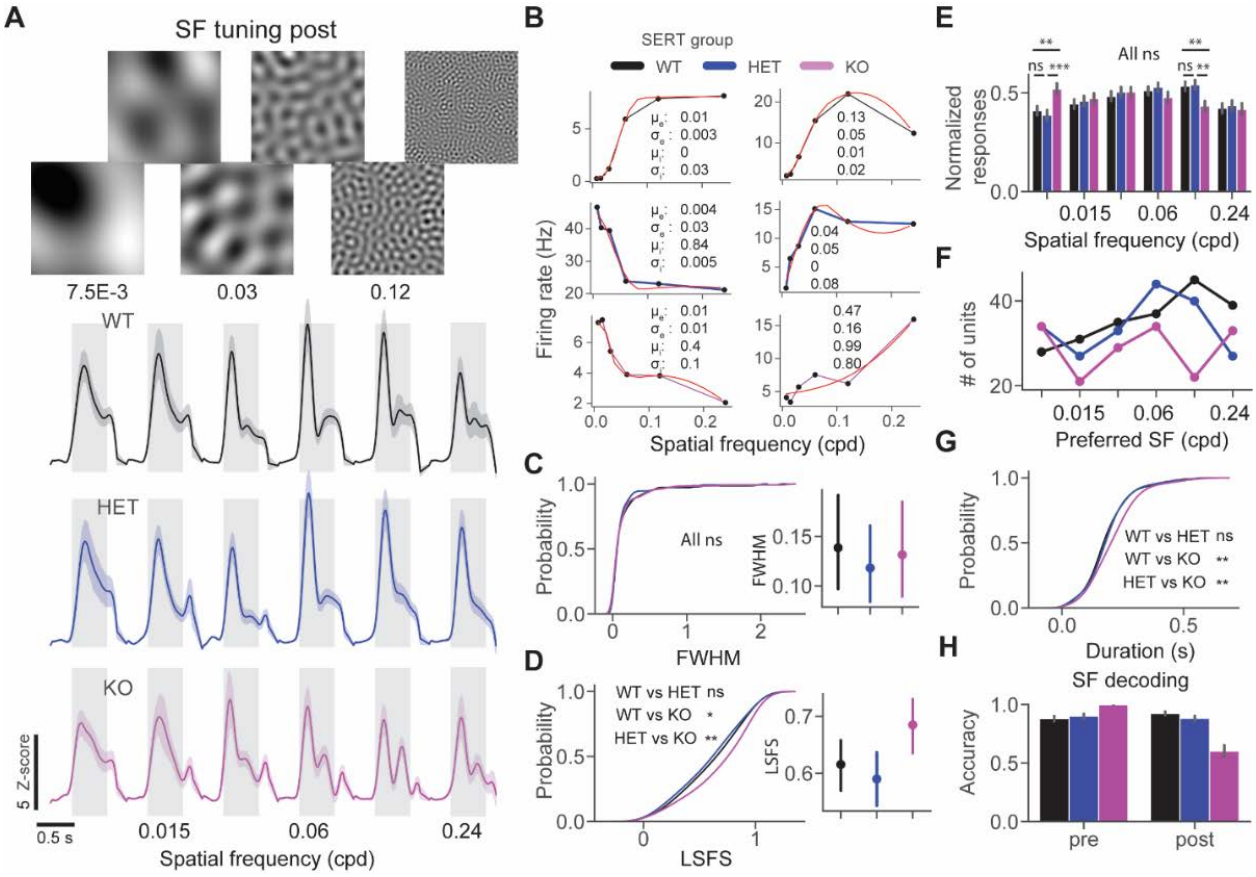

Figure 10. Spatial frequency non-specific oscillations in SERT KO mice.

A. Average unit z-score firing rate in response to spatial frequency tuning stimuli across three different genotypes. **B.** Example SF tuning curves fitted with a DOG **C.** Cumulative distribution function of FWHM of SF tuning curves. **D.** Cumulative distribution function of LSFS, larger values indicate a lower attenuation at low SF. **E.** Bar plots show the normalized responses across different SF and groups. **F.** Point plots show the number of units preferring different SF. **G.** Cumulative distribution function of oscillatory duration. **H.** SF decoding accuracy of classifiers trained on population spike counts from different groups using LDA.

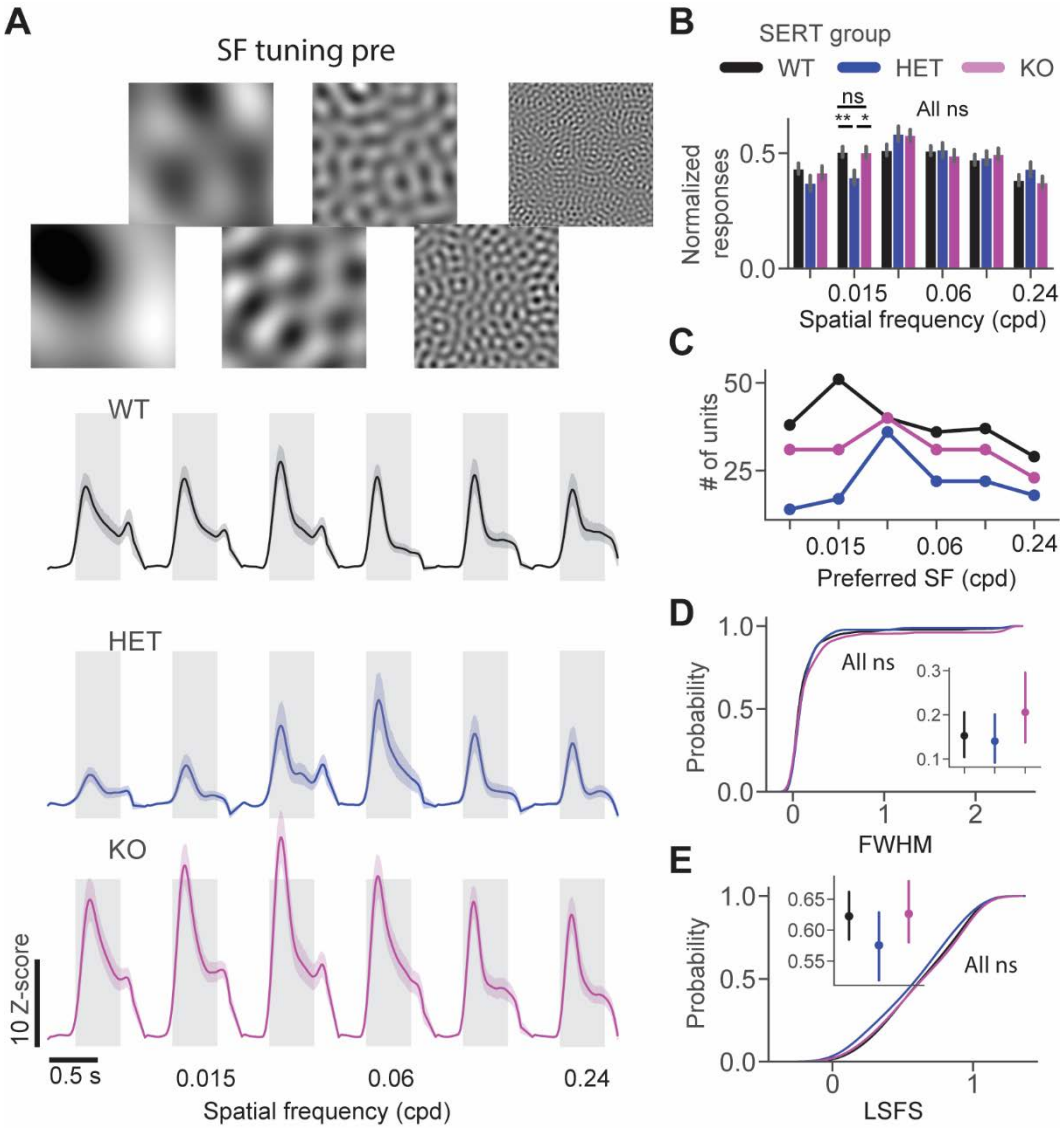

Figure 11. Intact spatial frequency tuning in naive SERT mice but weaker responses to low SF in SERT HET.

A. Average unit z-score firing rate in response to spatial frequency tuning stimuli. **B.** Bar plots show the normalized responses across different SF and groups (SF=7.5E-3 (P = 0.31), SF = 0.015 (P = 0.009), SF = 0.03 (P = 0.07), SF = 0.06 (P = 0.74), SF = 0.12 (P =0.77), and SF = 0.24 (P = 0.27), Kruskal-Wallis test, n = 231, 129, and 187, post hoc SF = 0.015 WT vs HET (P = 0.002), WT vs KO (P = 0.42), and HET vs KO (P = 0.004), Mann-Whitney U test) **C.** Point plots how the number of units preferring different SF. **D.** Cumulative distribution function of FWHM of SF tuning curves across three different genotypes (FWHM pre (P = 0.47), Kruskal-Wallis test, n = 177, 90, and 130 units). **E.** Cumulative distribution function of LSFS across three different groups (LSFS pre (P = 0.34), Kruskal-Wallis test, n = 200,m 111, and 140 units).

Consistent with these findings, we discovered significantly different responses at the SF of 7.5E-3 and 0.12 cpd (normalized SF responses post: genotype SF=7.5E-3 (P = 0.001), SF = 0.015 (P =

We next quantified the duration of oscillatory activity in response to different SF stimuli. The duration of oscillations was averaged across stimuli for each unit and compared across different genotypes (**Figure 10E**). Significantly longer oscillations were found in SERT KO mice compared to the two other groups (**Figure 10G**, duration post: genotype (P = 0.016), Kruskal-Wallis test, n = 208, 198, and 156 units, WT vs. HET (P = 0.26), WT vs. KO (P = 0.003), and HET vs. KO (P = 0.011), post hoc Mann-Whitney U test). We then investigated SF decoding pre vs. post visual learning. Classifiers were trained for different conditions on population spike counts using LDA in scikit-learn. SF decoding accuracy was reduced after learning in SERT KO but not in other groups (**Figure 10H**, SF decoding accuracy mean ± s.e.m. % WT vs HET vs KO: pre (87.8 ± 1.1 vs 90.2 ± 1.1 vs 99.8 ± 0.2), n = 241, 140, and 197 units; post (92.5 ± 0.8 vs 88.3 ± 1.0 vs 60.2 ± 2.5), n = 229, 209, and 174 units). Overall, our results suggest that there is altered spatial frequency processing in SERT KO after the perceptual experience.

2.7 Lower contrast sensitivity after perceptual experience in SERT HET mice

We next focused on contrast sensitivity properties of three genotypes pre and post perceptual experience. No significant alterations were found in contrast response function in naive SERT deficient mice (**Figure 13**). We then measured the contrast sensitivity after visual experience. Mean population z-score responses to 0º static grating at different contrast levels revealed oscillatory activity only in SERT KO mice. Normalized responses were differentially modulated by contrast in different groups (**Figure 12C,**, normalized responses at different contrast levels post: genotype C = 0.0625 genotype (P = 0.05); C = 0.125 genotype (P = 0.016), WT vs HET (P = 0.004), WT vs KO (P = 0.41), and HET vs KO (P = 0.01); C = 0.25 genotype (P = 0.03), WT vs HET (P = 0.02), WT vs KO (P = 0.24), and HET vs KO (P = 0.006); C = 0.5 genotype (P = 1.56E-6), WT vs HET (P = 0.0008), WT vs KO (0.02), and HET vs KO (P = 1.11E-7); C = 1.0 genotype (P = 0.003), WT vs HET (P = 0.0003), WT vs KO (P = 0.04), and HET vs KO (P = 0.05), Kruskal-Wallis test with post hoc Mann-Whitney U test, n = 209, 197, and 171 units). We fitted hyperbolic ratio functions to the contrast sensitivity curves (**Figure 12B**). Significantly lower contrast sensitivity (higher c_{50} values) was found In HET mice (**Figure 12D**, c_{50} post: genotype (P = 0.01), Kruskal-Wallis test, n = 74, 78, and 75 units, WT vs HET (P = 0.001), and WT vs KO (P = 0.25),

and HET vs KO (P = 0.01), post hoc Mann-Whitney U test). Furthermore, the exponent ("n" parameter) was significantly lower in HET vs WT (**Figure 12E**, exponent post: genotype (P = 0.008), Kruskal-Wallis test, n = 74, 78, and 75 units, WT vs HET (P = 0.0008), WT vs KO (P = 0.07), and HET vs KO (P = 0.05), post hoc Mann-Whitney U test). Despite qualitative differences in oscillatory dynamics, we did not find significant differences in duration of oscillations between genotypes (**Figure 12F**, duration post: genotype (P = 0.14), Kruskal-Wallis test, n = 165, 151, and 137 units). Using populations spike counts within 0.05-0.5s of the stimulus onset, we trained classifiers for different conditions to decode the contrast of the presented stimulus. We saw an overall decrease in the performance of the classifiers in SERT-deficient mice after perceptual experience (**Figure 12G**, contrast decoding accuracy mean ± s.e.m. % WT vs HET vs KO: pre (60.6 ± 1.6 vs 59.4 ± 1.7 vs 74.8 ± 1.3), n = 239, 137, and 189 units; post (60.4 ± 1.8 vs 42.8 ± 2.2 vs 43.6 ± 1.3), n = 211, 203, and 175 units). Together, our results suggest that contrast sensitivity is altered in SERT-deficient mice after perceptual experience, especially in HET.

2.8 Discussion

Here we investigated visual processing and experience-dependent learning in SERT-deficient mice. We did not find significant alterations in orientation, spatial frequency, and contrast tuning in naive mice. This finding is aligned with the prior operant conditioning study that demonstrated intact learning in visual discrimination tasks in SERT-deficient mice (Brigman et al., 2009). Furthermore, compensatory mechanisms might partially correct for the lack of functional SERT to maintain cortical development (Zhou, Lesch, & Murphy, 2002). However, we observed a lack of bias towards cardinal orientations in V1 of SERT-deficient mice before visual experience. It was partially recovered in SERT HET mice after perceptual experience but not in KO animals.

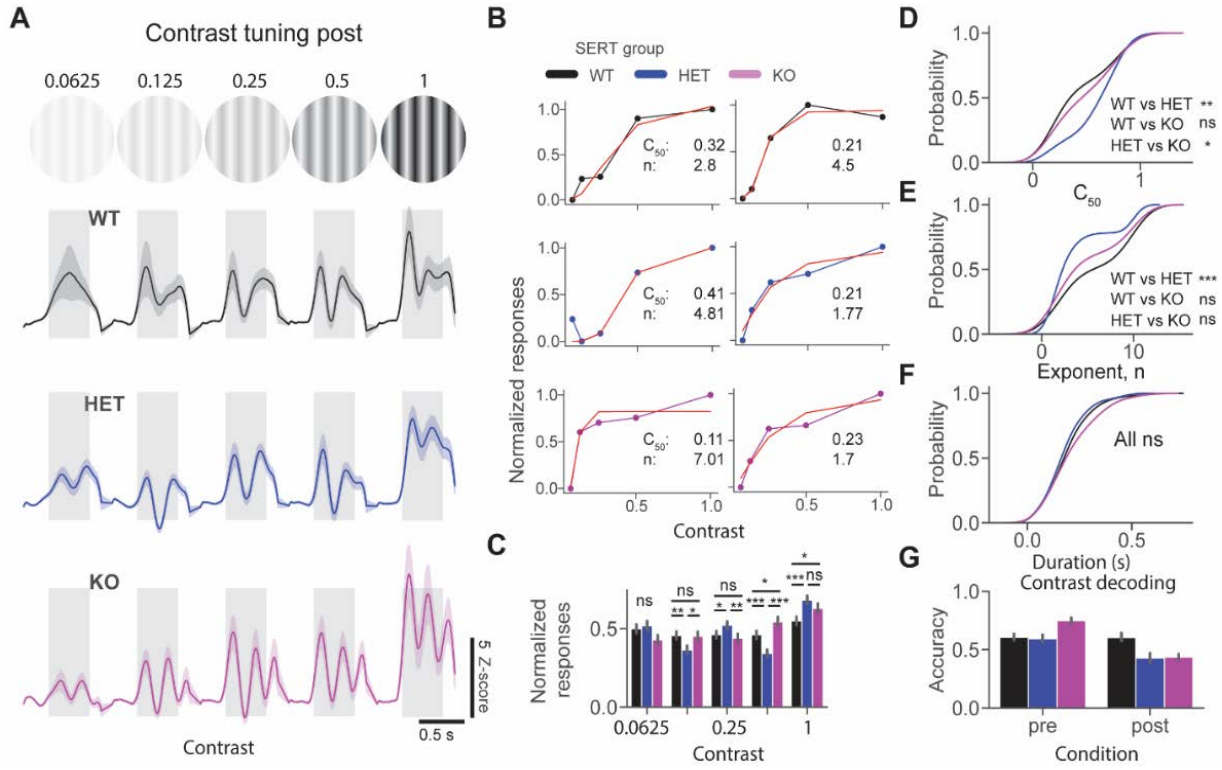

Figure 12. Lower contrast sensitivity after perceptual experience in SERT HET mice.

A. Average population z-score firing rate in response to grating stimulus at various contrast levels in three different groups. **B.** Example contrast response curves fitted with a ratio of hyperbolic function from three different groups. **C.** Bar plot shows the mean normalized response to the visual stimulus at different contrast levels. **D.** Cumulative distribution function of C_{50} (lower values indicate higher contrast sensitivity) across different genotypes. **E.** Cumulative distribution function of the "n" (exponent) parameter of the fitted curve. **F.** Cumulative distribution function of oscillatory duration across different genotypes. **G.** Contrast decoding accuracy of classifiers trained on population spike counts from different genotypes using LDA.

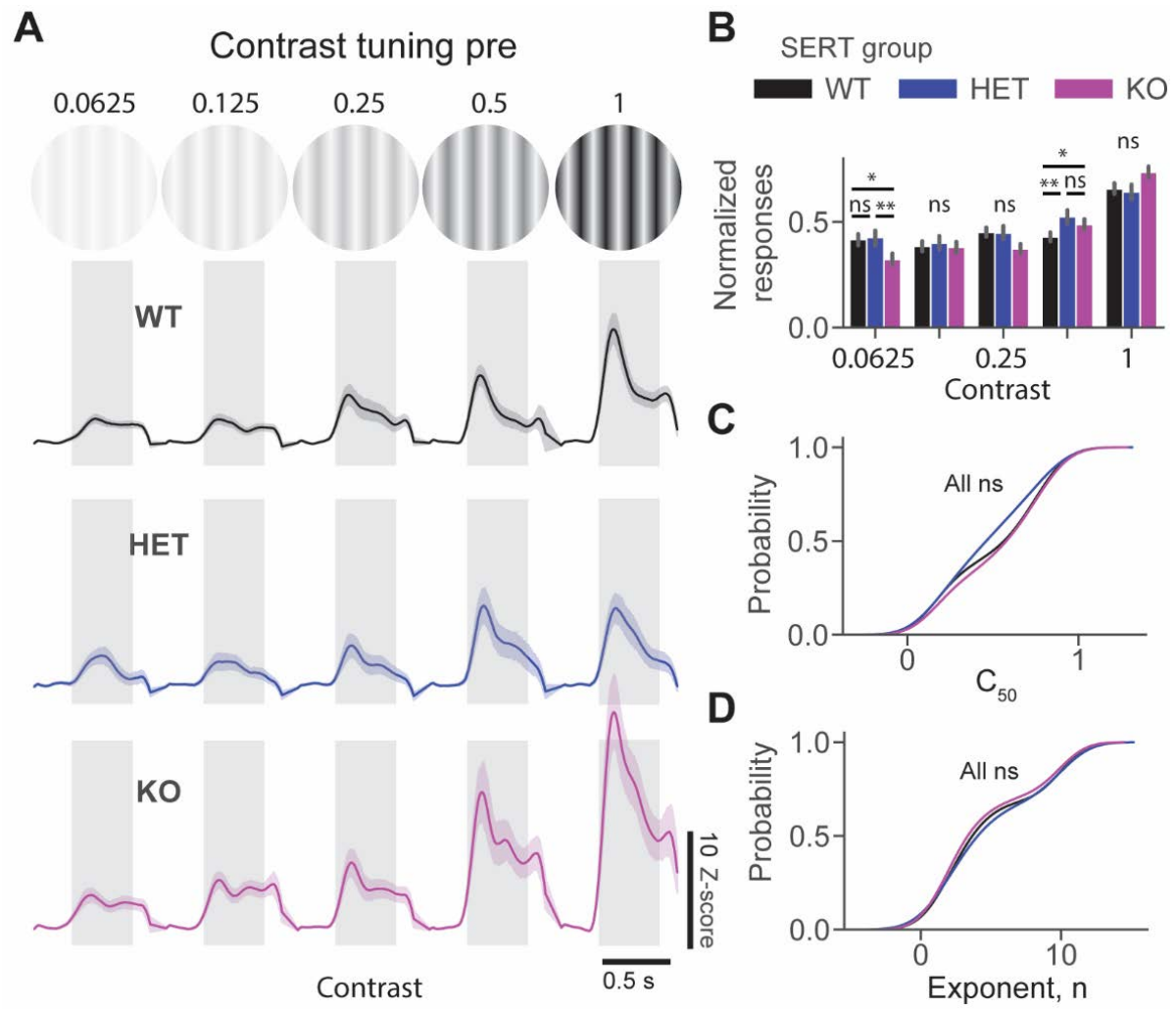

Figure 13. Weaker responses to low contrast stimuli in SERT KO and stronger responses to medium contrast stimuli in naive SERT deficient vs WT mice.

A. Average population z-score firing rate in response to the grating stimulus at various contrast levels in three different groups. **B.** Bar plot shows the mean normalized response to the visual stimulus at different contrast levels (C=0.0625 (P = 0.025), C = 0.125 (P = 0.891), C = 0.25 (P = 0.05), C = 0.5 (P = 0.03), C = 1.0 (P =0.05), Kruskal-Wallis test, n = 228, 131, and 183, post hoc C = 0.0625 WT vs HET (P = 0.41), WT vs KO (P = 0.01), and HET vs KO (P = 0.008), C = 0.5 WT vs HET (P = 0.008), WT vs KO (P = 0.03), and HET vs KO (P = 0.21), Mann-Whitney U test). **C.** Cumulative distribution function of c_{50} (lower values indicate higher contrast sensitivity) across different genotypes (c_{50} pre (P = 0.41), Kruskal-Wallis test, n = 109, 58, and 107 units). **D.** Cumulative distribution function of the "n" (exponent) parameter of the fitted curve (exponent pre (P = 0.58), Kruskal-Wallis test, n = 109, 58, and 107 units).

Table 1. Summary of alterations in SERT-deficient mice compared to WT

Table showing a summary of changes found in SERT-deficient mice compared to WT across different conditions. (↑) indicates stronger/longer, (↓) weaker/shorter, (NS) not significant, (pre) naive mice; (post) after perceptual experience, and (novel) in response to novel stimulus. Legend: ITPC, inter-trial phase coherence LSFS, low spatial frequency suppression; OSI, orientation selectivity index; SF, spatial frequency.

Condition	Alteration	HET	KO
Pre	stimulus-evoked theta	↑	↑
	stimulus-evoked beta	↓	↓
	stimulus-evoked low gamma	↑	↑
	population unit responses	NS	↑
	bias towards cardinal orientations	↓	↓
	responses to low contrast stimuli	NS	↓
	responses to medium contrast stimuli	↑	↑
Post	Duration of unit oscillatory activity	↑	↑
	OSI	NS	↓
	bias toward cardinal orientations	NS	↓
	orientation decoding accuracy	NS	↓
	LSFS	NS	↑
	SF decoding accuracy	NS	↓
	C_{50}	↑	NS
	contrast decoding accuracy	↓	↓
Novel	stimulus-evoked population unit responses	NS	↓
	pupillary surprise response	NS	↓
	stimulus-evoked alpha	↓	↓
	ITPC in low frequency oscillations	↓	↓

Visual experience dependent oscillations can be used as a global proxy for plasticity. We have previously shown that perceptual experience induces theta oscillations in both LFP and single unit activity (Kissinger et al., 2018). Furthermore, these oscillations were weaker in the Fmr1 KO

mouse model of autism (Kissinger et al., 2020). Our observations of longer oscillatory activity in SERT KO mice might indicate enhanced plasticity. It has been previously shown that serotonin signaling might be important for long-term depression and regulation of excitatory-inhibitory balance through various 5-HT receptors in cortical neurons (Berthoux, Barre, Bockaert, Marin, & Bécamel, 2019; He et al., 2015; William Moreau, Amar, Le Roux, Morel, & Fossier, 2009). We also observed reduced feature specificity of these oscillations in SERT KO mice. Such impairments might arise from cross-feature activation and non-specific tuning in the visual cortex after the perceptual experience.

Perceptual learning was shown to improve cortical tuning in the visual cortex (Jurjut et al., 2017). Furthermore, altered visual experience during development was shown to affect cortical orientation preference (Kreile et al., 2011). Fine-tuning of cortical circuits during adulthood is limited. However, a SERT inhibitor, fluoxetine, was shown to be able to restore critical period in adult rats' visual cortex, which supports the role of 5-HT in adult plasticity (Maya Vetencourt et al., 2008). Our observations of longer oscillatory activity after perceptual experience in SERT-deficient mice further support the theory that 5-HT may play role in cortical plasticity. We also observed a decreased orientation selectivity and broadened orientation tuning in SERT KO mice. Interestingly, decreased orientation selectivity and broadened orientation tuning are similar to the alterations in Fmr1 KO mice, which are known to be mediated by the hypoactivation of parvalbumin-positive fast spiking interneurons and their corresponding circuit alterations (Goel et al., 2018; Kissinger et al., 2020). Thus, one of the potential mechanisms underlying similar alterations in SERT KO mice may be mediated by the impaired plasticity of the cortical inhibitory circuitry following visual experience. Spatial frequency and contrast processing were also impaired after perceptual learning. While fluoxetine was shown to improve visual acuity in the adult rats, recent clinical trials in humans report diverse findings regarding the efficacy of the antidepressants in managing amblyopia (Huttunen et al., 2018; Lagas, Black, Russell, Kydd, & Thompson, 2019; Sharif, Talebnejad, Rastegar, Khalili, & Nowroozzadeh, 2019). Thus, it is possible that 5-HT mediated enhanced plasticity is not sufficient for functional recovery of vision in humans, and additional pharmacological or perceptual training protocols may also be required.

Our pupillometry recordings did not reveal significant alterations in SERT-deficient mice. Similar to our previous study, we observed a strong surprise response in pre and novel, but not in the familiar condition (Kissinger et al., 2018). There was a trend towards increased pupil size in

SERT KO mice, but it was not significant. We observed a smaller surprise response to the novel stimulus in SERT KO, which might arise from decreased sensitivity to novelty. Reduced novelty response might be associated with a reduced specificity of theta oscillations and activity of the noradrenergic system. Alternatively, a large baseline pupil size might limit the dynamic range of pupil dynamics in SERT KO mice.

It is important to note that transgenic animals lacking functional SERT variant might display various deficits beyond serotonergic system. They might arise, in part, due to the compensatory mechanisms during the development. Therefore, it would be important for future studies to use specific 5-HT receptor agonists/antagonists or transient pharmacological/optogenetic manipulations to establish a direct link between serotonin signaling and visual processing and learning.

The major findings of our study were related to impaired tuning after visual learning. Given that we observed largely intact tuning properties in single units in naïve SERT mice, similar oscillatory dynamics in LFP after visual learning in all groups, and similar pupil responses to familiar stimuli, it is likely that altered serotonin signaling is one of the major factors underlying our observations.

In conclusion, we provide evidence for the impaired fine-tuning of cortical selectivity and longer familiarity-evoked theta-locked spiking activity following perceptual experience in V1 of SERT-deficient mice. Our findings suggest that 5-HT signaling may be involved in the experience-dependent refinement of cortical circuitry and encoding of visual familiarity in mice. Future studies will dissect the molecular and circuit mechanisms of this signaling in V1 cortical plasticity.

2.9 References

Albrecht, D. G., & Hamilton, D. B. (1982). Striate cortex of monkey and cat: contrast response function. *Journal of Neurophysiology, 48*(1), 217-237. doi:10.1152/jn.1982.48.1.217

Ansorge, M. S., Zhou, M., Lira, A., Hen, R., & Gingrich, J. A. (2004). Early-Life Blockade of the 5-HT Transporter Alters Emotional Behavior in Adult Mice. *Science, 306*(5697), 879-881. doi:10.1126/science.1101678

Bengel, D., Murphy, D. L., Andrews, A. M., Wichems, C. H., Feltner, D., Heils, A., . . . Lesch, K.-P. (1998). Altered Brain Serotonin Homeostasis and Locomotor Insensitivity to 3,4-Methylenedioxymethamphetamine ("Ecstasy") in Serotonin Transporter-Deficient Mice. *Molecular Pharmacology, 53*(4), 649-655. doi:10.1124/mol.53.4.649

Berthoux, C., Barre, A., Bockaert, J., Marin, P., & Bécamel, C. (2019). Sustained Activation of Postsynaptic 5-HT2A Receptors Gates Plasticity at Prefrontal Cortex Synapses. *Cerebral cortex (New York, N.Y. : 1991), 29*(4), 1659-1669. doi:10.1093/cercor/bhy064

Brigman, J. L., Mathur, P., Harvey-White, J., Izquierdo, A., Saksida, L. M., Bussey, T. J., . . . Holmes, A. (2009). Pharmacological or Genetic Inactivation of the Serotonin Transporter Improves Reversal Learning in Mice. *Cerebral Cortex, 20*(8), 1955-1963. doi:10.1093/cercor/bhp266

Celada, P., Puig, M. V., & Artigas, F. (2013). Serotonin modulation of cortical neurons and networks. *Frontiers in Integrative Neuroscience, 7*(25). doi:10.3389/fnint.2013.00025

Chubykin, A. A., Roach, E. B., Bear, M. F., & Shuler, M. G. (2013). A cholinergic mechanism for reward timing within primary visual cortex. *Neuron, 77*(4), 723-735. doi:10.1016/j.neuron.2012.12.039

Cohen, J. Y., Amoroso, M. W., & Uchida, N. (2015). Serotonergic neurons signal reward and punishment on multiple timescales. *eLife, 4*, e06346. doi:10.7554/eLife.06346

Cohen, M. X. (2014). *Analyzing neural time series data: theory and practice*: MIT press.

Cooke, S. F., & Bear, M. F. (2010). Visual Experience Induces Long-Term Potentiation in the Primary Visual Cortex. *The Journal of Neuroscience, 30*(48), 16304-16313. doi:10.1523/jneurosci.4333-10.2010

Cooke, S. F., Komorowski, R. W., Kaplan, E. S., Gavornik, J. P., & Bear, M. F. (2015). Visual recognition memory, manifested as long-term habituation, requires synaptic plasticity in V1. *Nat Neurosci, 18*(2), 262-271. doi:10.1038/nn.3920

Frenkel, M. Y., Sawtell, N. B., Diogo, A. C., Yoon, B., Neve, R. L., & Bear, M. F. (2006). Instructive effect of visual experience in mouse visual cortex. *Neuron, 51*(3), 339-349. doi:10.1016/j.neuron.2006.06.026

Gavornik, J. P., & Bear, M. F. (2014). Learned spatiotemporal sequence recognition and prediction in primary visual cortex. *Nat Neurosci, 17*(5), 732-737. doi:10.1038/nn.3683 http://www.nature.com/neuro/journal/v17/n5/abs/nn.3683.html#supplementary-information

Gilbert, C. D., & Li, W. (2012). Adult visual cortical plasticity. *Neuron, 75*(2), 250-264. doi:10.1016/j.neuron.2012.06.030

Goel, A., Cantu, D. A., Guilfoyle, J., Chaudhari, G. R., Newadkar, A., Todisco, B., . . . Portera-Cailliau, C. (2018). Impaired perceptual learning in a mouse model of Fragile X syndrome is mediated by parvalbumin neuron dysfunction and is reversible. *Nat Neurosci, 21*(10), 1404-1411. doi:10.1038/s41593-018-0231-0

Gu, Q. (2002). Neuromodulatory transmitter systems in the cortex and their role in cortical plasticity. *Neuroscience, 111*(4), 815-835. doi:10.1016/s0306-4522(02)00026-x

Hawken, M. J., & Parker, A. J. (1987). Spatial properties of neurons in the monkey striate cortex. *Proceedings of the Royal Society of London. Series B, Biological sciences, 231*(1263), 251-288. doi:10.1098/rspb.1987.0044

He, K., Huertas, M., Hong, Su Z., Tie, X., Hell, Johannes W., Shouval, H., & Kirkwood, A. (2015). Distinct Eligibility Traces for LTP and LTD in Cortical Synapses. *Neuron, 88*(3), 528-538. doi:10.1016/j.neuron.2015.09.037

Hua, T., Bao, P., Huang, C.-B., Wang, Z., Xu, J., Zhou, Y., & Lu, Z.-L. (2010). Perceptual learning improves contrast sensitivity of V1 neurons in cats. *Curr Biol, 20*(10), 887-894. doi:10.1016/j.cub.2010.03.066

Huttunen, H. J., Palva, J. M., Lindberg, L., Palva, S., Saarela, V., Karvonen, E., . . . Uusitalo, H. (2018). Fluoxetine does not enhance the effect of perceptual learning on visual function in adults with amblyopia. *Scientific Reports, 8*(1), 12830-12830. doi:10.1038/s41598-018-31169-z

Jurjut, O., Georgieva, P., Busse, L., & Katzner, S. (2017). Learning Enhances Sensory Processing in Mouse V1 before Improving Behavior. *The Journal of Neuroscience, 37*(27), 6460-6474. doi:10.1523/jneurosci.3485-16.2017

Kissinger, S. T., Pak, A., Tang, Y., Masmanidis, S. C., & Chubykin, A. A. (2018). Oscillatory Encoding of Visual Stimulus Familiarity. *J Neurosci, 38*(27), 6223-6240. doi:10.1523/JNEUROSCI.3646-17.2018

Kissinger, S. T., Wu, Q., Quinn, C. J., Anderson, A. K., Pak, A., & Chubykin, A. A. (2020). Visual Experience-Dependent Oscillations and Underlying Circuit Connectivity Changes Are Impaired in Fmr1 KO Mice. *Cell Rep, 31*(1), 107486. doi:10.1016/j.celrep.2020.03.050

Kojic, L., Dyck, R. H., Gu, Q., Douglas, R. M., Matsubara, J., & Cynader, M. S. (2000). Columnar distribution of serotonin-dependent plasticity within kitten striate cortex. *Proceedings of the National Academy of Sciences, 97*(4), 1841-1844. doi:10.1073/pnas.97.4.1841

Kreile, A. K., Bonhoeffer, T., & Hübener, M. (2011). Altered visual experience induces instructive changes of orientation preference in mouse visual cortex. *The Journal of neuroscience : the official journal of the Society for Neuroscience, 31*(39), 13911-13920. doi:10.1523/JNEUROSCI.2143-11.2011

Lagas, A., Black, J., Russell, B., Kydd, R., & Thompson, B. (2019). The Effect of Combined Patching and Citalopram on Visual Acuity in Adults with Amblyopia: A Randomized, Crossover, Placebo-Controlled Trial. *Neural plasticity, 2019*, 5857243. doi:10.1155/2019/5857243

Lanfumey, L., La Cour, C. M., Froger, N., & Hamon, M. (2000). 5-HT-HPA Interactions in Two Models of Transgenic Mice Relevant to Major Depression. *Neurochemical Research, 25*(9), 1199-1206. doi:10.1023/A:1007683810230

Lira, A., Zhou, M., Castanon, N., Ansorge, M. S., Gordon, J. A., Francis, J. H., . . . Gingrich, J. A. (2003). Altered depression-related behaviors and functional changes in the dorsal raphe nucleus of serotonin transporter-deficient mice. *Biological Psychiatry, 54*(10), 960-971. doi:10.1016/s0006-3223(03)00696-6

Lottem, E., Banerjee, D., Vertechi, P., Sarra, D., Lohuis, M. o., & Mainen, Z. F. (2018). Activation of serotonin neurons promotes active persistence in a probabilistic foraging task. *Nature Communications, 9*(1), 1000. doi:10.1038/s41467-018-03438-y

Lottem, E., Lörincz, M. L., & Mainen, Z. F. (2016). Optogenetic Activation of Dorsal Raphe Serotonin Neurons Rapidly Inhibits Spontaneous But Not Odor-Evoked Activity in Olfactory Cortex. *The Journal of Neuroscience, 36*(1), 7-18. doi:10.1523/jneurosci.3008-15.2016

Makino, H., & Komiyama, T. (2015). Learning enhances the relative impact of top-down processing in the visual cortex. *Nature Neuroscience, 18*(8), 1116-1122. doi:10.1038/nn.4061

Mathis, A., Mamidanna, P., Cury, K. M., Abe, T., Murthy, V. N., Mathis, M. W., & Bethge, M. (2018). DeepLabCut: markerless pose estimation of user-defined body parts with deep learning. *Nature Neuroscience, 21*(9), 1281-1289. doi:10.1038/s41593-018-0209-y

Matias, S., Lottem, E., Dugué, G. P., & Mainen, Z. F. (2017). Activity patterns of serotonin neurons underlying cognitive flexibility. *eLife, 6*, e20552. doi:10.7554/eLife.20552

Maya Vetencourt, J. F., Sale, A., Viegi, A., Baroncelli, L., De Pasquale, R., O'Leary, O. F., . . . Maffei, L. (2008). The antidepressant fluoxetine restores plasticity in the adult visual cortex. *Science (New York, N.Y.), 320*(5874), 385-388. doi:10.1126/science.1150516

Miceli, S., Nadif Kasri, N., Joosten, J., Huang, C., Kepser, L., Proville, R., . . . Schubert, D. (2017). Reduced Inhibition within Layer IV of Sert Knockout Rat Barrel Cortex is Associated with Faster Sensory Integration. *Cerebral cortex (New York, N.Y. : 1991), 27*(2), 933-949. doi:10.1093/cercor/bhx016

Michaiel, A. M., Parker, P. R. L., & Niell, C. M. (2019). A Hallucinogenic Serotonin-2A Receptor Agonist Reduces Visual Response Gain and Alters Temporal Dynamics in Mouse V1. *Cell Rep, 26*(13), 3475-3483.e3474. doi:10.1016/j.celrep.2019.02.104

Murphy, D. L., & Lesch, K.-P. (2008). Targeting the murine serotonin transporter: insights into human neurobiology. *Nature Reviews Neuroscience, 9*(2), 85-96. doi:10.1038/nrn2284

Niell, C. M., & Stryker, M. P. (2008). Highly Selective Receptive Fields in Mouse Visual Cortex. *The Journal of Neuroscience, 28*(30), 7520-7536. doi:10.1523/jneurosci.0623-08.2008

Pachitariu, M., Steinmetz, N., Kadir, S., Carandini, M., & Harris, K. (2016). *Fast and accurate spike sorting of high-channel count probes with KiloSort.* Paper presented at the Proceedings of the 30th International Conference on Neural Information Processing Systems, Barcelona, Spain.

Peirce, J. W. (2009). Generating Stimuli for Neuroscience Using PsychoPy. *Frontiers in Neuroinformatics, 2*, 10-10. doi:10.3389/neuro.11.010.2008

Poort, J., Khan, A. G., Pachitariu, M., Nemri, A., Orsolic, I., Krupic, J., . . . Hofer, S. B. (2015). Learning Enhances Sensory and Multiple Non-sensory Representations in Primary Visual Cortex. *Neuron, 86*(6), 1478-1490. doi:10.1016/j.neuron.2015.05.037

Puig, M. V., Artigas, F., & Celada, P. (2004). Modulation of the Activity of Pyramidal Neurons in Rat Prefrontal Cortex by Raphe Stimulation In Vivo: Involvement of Serotonin and GABA. *Cerebral Cortex, 15*(1), 1-14. doi:10.1093/cercor/bhh104

Ringach, D. L., Shapley, R. M., & Hawken, M. J. (2002). Orientation selectivity in macaque V1: diversity and laminar dependence. *The Journal of neuroscience : the official journal of the Society for Neuroscience, 22*(13), 5639-5651. doi:10.1523/JNEUROSCI.22-13-05639.2002

Rossant, C., Kadir, S. N., Goodman, D. F. M., Schulman, J., Hunter, M. L. D., Saleem, A. B., . . . Harris, K. D. (2016). Spike sorting for large, dense electrode arrays. *Nature Neuroscience, 19*(4), 634-641. doi:10.1038/nn.4268

Scholl, B., Tan, A. Y. Y., Corey, J., & Priebe, N. J. (2013). Emergence of orientation selectivity in the Mammalian visual pathway. *The Journal of neuroscience : the official journal of the Society for Neuroscience, 33*(26), 10616-10624. doi:10.1523/JNEUROSCI.0404-13.2013

Sharif, M. H., Talebnejad, M. R., Rastegar, K., Khalili, M. R., & Nowroozzadeh, M. H. (2019). Oral fluoxetine in the management of amblyopic patients aged between 10 and 40 years old: a randomized clinical trial. *Eye (London, England), 33*(7), 1060-1067. doi:10.1038/s41433-019-0360-z

Shobe, J. L., Claar, L. D., Parhami, S., Bakhurin, K. I., & Masmanidis, S. C. (2015). Brain activity mapping at multiple scales with silicon microprobes containing 1,024 electrodes. *Journal of neurophysiology, 114*(3), 2043-2052. doi:10.1152/jn.00464.2015

Shuler, M. G., & Bear, M. F. (2006). Reward timing in the primary visual cortex. *Science, 311*(5767), 1606-1609. doi:10.1126/science.1123513

Sora, I., Wichems, C., Takahashi, N., Li, X. F., Zeng, Z., Revay, R., . . . Uhl, G. R. (1998). Cocaine reward models: conditioned place preference can be established in dopamine- and in serotonin-transporter knockout mice. *Proc Natl Acad Sci U S A, 95*(13), 7699-7704. doi:10.1073/pnas.95.13.7699

Virtanen, P., Gommers, R., Oliphant, T. E., Haberland, M., Reddy, T., Cournapeau, D., . . . SciPy, C. (2020). SciPy 1.0: fundamental algorithms for scientific computing in Python. *Nature Methods*. doi:10.1038/s41592-019-0686-2

Wang, Y., Gu, Q., & Cynader, M. S. (1997). Blockade of serotonin-2C receptors by mesulergine reduces ocular dominance plasticity in kitten visual cortex. *Experimental brain research, 114*(2), 321-328. doi:10.1007/pl00005640

William Moreau, A., Amar, M., Le Roux, N., Morel, N., & Fossier, P. (2009). Serotoninergic Fine-Tuning of the Excitation–Inhibition Balance in Rat Visual Cortical Networks. *Cerebral Cortex, 20*(2), 456-467. doi:10.1093/cercor/bhp114

Xiang, Z., & Prince, D. A. (2003). Heterogeneous actions of serotonin on interneurons in rat visual cortex. *J Neurophysiol, 89*(3), 1278-1287. doi:10.1152/jn.00533.2002

Zhou, F. C., Lesch, K.-P., & Murphy, D. L. (2002). Serotonin uptake into dopamine neurons via dopamine transporters: a compensatory alternative. *Brain Research, 942*(1), 109-119. doi:https://doi.org/10.1016/S0006-8993(02)02709-9

Zold, C. L., & Hussain Shuler, M. G. (2015). Theta Oscillations in Visual Cortex Emerge with Experience to Convey Expected Reward Time and Experienced Reward Rate. *The Journal of Neuroscience, 35*(26), 9603-9614. doi:10.1523/JNEUROSCI.0296-15.2015

CHAPTER 3. TOP-DOWN FEEDBACK CONTROLS THE CORTICAL REPRESENTATION OF ILLUSORY CONTOURS IN MOUSE PRIMARY VISUAL CORTEX

Adopted from: Pak, A., Ryu, E., Li, C., & Chubykin, A. A. (2020). Top-Down Feedback Controls the Cortical Representation of Illusory Contours in Mouse Primary Visual Cortex. The Journal of neuroscience : the official journal of the Society for Neuroscience, 40(3), 648–660. https://doi.org/10.1523/JNEUROSCI.1998-19.2019

3.1 Abstract

Visual systems have evolved to recognize and extract features from complex scenes using limited sensory information. Contour perception is essential to this process and can occur despite breaks in the continuity of neighboring features. Such robustness of the animal visual system to degraded or occluded shapes may also give rise to an interesting phenomenon of optical illusions. These illusions provide a great opportunity to decipher neural computations underlying contour integration and object detection. Kanizsa illusory contours have been shown to evoke responses in the early visual cortex despite the lack of direct receptive field activation. Recurrent processing between visual areas has been proposed to be involved in this process. However, it is unclear whether higher visual areas directly contribute to the generation of illusory responses in the early visual cortex. Using behavior, in vivo electrophysiology and optogenetics, we first show that the primary visual cortex (V1) of male mice responds to Kanizsa illusory contours. Responses to Kanizsa illusions emerge later than the responses to the contrast-defined real contours in V1. Second, we demonstrate that illusory responses are orientation-selective. Finally, we show that top-down feedback controls the neural correlates of illusory contour perception in V1. Our results suggest that higher-order visual areas may fill in the missing information in the early visual cortex necessary for illusory contour perception.

3.2 Introduction

Contours contain essential information about the shapes of objects in the environment. Correct identification of these objects in the visual scene and their segregation from the background are necessary for animal survival. Consequently, the visual system has developed the ability to recognize shapes in diverse conditions, including various levels of illumination, colors, texture,

and crowding (Nieder, 2002; Wyatte, Jilk, & O'Reilly, 2014). One example of this ability is the perception of illusory (or subjective) contours, such as those found in Kanizsa's triangle (Gaetano Kanizsa, 1976). If three "pacmen" inducers are arranged in a particular configuration, one can perceive a triangle despite the lack of a physical basis for that triangle. If these illusory contours are positioned on the receptive field (RF) of a neuron, no neural response is expected because there is no bottom-up input directly activating that RF. However, single-unit recordings in cats and primates have demonstrated that a subset of neurons in early visual cortex responds to subjective contours similarly to real lines (Grosof, Shapley, & Hawken, 1993; Lee & Nguyen, 2001; Peterhans & von der Heydt, 1989; Sheth, Sharma, Rao, & Sur, 1996; von der Heydt & Peterhans, 1989). Importantly, responses in the secondary visual area V2 emerged earlier compared to V1 (Lee & Nguyen, 2001). Furthermore, recurrent processing is involved in the perception of various illusions across species, suggesting that higher-order processing may be important for the generation of illusory perception. (De Weerd, Desimone, & Ungerleider, 2009; Luo et al., 2019; Mendola, Dale, Fischl, Liu, & Tootell, 1999; Murray et al., 2002; Pan et al., 2012). These observations led to the hypothesis that top-down feedback from V2 might supply the missing information about subjective contours to V1.

Several recent studies support the importance of top-down feedback in learning and perception (Bar et al., 2006; Gilbert & Li, 2013; Li, Piëch, & Gilbert, 2004; Polley, Steinberg, & Merzenich, 2006; Schnabel et al., 2018; Wyatte, Curran, & O'Reilly, 2012). However, it is poorly understood at the mechanistic level how top-down feedback influences sensory processing in cases where there is no bottom-up input. We decided to test the hypothesis that top-down feedback supplies missing information about subjective contours to V1 and dissect the neural circuits involved in this process.

Here, we first show that mice can learn to discriminate between Kanizsa illusory contours. Second, mouse V1 responds to Kanizsa illusory contours at the population level. Illusory responses emerge later than the responses to the contrast-defined contours in V1. Third, we demonstrate that illusory responses are orientation selective. Finally, we provide neurophysiological evidence that neural correlates of illusory contour perception can be downregulated by optogenetic inhibition of lateromedial area.

3.3 Materials and Methods

3.3.1 Mice

All animal procedures were approved by the Purdue University Animal Care and Use Committee (PACUC). Animals were group-housed on a 12 hr light/dark cycle with full water and food access. 12 male C57BL/6 mice (Jackson Lab) aged 2-4 month were used for behavioral studies. 2-3 month-old 10 males and 3 females were used for optogenetic experiments. 2-month-old 5 male animals were used for illusory contours orientation tuning experiments.

3.3.2 Initial surgery and viral injections

Surgical procedures were done as previously described (Kissinger, Pak, Tang, Masmanidis, & Chubykin, 2018). Briefly, 1-month-old animals were induced with 5% isoflurane and maintained at 1.5-2% isoflurane during surgery. They were placed on a motorized stereotaxic apparatus (Neurostar). Animal body temperature was controlled using a heating pad. The scalp was opened to expose the lambda and bregma sutures. A small head post and a reference pin were installed 3.5 and 0.2 mm anterior of the bregma, respectively. Neurostar software with an integrated mouse brain atlas was used to mark coordinates above V1 (from lambda AP 0.8 mm, LM: ±3.1 mm) and lateromedial area (from lambda AP 1.4mm, LM ±4.1 mm). A small craniotomy was drilled above LM for a viral injection. A glass micropipette was loaded with undiluted AAV5-CAG-ArchT-GFP-WPRE (Addgene, cat # 29777-AAV5). Injections were performed at 60 nl/min using Nanoject II (Drummond Scientific) at two depths: 0.7 and 0.3 mm below the cortical surface. 25 or 50 nl of the virus was injected at each depth and 5 min was allowed before the glass pipette was withdrawn. We found that both of these concentrations resulted in a localized injection. Medical grade Metabond™ was then used to seal exposed areas of the scalp to form a head cap. Animals usually recovered within 30 min after surgery and were followed for 3 days.

3.3.3 Behavioral training paradigm

Mice were trained to an operant conditioning paradigm through which they learned to discriminate between two visual stimuli, illusory bars in opposite orientations (45 vs 135 deg). The mice advanced through a sequence of pre-training, training, and transfer testing sessions, designed for them to progress from simple visual discrimination tasks to more complex ones. The entire

training process lasted about 8 weeks. Training sessions took place in three Sound Attenuation chambers (Lafayette Instrument Series 83017, 83018) for a duration of 30 minutes. Each chamber contains a reward tray with an indicator light, a water pump attached to the reward tray (Campden Instruments Calibrate-able Liquid Pump Model 80204-0.5), and a touchscreen display (Planar PLL2010MW LED LCD Monitor). ABET II VideoTouch software (Lafayette Instrument, http://lafayetteneuroscience.com/products/abetii-touch-audio-video-stimulus) was used to design and execute each stage, and WhiskerServer (Cambridge University Technical Services Ltd, http://whiskercontrol.com) was used to set up hardware functionality, e.g., water pump, screen display.

Each mouse was put on water restriction to ensure high motivation during training sessions. Water bottles were removed from the cages, while food pellets were available for free feeding. The mice were each given 900 µL water daily in a small falcon tube cap. Pre-training sessions began once all mice were within 75-85% of their original weights, which was 7 days after the start of water restriction. Mice were given a total of 1000 µL water daily, so usually, additional water was given following training sessions. Their weights were recorded every day from the start of water restriction to the end of the training, and the amount of water given at the end of a session was adjusted if a mouse was outside of the desired range.

Pre-training: Pre-training consisted of five stages that familiarized the mice with the chamber. The first stage was a free reward stage, where a 160 µL water reward was given every 5 minutes. The reward tray was locked in the open position and the tray light remained on during the entire session. After three sessions of Pre-training Stage 1, mice moved on to Pre-training Stage 2. Mice were given a 20 µL reward at the start of the session, and then each time 30 s after a reward was collected. Rewards were signaled by the reward tray light, and the tray was no longer locked during this stage. Mice passed this stage if they reached at least 20 trials in one session, indicating competence retrieving rewards. All mice passed Pre-training Stage 2 in 1 session. In each trial of Pre-training Stages 3, 4, and 5, a white square on a black background was displayed to one side of the screen that was pseudorandomly determined. If the side containing the square was touched, it was counted as a correct response. In Pre-training Stage 3, the white square was presented to one side of the screen. After an incorrect response or 30s without a response, a 10 µL reward was given. After a correct response, a 20 µL reward was given to encourage the same behavior. To pass the stage, the mice had to reach at least 20 trials in one session and pass two consecutive sessions. All

mice passed Pre-training Stage 3 in 2 sessions. In Pre-training Stage 4, or the Must Touch stage, the white square was presented and remained on the screen until the correct side was touched. Once touched, a 20 µL reward was given. Mice passed if they reached at least 20 trials in one session. On average, the mice passed in 1.2 sessions. The last stage of Pre-training was Stage 5, or the Must Initiate stage, where mice had to initiate trials with head entry to the reward tray. Incorrect responses to the blank side prompted a 20s timeout and subsequent correction trial, which displayed the image in the same position each trial until a correct response was made. A 20 µL reward was given for correct responses, and a 10 µL reward was given for correct correction responses. To pass, mice had to reach at least 75% performance on normal trials, or non-correction trials averaged over two consecutive days. On average, the mice took 4 sessions to pass Pre-training Stage 5. In Pre-training Stages 2, 3, 4, and 5, the intertrial interval (ITI) was 30 s. Once a mouse passed the last Pre-training stage, it proceeded to Training Stage 1.

Training: Training consisted of three stages designed for the mice to learn to discriminate between illusory bars of 45° and 135° orientations, where the 135° bar was the correct image. In each stage, mice were required to initiate trials with a nose poke to the reward tray, which prompted the images to be displayed in pseudorandom positions. Correct responses were rewarded with 20 µL water while correct correction responses were rewarded with 10 µL. The ITI was 5s, and incorrect touches prompted a 15s timeout. The passing criteria for each stage were at least 75% performance on normal trials averaged over two days, with at least 65% performance each day. In Stage 1, two black illusory bars were presented, each composed of two white pacmen inducers on a black background. In Stage 2, the illusory bars were presented with two distractor inducers added to each image. Stage 3 used the same stimuli as in Stage 2 and included a color inverted version, in which the inducers were black and the background was white. The color scheme of each trial was pseudorandom and was not presented more than three times in a row. Once a mouse passed Stage 3, it advanced to the transfer testing stage.

Transfer testing: Stage 4, or the transfer testing stage, incorporated real bar transfer tests into the Stage 3 training trials to test if the mice had learned to distinguish between the two illusory bars rather than to focus solely on local stimuli. During training trials, stimuli, rewards, ITI, and timeouts were administered exactly as they were in Stage 3. Testing trials were interleaved every five correct responses during normal trials, and two real bars at 45° and 135° orientations were presented. Both stimuli positions and color scheme for real bar testing trials were pseudorandomly

determined. No reward was given after testing trials, regardless of correct or incorrect responses. Following responses to testing trial stimuli, there was a 5 s ITI before the next training trial. Mice continued in Stage 4 until they accumulated at least 30 testing trials across all sessions.

Control testing: In addition to Stage 4 transfer testing, the mice were also subjected to a control test of differentiating two visual stimuli with rotated distractor inducers. Retaining the Stage 3 training trials exactly as they were, control trials were incorporated after every five correct responses during normal trials. During control trials, the two illusory bars were each shown with two distractor inducers rotated at angles perpendicular to those in Stages 2, 3, and 4. The stimuli positions and color scheme for control trials were pseudorandomly determined.

3.3.4 Pre-recording surgery

3 weeks after the viral injection, electrophysiological experiments were performed. 2-month-old mice were induced with 5% isoflurane and placed on the stereotaxic apparatus. Two small craniotomies were performed under 1.5% isoflurane anesthesia: one above V1 and another one above LM. Mice were then transferred to the recording room and head-fixed in the apparatus in front of the monitor.

3.3.5 Electrophysiology

Animals were habituated in a head-fixation set-up for at least three days before the actual experiment. We used 64-channel silicon probes (Shobe, Claar, Parhami, Bakhurin, & Masmanidis, 2015) (channel separation: vertical 25 µm, horizontal 20 µm, 3 columns, 1.05 mm in length) for acute extracellular electrophysiology in awake head-fixed mice. The probe was inserted only once per hemisphere so that each animal went through a maximum of two recording sessions. Data acquisition was performed at 30 kHz using OpenEphys hardware and software. Recordings were triggered by a TTL signal sent from an Arduino UNO board. PsychoPy software was used to present visual stimuli and trigger both electrophysiology recordings and laser stimulation. This was achieved through serial communication (pyserial package) with Arduino boards. The typical experiment lasted for about 2 hours. 30 min for the electrode to settle down, 15 min for RF mapping with locally sparse noise, 40 min for spike detection/sorting, RF analysis, and alignment of RF maps with the Kanizsa figure, 30 min for recording blocks with the Kanizsa illusion.

3.3.6 Histology

Mice were anesthetized with 100 mg/kg ketamine and 16 mg/kg xylazine solution. They were perfused transcardially with 4% paraformaldehyde. After decapitation, their brain was extracted and sliced in 0.1 mm in PBS using a vibratome. Coronal slices were mounted on slides and imaged on a fluorescence scope. We verified the expression of the GFP in LM (visual lateromedial area in the atlas) but not in V1 by aligning slice images with the mouse atlas (Allen Institute). Histology was performed for all animals to verify GFP expression.

3.3.7 Optogenetic stimulation

We used a 532 nm DPSS laser (OEM Laser Systems) for all optogenetic experiments. The light was delivered through an optical fiber (200 µm, NA 0.39) coupled to the laser through patch cable (Thorlabs, SMA connection and 1.25 mm ceramic ferrules at the ends). Laser power was measured using a Powermeter (Thorlabs) before each experiment. We typically used 8-15 mW of continuous laser stimulation to activate ArchT for 0.8s starting at -0.1s and ending at 0.7a relative to the test stimulus onset. The laser was triggered by a TTL signal from the Arduino board interacting with the running visual stimulation software PsychoPy via serial communication. To protect mouse eyes from laser stimulation and minimize light artifacts on the electrode, we painted optical fibers with black ink and covered the connection between ferrules with foil. Optogenetic trials were interleaved with regular trials.

3.3.8 Visual stimulation

PsychoPy, open-source Psychology software in Python, was used to generate and present all visual stimulations (Peirce, 2009). We used a gamma calibrated monitor (22’ ViewSonic VX2252, 60 Hz) for stimulus presentation. The mean luminance of the monitor was 30 cd/m^2. The monitor was positioned 17 cm in front of the mouse to ensure the binocular presentation of the stimuli. The size of the illusory and white squares was 44.4 degrees, the width of the black line was 1 degree, and the radius of the circular disc was 9.2 degrees. There was a 26 degrees gap between inducers that formed the Kanizsa square illusion. Each trial lasted for 2 seconds. Each recording session consisted of 200 trials, 4 test stimuli x (25 regular + 25 optogenetic) trials. Four circular discs were presented first at 0.5s, then they abruptly changed to one of the test stimuli at 1 s. Four test

stimuli included a Kanizsa square with illusory contours (KIC), rotated corners control (ROT), a filled white square (SQR), and a black square line (LINE). Each test stimulus was presented for 0.5 s. Stimuli were presented in a pseudorandom manner; optogenetic trials were interleaved with regular trials. Two blocks of 200 trials (25 trials for each condition) were presented. The first block was used to pre-expose animals to test stimuli, both illusory and real squares were shown. Neural responses from the second block were included in the final analysis. For a receptive field (RF) mapping, we used a locally sparse noise with 3.55 degrees black/white squares (Zhuang et al., 2017). In total, 3002 different frames were presented to the animal. Each frame contained 3-5 black/white squares and lasted for 150 ms. After recording, spike detection and sorting were performed (see Analysis of units). We then computed the spike-triggered average (STA) map for each recorded neuron. A putative RF map was identified by finding the hotspot in the map. After that, we manually aligned the Kanisza square with RF maps in Adobe Illustrator, so that the illusory contour was on the RF, but inducers were outside it. We tried different coordinates for the Kanizsa square presentation in PsychoPy and used the one that aligned with the majority of units. Depending on the location of the RF, we positioned subjective contours either in a horizontal or vertical orientation, which is different from the previous single unit studies (KIC of preferred orientation was presented). This was done because we recorded many units at the same time and could not adjust the orientation and position for each cell.

To test the orientation selectivity of KIC, we made several adjustments to our experimental design. First, we used a bigger monitor (27’ ViewSonic VA2746, 60 Hz) with 1920x1080 resolution binocularly positioned at 17 cm viewing distance. Second, we used 3.96 degrees black/white squares for RF mapping. The radius of inducers was 6.6 degrees and the square was 33x33 degrees. There was a 20 degrees gap between inducers. The line width was 0.83 degrees. Third, we recorded 8 drifting gratings before KIC sessions to obtain direction tuning curves. KIC of four different orientations (0, 45, 90, and 135 deg) were presented to the animal. Overall, we had 16 different stimuli (4 test stimuli x 4 different orientations). Test stimuli were presented in a pseudorandom manner, each stimulus was presented for at least 25 trials.

We generally observed a good correspondence of RF positions across cortical depth (**Figure 16**). To quantify the size of the receptive fields, we performed a thresholding of STA RF maps and then fit a two-dimensional (2D) Gaussian function (**Figure 16**). Thresholding was done by identifying outlier pixels that were brighter/darker (On/Off) than 97.5% of pixels within the map.

All other pixels were masked and not considered for further analysis. A 2D Gaussian was fitted with optimize.curvefit function from the Python Scipy library. Starting parameters such as x-,y-position of the center and amplitude were calculated from the thresholded map, whereas initial sigma was set to 20. RF size was calculated by averaging a half-width at half maximum of two axes of the 2D Gaussian fit. Depending on the recording, we were able to obtain On RF maps for about 50% and Off maps for 12% of neurons. Given the size of the squares used in the RF mapping, it is possible that they best worked for obtaining RF maps of particular units. As it was reported previously, there is a big diversity in the shape and size of RF maps of mouse V1 neurons. (Niell & Stryker, 2008).

3.3.9 Analysis of units

We used Kilosort software for spike detection and sorting. It implements a template matching algorithm written in Matlab that allows GPU acceleration (Pachitariu, Steinmetz, Kadir, Carandini, & Harris, 2016). Speed and quality of the spike sorting were important for our experimental design because the RF mapping and analysis were a critical step to properly position the Kanizsa square. We used default configuration parameters but the standard deviation for spike detection was changed from -4 to -6. Templates were initialized from the data. Kilosort was run on NVIDIA GeForce GTX960 on Windows 10 running machine. Results were visualized with Klusta/Phy software to manually remove, split, and merge units (Rossant et al., 2016). Units were excluded from the further analysis in case they had less than 100 spikes for each testing condition, more than 5% of spikes violated absolute refractory period, aberrantly shaped waveform. Splitting and merging required more manual curation and was done according to the guide available online (https://github.com/kwikteam/phy-contrib/blob/master/docs/template-gui.md). We also used Kilosort2 for a subset of data. Both algorithms gave qualitatively the same result, but Kilosort2 required less manual curation. RF mapping and the Kanizsa figure recording blocks were concatenated and clustered together so that we were able to track single units across time. All further analysis was done in Python 2.7 using custom written Jupyter Notebooks and publicly available packages including numpy, pandas, scipy, and seaborn. Peristimulus time histograms (PSTH) were generated by binning spike times with a 10 ms window and convolving with a Gaussian kernel (width 100 ms). Z-score (z = (FR – mean FR)/SD FR), where FR represents a firing rate during the whole trial, so that mean and standard deviation (SD) were computed for the

whole 2 s period of the trial. We computed a response modulation indices for KIC: I_m (X) = (FR KIC – FR X)/(FR KIC + FR X), where X is firing rate (FR) to the circular discs - I_m (CIR), rotated corners – I_m (ROT), or to the subjective contours during the laser stimulation – I_m (laser). Mean firing rate was calculated by averaging a response between 50 and 500 ms after stimulus onset. These indices range from -1 to 1 with positive values indicating a stronger response to the illusory contours and negative ones vice versa. To identify illusory responsive units, we first found units that were not significantly modulated by CIR. We used Wilcoxon signed-rank test to compare baseline firing rate (0.05-0.5 s) vs CIR (0.55-1 s) response during KIC trials. Second, we used selected units with a positive I_m (CIR) indices. This was done to remove CIR responsive units that were not eliminated by the first criteria. Careful examination of those units revealed that they initially increased their response to CIR (50-200 ms) and then their firing rate dropped below the baseline activity (200-500 ms). This is why their CIR response was not significantly different from the baseline. For experiments with KIC of different orientations, we selected units that had minimal response to CIR in at least two orientations and were illusory responsive. Given that KIC position was not adjusted separately for every unit, it was challenging to find units that did not respond to CIR in all four orientations. This is why we allowed small CIR responses in a subset of conditions. To adjust for these CIR responses, we used I_m(CIR) modulation indices that represent test stimuli responses normalized by CIR response.

For a direction tuning using drifting grating stimuli, we averaged responses for each direction between 0.35-0.8 s. For the orientation tuning, responses were averaged between opposite directions. To construct a population tuning curve, we first identified a preferred orientation (the one with the maximal response). After that, we averaged tuning curves aligned by their preferred orientation, so that 0 degrees represents the responses to the preferred orientation. All other orientations were then presented relative to the preferred one. To compute putative population tuning curves for KIC and other test stimuli, we used I_m(CIR) to adjust for possible direct RF activation in a subset of conditions. I_m(CIR) was computed separately for each test stimuli and represents normalized to CIR response. For example, I_m(CIR) for SQR would show how much SQR was upregulated relative to the CIR preceding it. We only included conditions with positive I_m(CIR) values. We averaged putative test stimuli tuning curves aligned on the maximal response. Other orientations were relative to the one with the maximal response.

3.3.10 Statistical Analysis

All statistical tests were performed in Python using scipy.stats. Data were not checked for normality of residuals and only non-parametric tests were used. Kruskal-Wallis test was used to determine whether at least one group median is different from others. It was used to test whether population orientation tuning curves were significantly different. Pairwise Mann-Whitney U tests were used to compare the firing rate to illusory contours vs rotated corners, white square, and black line square. Kolmogorov-Smirnov 2 sample tests were used to compare the distribution of peak times of units, cortical depth, and RF sizes. We used the Wilcoxon signed-rank test to compare the firing rate in response to test stimuli with vs without LM inhibition.

3.4 Behavioral correlates of illusory contour perception in mice

Illusory perception has been described in various species, including insects, birds, and fish (Nieder, 2002). Surprisingly, there are only a couple of studies of illusory perception in rodents (G. Kanizsa, Renzi, Conte, Compostela, & Guerani, 1993; Okuyama-Uchimura & Komai, 2016). A recent report suggests that mice can discriminate illusory bars in a touchscreen-based visual discrimination task (Okuyama-Uchimura & Komai, 2016). Animals were first trained to discriminate between real bars of different orientations in an operant conditioning chamber. After several training stages, they were exposed to transfer trials in which Kanizsa-type illusory bars were presented. Mice were able to discriminate the illusory bars formed by pacmen inducers.

We decided to test whether mice can learn to discriminate between illusory bars of different orientations. Using a similar touchscreen operant conditioning chamber, we trained mice to discriminate between illusory bars formed by two pacmen inducers (**Figure** 1A) (Horner et al., 2013). We then performed a reverse transfer experiment to test whether they can differentiate between two real bars (formed by the luminance contours) that they were not explicitly trained on. Our training paradigm consisted of pre-training and four training stages. Pre-training included habituation of water-restricted animals to the behavioral apparatus. During the first training stage, mice were trained to discriminate between two Kanizsa illusory bars (45 vs 135 deg) formed by pacmen. We then added two additional pacmen, to ensure that animals were not relying on the local configuration of pacmen. During the third stage, we added color inverted versions of our stimuli to equalize luminance distribution across stimuli (**Figure 14B**). During the test stage 1,

trials with illusory and real bars were interleaved. During the test stage 2, we presented illusory bars with rotated distractor pacmen that the animals have not previously seen, to control for the local pacmen inducer configurations. On average, it took animals 7.85 days to pass the Stage 1, which required an average performance of 0.75 over the last two days (**Figure 14D**). Stage 2 and 3 took 5.71 and 6.42 days to pass, respectively. Seven out of twelve animals were able to pass to the test stages. We found that animals had a high performance in normal trials with illusory bars throughout both test stages (**Figure 14E**, mean ± s.e.m performance test 1: 0.76 ± 0.02 (t = 10.7, P = 3.92E-5), test 2: 0.77 ± 0.04 (t = 6.3, P = 0.001), one sample t-test against a chance level of 0.5, n = 7 and 5 mice). They also had a significantly higher than chance performance in the transfer testing trials with real bars (**Figure 14E** (left), mean ± s.e.m performance: 0.63 ± 0.04 (t = 3.03, P = 0.02), one sample t-test against a chance level of 0.5, n = 7) and rotated distractor pacmen (Fig 1E (right), 0.65 ± 0.03 (t = 4.3, P = 0.01), one sample t-test against a chance level of 0.5, n = 5). These results suggest that animals were able to learn to differentiate between illusory bars. In particular, their ability to discriminate real bars strongly supports the idea that mice have learned to differentiate between illusory bars rather than the local features in the stimuli. Our results provide additional behavioral evidence for illusory contour perception in mice.

3.5 Neural correlates of illusory contour perception in mouse V1

To determine whether mouse V1 responds to subjective contours, we performed extracellular electrophysiology with 64 channel silicon probes (Shobe et al., 2015) (Fig 2A,B). We employed a similar visual paradigm as in the prior single-unit and fMRI studies in primates and humans involving the perception of illusory contours in a Kanizsa square (**Figure**. **15C**) (Lee & Nguyen, 2001; Maertens, Pollmann, Hanke, Mildner, & Möller, 2008). The experiment consisted of several stages: 1) RF mapping 2) Spike sorting and RF analysis, 3) alignment of RF maps and Kanizsa illusory contours, and 4) recording responses to Kanizsa illusory contours aligned to the RF. We first mapped RF in mouse V1 using locally sparse noise (Zhuang et al., 2017) (**Figure 16**).

Figure 14. Behavioral correlates of illusory contour perception in mice.

A. Schematic of an operant conditioning chamber with a touchscreen. **B.** The schedule of the behavioral task. Animals were trained to a touchscreen-based visual discrimination task. It consisted of pre-training (see Methods), 3 training stages, and a test stage. During training stages, mice were trained to discriminate between illusory bars of two different orientations (45 vs 135 deg). Stages with additional pacmen and color reversal were added to promote animals to learn global rather than local features of the visual stimuli. **C.** During the test stage 1, normal trials (with illusory bars) were interleaved with testing trials that contained real bars. Test 2 contained rotated distractor pacmen as an additional control for the local pacmen configuration. **D.** Animals (n=7) were able to learn to discriminate illusory bars of different orientations with a high performance (75%). Learning curve by mouse (grey lines) with an overlaid mean (black solid line) shows an increase in performance across several days. **E.** Bar plots show the mean ± s.e.m of the performance during normal and testing trials. High performance was observed in normal trials (illusory bars) in both testing stages. During test stage 1 trials, animals were able to discriminate real bars with a significantly higher than chance performance despite never being explicitly trained to them. Furthermore, during test stage 2 trials, animals were able to discriminate illusory bars despite rotated distractor pacmen. (*P<0.05, **P<0.01, ***P<0.001)

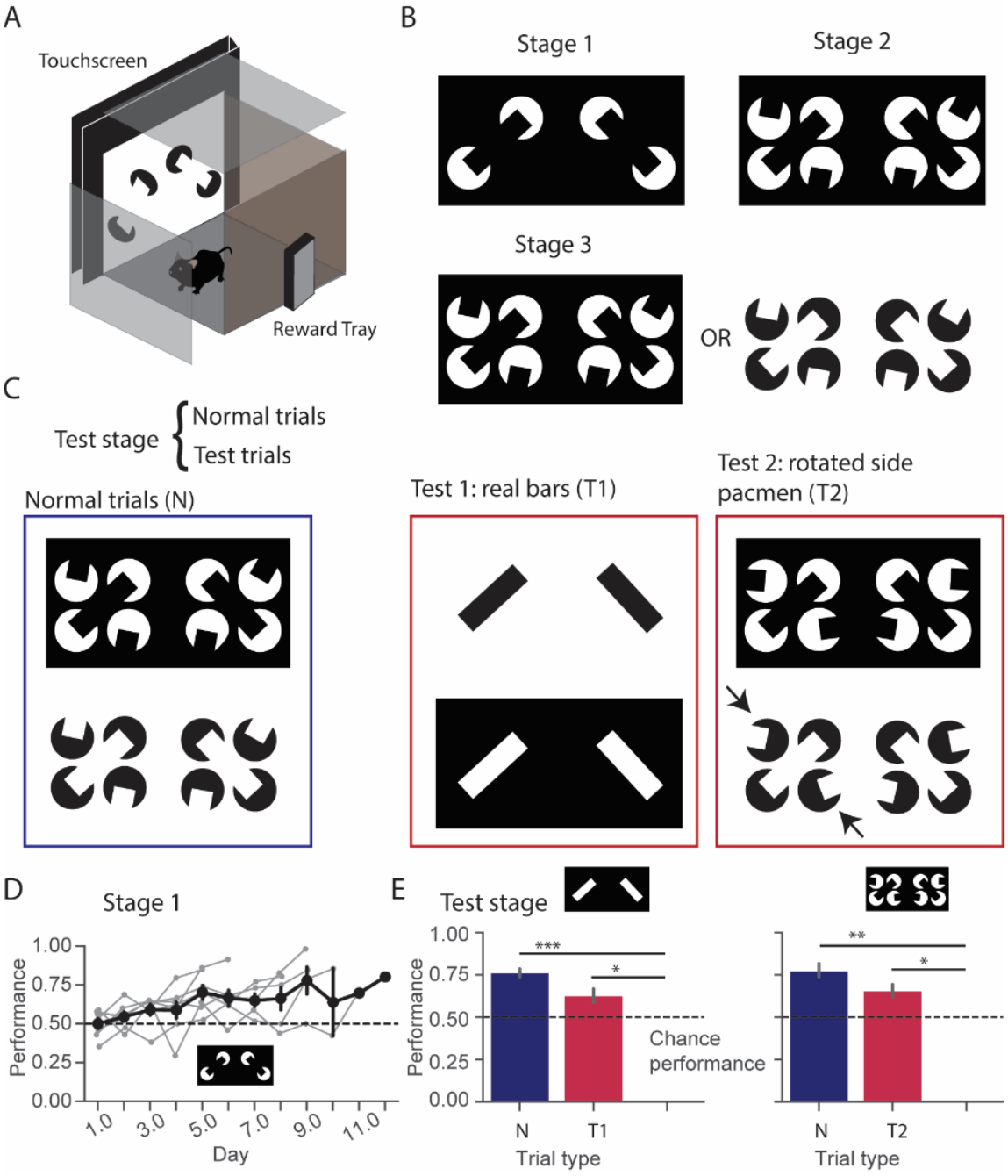
A
Touchscreen
Reward Tray
B
Stage 1
Stage 2
Stage 3
OR
C
Test stage
Normal trials
Test trials
Normal trials (N)
Test 1: real bars (T1)
Test 2: rotated side pacmen (T2)
D
Stage 1
Performance
1.00
0.75
0.50
0.25
0.00
1.0
3.0
5.0
7.0
9.0
11.0
Day
E
Test stage
Performance
***
*
Chance performance
N
T1
Trial type
**
*
N
T2
Trial type

After fast spike sorting using Kilosort software (Pachitariu et al., 2016), we computed spike-triggered average RF maps of the individual units. The Kanizsa square was then aligned to the RF maps so that an illusory contour was on the hotspot of the map but the inducers (pacmen) were outside of it (**Figure 15E**). The radius of inducers was 9.2 degrees and the side of the square was 44.4 degrees so that there was a 26 degrees gap between inducers. Proper positioning of the Kanizsa figure on the monitor screen was chosen to maximize the number of units activated by the subjective contour but not the inducers. Four different types of trials were presented to the animal (**Figure 15D**). Each trial started with four circular disks (CIR) followed by one of the four test stimuli: the Kanizsa square containing illusory contours (KIC, red), rotated corners (ROT, green), a filled white square (SQR, dark blue), and a black line square (LINE, purple). Different types of trials were presented in a pseudorandom manner.

We observed that a subset of units in mouse V1 responds to KIC. They had a much stronger response to KIC compared to ROT and CIR (Fig 2F). To analyze the population-level response to the Kanizsa square, we computed a modulation index by normalizing the responses to the Kanizsa square by those elicited by the circular discs and rotated control: I_m (CIR) = FR (KIC) – FR (CIR)/(FR (KIC) + FR (CIR)) and I_m (ROT) = FR (KIC) – FR (ROT) /(FR (KIC) + FR (ROT)), where FR refers to the firing rate over 0.05-0.5s relative to the stimulus onset, and the I_m (CIR) and I_m (ROT) indices represent how much KIC was enhanced compared to the CIR and ROT, respectively. For example, positive I_m (CIR) values indicate enhanced responses to the KIC compared to the CIR, whereas negative values mean the opposite. Scatter plot shows the distribution of I_m (CIR) and I_m (ROT) indices for 819 units across 17 recording sessions from 11 mice (Fig 2E). Distributions of both indices were wide. The top right quadrant represents units with enhanced responses to the KIC compared to CIR and ROT (**Figure 15E**). This finding suggests that mouse V1 contains illusory responsive units. Given that we simultaneously recorded many units, we could not adjust the position and orientation of KIC for every single cell. We presented either horizontal or vertical KIC because mouse V1 has a preference for cardinal orientations.

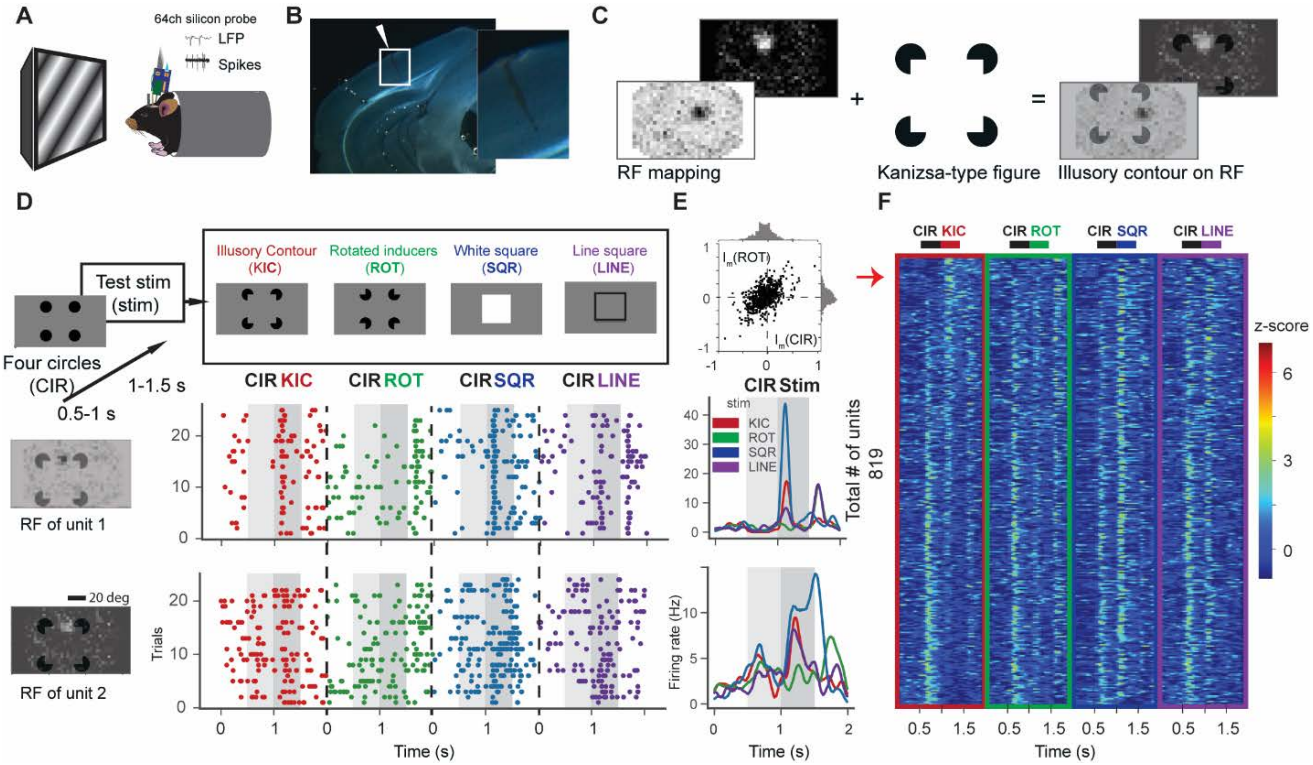

Figure 15. Illusory contour responses in a mouse primary visual cortex (V1).

A. In vivo extracellular electrophysiology with 64ch silicon probes in V1 of awake mice. **B.** Histological identification of recording location in V1. **C.** A Kanizsa figure was presented such that the illusory contour was on the RF of the neuron. Proper positioning of the stimulus on the monitor screen was done by manually aligning the hotspot of the RF maps with an illusory contour of the Kanizsa figure. **D.** Experimental paradigm: Each trial started with four circles (CIR) presented at 0.5-1 s followed by one of the four test stimuli from 1-1.5 s: Kanizsa illusory contours (red, KIC), rotated corners (green, ROT), white square (blue, SQR), and black line square (purple, LINE). Bottom: Two representative units that responded to an illusory contour but not to rotated corners or circles preceding test stimuli. Raster and PSTH plots show stronger responses to KIC vs ROT or CIR. RF maps of these units are shown on the left and overlaid with Kanizsa illusory contours. **E.** Scatter plot shows the distribution of I_m (CIR) and I_m (ROT) indices across all units. **F.** Heat map of unit z-score responses to four different stimuli, n = 819 units across 17 recordings from 11 mice. Units were sorted by FR(KIC) - FR(CIR) responses. Note: red arrow points to a small portion of units at the top of the heat map that show minimal responses to CIR but respond to Kanizsa illusory contour presentation.

Additionally, when considering the relatively large RF size of neurons in mouse V1 and the small proportion of units responsive to KIC that have been found in primate V1 (around 14%) (Lee & Nguyen, 2001), we did not expect to find many illusory responsive units. As can be seen from the heat map of all recorded units, we did observe a small portion of cells that exhibited a minimal response to inducers but were upregulated by KIC (**Figure 15F**, red arrow). Overall, we found single cells that were responsive to illusory contours but not to the circles or the rotated control.

3.6 Mouse V1 Responds to Kanizsa Illusory Contours at the Population Level

To investigate whether mouse V1 responds to illusory contours at the population level, we averaged unit responses to KIC across the population. We used several criteria to identify illusory modulated units. 1) We identified units that did not have statistically significant responses to four circular discs preceding the KIC stimulus. This was done to ensure that the inducers were outside of the RF. We compared the mean firing rate (FR) between the baseline (0.05-0.5) and CIR (0.55-1.0s) using Wilcoxon signed-rank test. 2) We then used a I_m(CIR) index to identify illusory modulated units, which should have positive indices. In total, 54 units (6.54 %) satisfied these conditions and were included in further analysis. It is important to note that this is not the proportion of illusory responsive units as the majority of units responsive to KIC were not included because their RF was directly activated by circular discs. The heat maps and line plots show the neural responses of illusory modulated units to both illusory and real contours (**Figure 17A and B**). Note that the line plots reveal responses to CIR because a small portion of the included units was slightly activated by CIR. We observed that illusory responsive units had significantly stronger population average responses compared to those elicited by the rotated inducers (**Figure 17C**, mean ± s.e.m firing rate: KIC vs ROT (7.03 ± 0.77 vs 5.67 ± 0.61 Hz, U = 871, P = 0.02), vs SQR (8.37 ± 0.98 Hz, U= 1096, P = 0.34), and vs LINE (7.01 ± 0.68 Hz, U = 1127, P = 0.42), Mann-Whitney U test, n = 48 for all comparisons). The selection criteria were not dependent on the ROT responses as only KIC trials and responses to CIR were used to identify illusory responsive units. The contrast square contour (SQR) elicited the strongest responses. Overall, we found significantly stronger responses to KIC vs ROT at the population level.

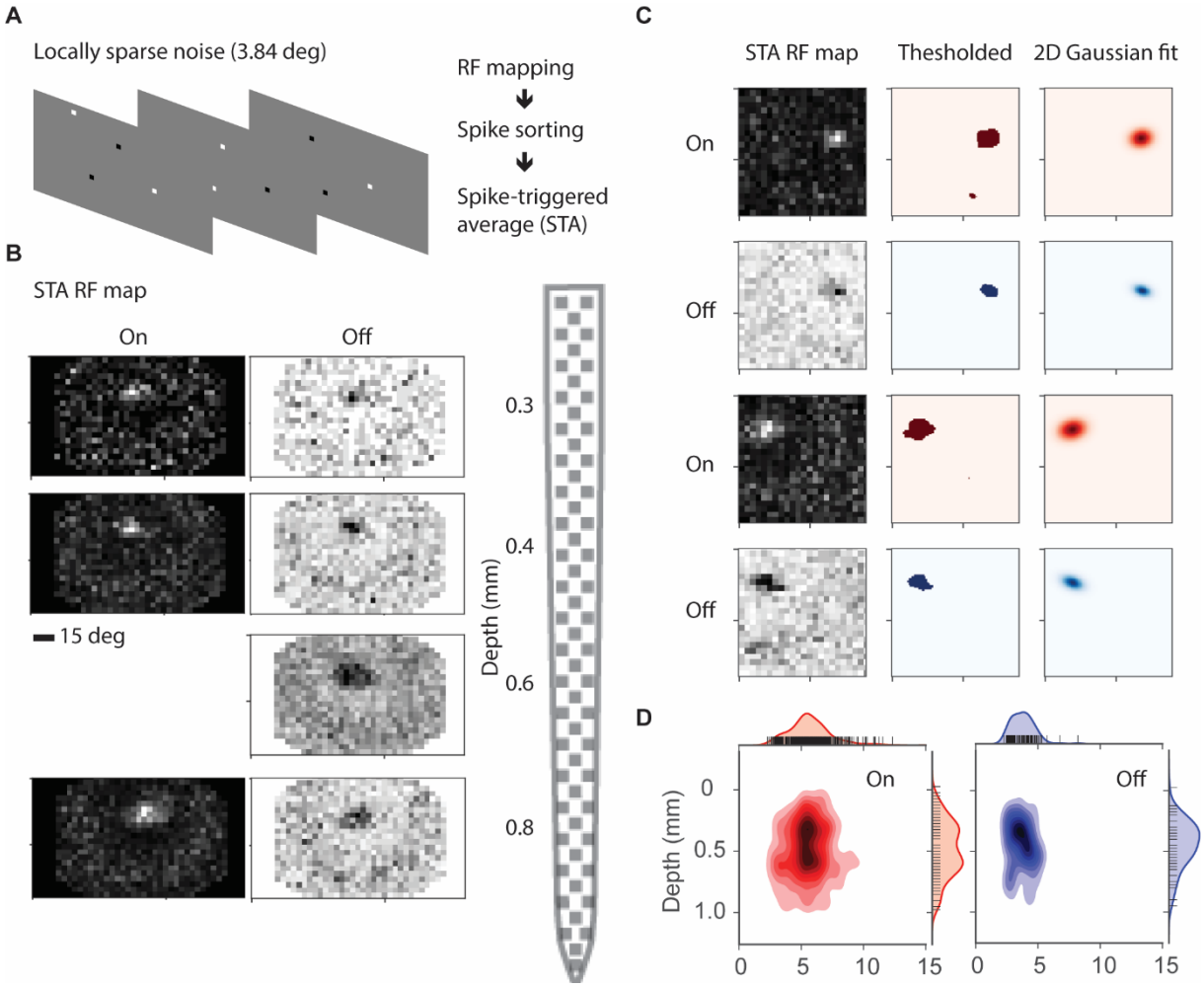

Figure 16. Receptive field (RF) mapping and analysis.

A. Example frames of locally sparse stimuli used for RF mapping. After recording, single units were isolated by spike sorting. RF maps were computed by using spike-triggered average (STA). **B.** On and Off RF maps across the cortical depth obtained from one mouse. Hotspots represent the putative RF. Cartoon of the 64 channel silicon probe is on the right. **C.** STA RF maps were further analyzed by thresholding outlier pixels and fitting 2D Gaussian. RF size was calculated as the average of horizontal and vertical half width at half maximum (HWHM) of the fitted 2D Gaussian. **D.** On/Off RF sizes of units were plotted against their putative depth and fitted with KDE. The on RF size was identified for 393 units (48%) and Off for 101 units (12%).

It has been previously demonstrated in primate V1 that responses to illusory contours are delayed relative to real contours (Lee & Nguyen, 2001). To quantify the response time, we computed the time of the maximal response. Our analysis revealed that KIC responses were significantly delayed relative to SQR but not LINE (**Figure 17D**, mean ± s.e.m peak time: KIC vs ROT (0.17 ± 0.011 vs 0.185 ± 0.012s, U = 372, P = 0.09), vs SQR (0.15 ± 0.006s, U = 336, P = 0.009), and LINE (0.17 ± 0.011s, U = 517, P = 0.44), Mann-Whitney U test, n = 33, 28, 31, 32 respectively). We also analyzed illusory responses across the cortical depth. We found that the largest mean I_m(ROT) index was observed for the neurons in the superficial layers (**Figure 17F**, mean ± s.e.m I_m(ROT): 0.23 ± 0.079, 0.11 ± 0.028, and 0.058 ± 0.024). The I_m(ROT) indeces were significantly different between neurons within different cortical layers: L2/3 vs L4 (U = 34, P = 0.03), vs L5/6 (U = 50, P = 0.01), L4 vs L5/6 (U = 118, P = 0.09), Mann-Whitney U test, n = 9, 14, and 23 respectively.

Figure 17. Mouse V1 responds to Kanizsa illusory contours at the population level

A. Heatmap of unit z-scores in response to illusory contours. Rows represent units, columns – different stimuli. Four circular discs (CIR) were presented at 0.5-1 s and test stimuli at 1-1.5s. Bottom: line plots show the time course of the population mean firing rate to illusory contours, shaded areas represent s.e.m. **B.** Heatmap of unit z-scores in response to real contours. Bottom: line plots represent population mean firing rate to real contours, shaded areas represent s.e.m. **C.** Bar plot showing the mean ± s.e.m. of firing rate between 1.05-1.5s across four different test stimuli **D.** CDF of peak times (relative to the stimulus onset) of four test stimuli. Inset shows the mean ± s.e.m. peak times across four conditions **E.** Scatter plot show the distribution of I_m (CIR) and I_m (ROT) indices of units responsive to illusory contours. (F) Distribution of I_m(ROT) indices in Layer 2/3, L4, and Layer 5/6. $P<0.05$ was considered significant (*$P<0.05$, **$P<0.01$, ***$P<0.001$)

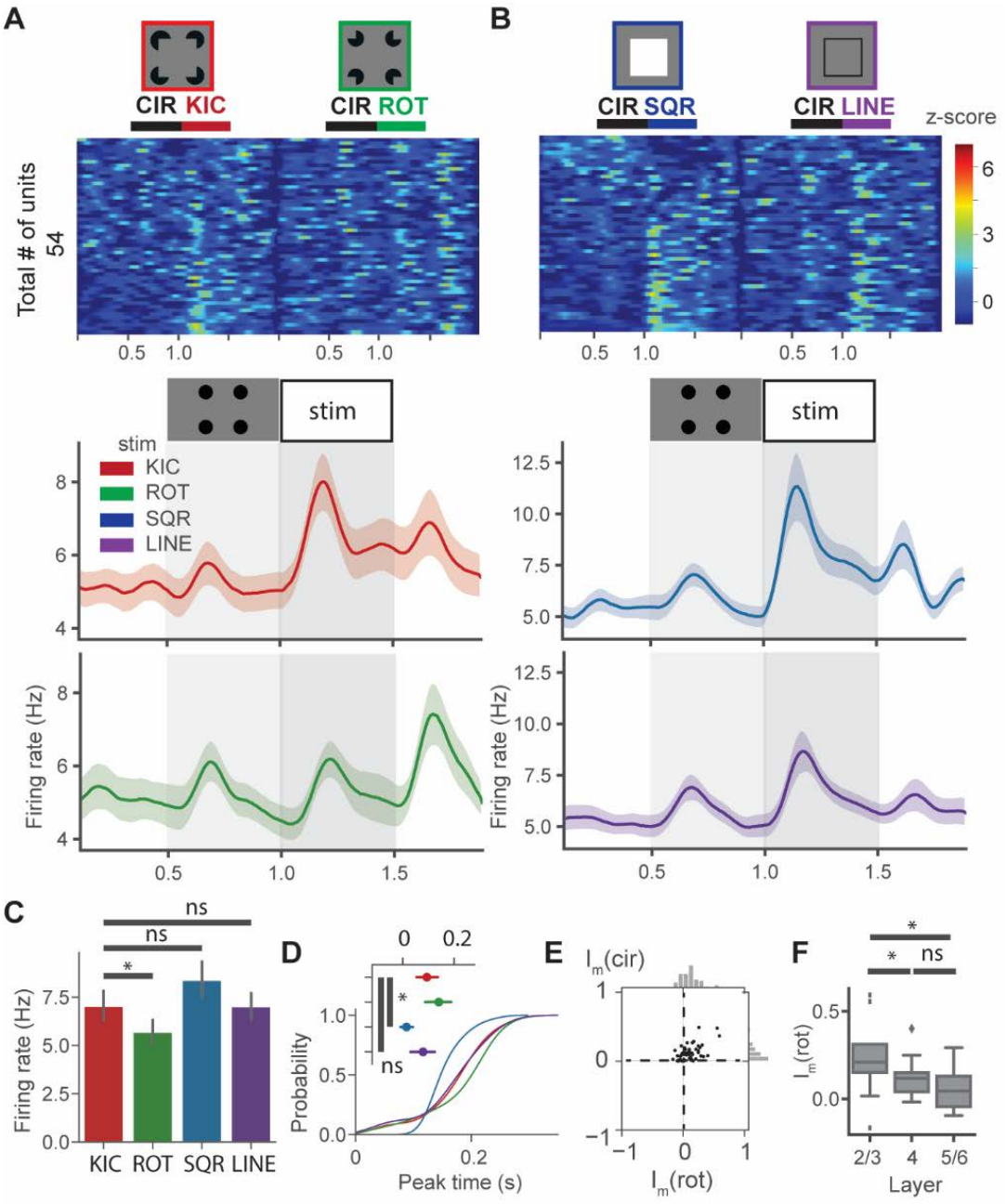
A
B
CIR KIC
CIR ROT
CIR SQR
CIR LINE
z-score
Total # of units
54
stim
KIC
ROT
SQR
LINE
Firing rate (Hz)
C
ns
*
KIC ROT SQR LINE
D
Probability
Peak time (s)
E
I_m(cir)
I_m(rot)
F
2/3 4 5/6
Layer

3.7 Illusory Contours are Orientation-Selective in Mouse V1

Illusory contours were shown to be orientation-selective in primates and cats using both Kanizsa type illusions and subjective contours defined by abutting gratings (Grosof et al., 1993; Peterhans & von der Heydt, 1989; Sheth et al., 1996; von der Heydt & Peterhans, 1989). To determine whether mouse V1 KIC responses are orientation selective, we modified our paradigm and presented KIC and other test stimuli of four different orientations (**Figure** 5A). We also presented drifting gratings of eight different directions for direction tuning. We ensured that KICs of various orientations overlapped with the RF of the unit, because the absence of responses to KIC of a particular orientation may be due to the RF being outside of the visual stimulation. To address this potential issue, we determined whether units still responded to real contours while not responding to KIC. We found that a subset of units responded to KIC of only one orientation but had responses to real contours (SQR or LINE) of various orientations (**Figure 18B**). We manually identified units that showed minimal responses to CIR in at least two conditions (KIC orientations). In total, we identified 15 units from 6 recording sessions from 3 animals. However, a subset of the units had observable responses to CIR. To account for that, we used I_m(CIR) indices to construct a putative population KIC tuning curve. One of the limitations of this experiment is the use of static KIC stimuli because the response magnitude will depend on the relative position of the contour relative to the RF of each neuron. We also analyzed the direction tuning of these units using drifting grating stimuli (**Figure 18A**). To generate population tuning curves for gratings and illusory contours, we first identified the orientation that induced the maximal response. Responses were then rescaled to 0-1 and plotted relative to the preferred orientation. We then set the preferred orientation as 0 degrees and shifted all the other orientations accordingly. For example, if the preferred orientation of the unit was 45 degrees, then 45 degrees was subtracted from all the orientations. The unit responses were then plotted against -45, 0, 45, 90 degrees instead of 0, 45, 90, and 135 degrees. The response at 0 degrees would be equal to 1 as it was the maximal response. Given the clear peak in the population tuning curve obtained with drifting gratings, these units were determined to be orientation-selective (**Figure 18F** at least one group median is different from others ($H = 29.4$, $P = 1.87E\text{-}5$), $n = 14$, Kruskal Wallis test). The putative population KIC tuning curve had a similar shape and at least one group was significantly different from others (**Figure 18D**, ($H = 16.6$, $P = 0.005$), $n = 15$, Kruskal Wallis test). We also performed the same analysis for ROT, SQR, and LINE. I_m(CIR) was computed separately for each stimulus by

normalizing their responses by CIR similarly as for KIC. We did not observe significant orientation tuning for rotated inducers, which further supports that putative KIC tuning was due to the illusory contours (**Figure 18D** (H = 9.84, P = 0.07), n = 14, Kruskal Wallis test). Interestingly, we also observed significant orientation tuning for LINE (**Figure 18E** (H = 11.5, P = 0.04), n = 14, Kruskal Wallis test) but not for SQR responses (**Figure 18E** (H = 7.5, P = 0.18), n = 15, Kruskal Wallis test). We also analyzed the distribution of preferred orientations obtained with drifting gratings vs KIC (**Figure 18G**) and found a good correspondence between them. Together, our results suggest that illusory responses are orientation-selective in mouse V1.

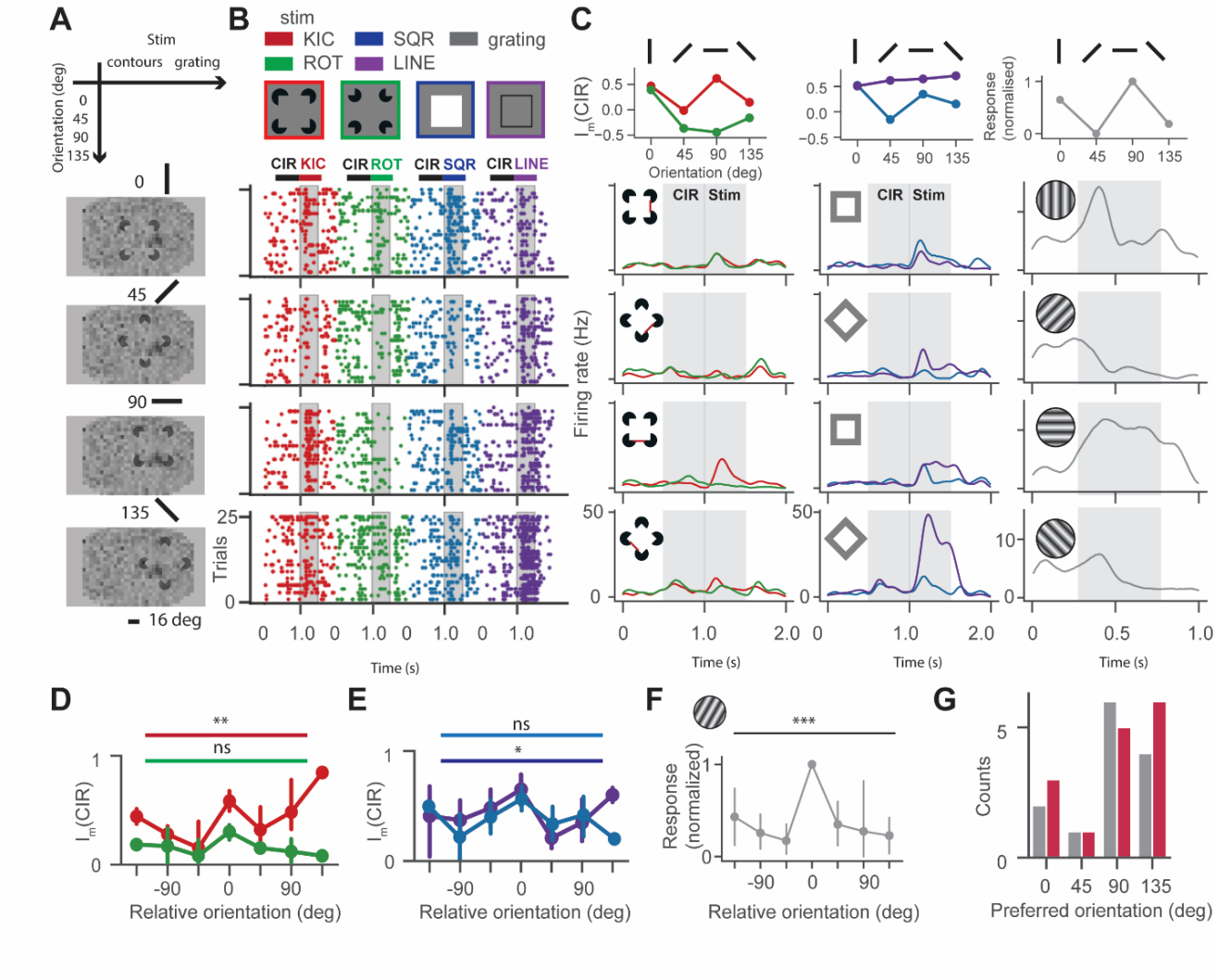

Figure 18. Illusory contours are orientation selective in mouse V1.

A. Arrows point to different stimuli vs orientations. RF map below is overlaid with KIC and show the orientation of illusory contours presented to the mouse. **B.** Raster plots for the representative units show responses in 16 different conditions (4 test stimuli vs 4 orientations). Columns represent four different stimuli while rows show the responses of real and illusory contours of different orientations. **C.** Line plot shows the mean firing rate in response to four test stimuli and grating (rightmost) across four different orientations. Putative tuning plots are shown at the top. **D.** Putative population KIC and ROT tuning curve of I_m(CIR) responses relative to maximum response orientation: We used positive I_m(CIR) values to only include units with minimal CIR responses. . **E.** Same as in (D) but for SQR and LINE. Note: I_m(CIR) represents normalized to CIR responses for different test stimuli **F.** Population tuning curve obtained with drifting grating stimuli. Reponses were rescaled to 0-1 before averaging. Responses were plotted relative to the preferred orientation of the unit **G.** Bar plot shows the counts of units preferring different orientations mapped with either drifting gratins or KIC. P<0.05 was considered significant (*P<0.05, **P<0.01, ***P<0.001).

3.8 Top-down Feedback from LM Modulates Illusory Contour Responses in V1

To test the hypothesis that top-down feedback is important for the responses to illusory contours in V1, we used electrophysiological recordings in V1 combined with optogenetic inhibition of the lateromedial (LM) visual area. We injected adeno-associated virus (AAV) expressing Archaerhodopsin-T (ArchT), a light-sensitive outward proton pump (Han et al., 2011), and green fluorescent protein (GFP) into LM, which is analogous to primate V2 and is known to send feedback projections to V1 and is the most interconnected area with V1 (**Figure 19 A and B**) (Pan et al., 2012; Wang & Burkhalter, 2007). Three weeks after injection, we performed in vivo electrophysiology with optogenetics. We first verified that optogenetic inactivation of LM suppressed responses to grating stimuli in LM but only modulated responses in V1. We recorded neural activity in V1 while an optical fiber was positioned above LM. Optogenetic trials were interleaved with regular trials (data presented in **Figure 15**). First, we calculated a KIC optogenetic modulation index for each unit: I_m (laser) = (FR (KIC) – FR (KIC + laser))/ (FR (KIC) + FR (KIC + laser)). This index represents the KIC response normalized by the KIC response during LM inhibition. Positive I_m (laser) values indicate a decrease in response to KIC during LM inhibition compared to the absence of LM inhibition, whereas negative values indicate the opposite. Scatter plots show the distribution of I_m (laser) and I_m (ROT) indices (**Figure 19C**). The majority of illusory modulated units were in the top right quadrant of the scatter plot, suggesting that optogenetic silencing of LM decreased KIC responses. Three representative units show responses to KIC with (solid colors) and without (light colors) LM inhibition (**Figure 19D**). We saw a clear decrease in KIC but not ROT responses during LM inhibition. Heat maps and line plots show the population responses during the optogenetic experiment (**Figure 19E and F**). We found that the mean KIC but not ROT responses significantly decreased during optogenetic inhibition of LM (**Figure 19G**, mean ± s.e.m of firing rate: KIC vs KIC+laser (6.69 ± 0.72 vs 5.72 ± 0.52 Hz, W = 306, P = 0.0004), ROT vs ROT+laser (5.43 ± 0.58 vs 5.65 ± 0.61 Hz, W = 572, P = 0.28), Wilcoxon signed-rank test, n = 52 for both comparisons). Scatter plots show the single unit responses during LM inhibition. Together, these results suggest that top-down feedback controls Kanizsa illusory contour responses in mouse V1.

Optogenetic stimulation did not affect responses to SQR and LINE in illusory responsive units (**Figure 20**). This suggests that the downregulation of KIC responses cannot be attributed to direct optogenetic inhibition of V1. Interestingly, laser stimulation did modulate responses to SQR but

Figure 19. Top-down feedback from LM controls illusory responses in mouse V1.

A. ArchT was injected into the lateromedial visual area (LM) and electrophysiological recordings were performed in V1. An optical fiber was positioned above LM to inactivate the region with green light (532 nm). **B.** Injection location and viral spread were verified using histology. **C.** The scatter plot shows the distribution of I_m (ROT) and I_m (laser) indices. **D.** Representative raster plots along with line plots show illusory responses with (solid colors) and without (light colors) LM inactivation. **E.** Heat map of unit z-scores in response to KIC with (left) and without (right) LM inactivation. Bottom: Responses to the ROT stimulus. **F.** Line plots show the mean firing rate of units in the heat map. Responses to KIC (red) and ROT (green) stimuli with (solid colors) and without (lighter colors) LM inactivation. Circular discs (CIR) were presented at 0.5-1 s and test stimuli at 1-1.5s. Laser light was applied from 0.9-1.7s as shown with the green rectangle at the bottom of the line plots. **G.** Bar plots show the mean ± s.e.m. of firing rate between 1.05-1.5s across four different conditions: **H.** Scatter plots of single unit responses to KIC (top) and ROT (bottom) during optogenetic inactivation of LM (x-axis) and without it (y-axis). $P<0.05$ was considered significant (*$P<0.05$, **$P<0.01$, ***$P<0.001$)

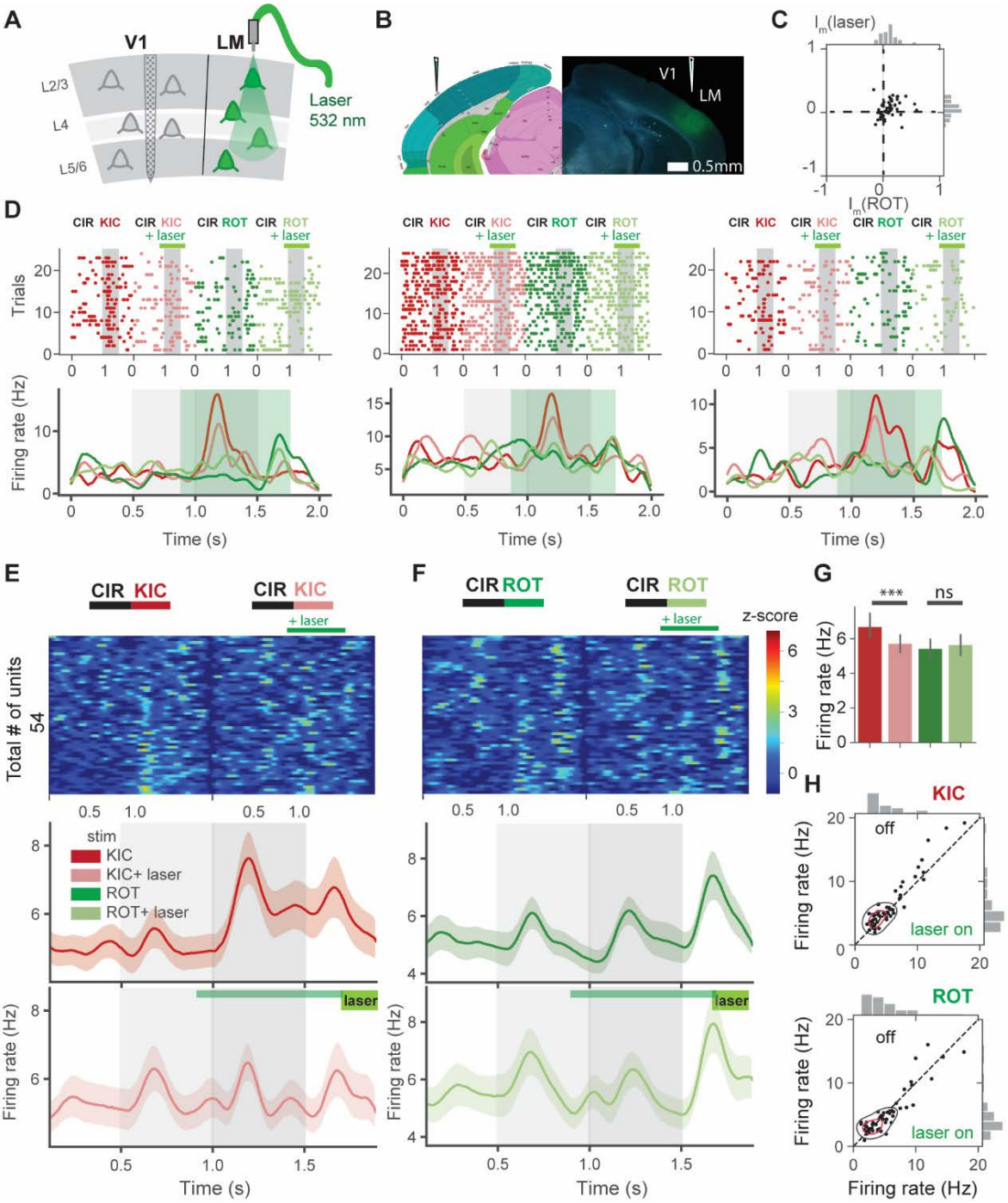
A
V1
LM
L2/3
L4
L5/6
Laser
532 nm
B
V1
LM
0.5mm
C
I_m(laser)
I_m(ROT)
D
CIR KIC
CIR KIC + laser
CIR ROT
CIR ROT + laser
Trials
Firing rate (Hz)
Time (s)
E
CIR KIC
CIR KIC + laser
Total # of units
54
stim
KIC
KIC+ laser
ROT
ROT+ laser
laser
Firing rate (Hz)
Time (s)
F
CIR ROT
CIR ROT + laser
z-score
G
***
ns
Firing rate (Hz)
H
KIC
ROT
off
laser on
Firing rate (Hz)

Figure 20. Inactivation of top down feedback does not affect real contour responses in illusory modulated units.

A. Heat maps of unit z-scores to real contours. Each column represents responses to different stimuli. Responses to SQR (blue) and LINE (purple) with (lighter colors) and without (darker colors) green (532 nm) laser light to optogenetically inhibit LM. Circular discs (CIR) were presented at 0.5-1 s and test stimuli at 1-1.5s. Laser stimulation was applied from 0.9 to +1.7s. **B.** Line plots represent time course of mean firing rate to the SQR (top) and LINE (bottom). **C.** Bar plots shows the mean ± s.e.m. of firing rate between 1.05-1.5s of across four different conditions: SQR vs SQR+laser (8.64 ± 1.00 vs 8.32 ± 1.03 Hz, P = 0.18), LINE vs LINE+laser (7.21 ± 0.69 vs 6.90 ± 0.79 Hz, P = 0.09), Wilcoxon signed rank test, n = 46 for both comparisons. **D.** Scatter plots show single unit z-score responses with (x-axis) and without (y-axis) LM inactivation. Dashed line represents unity line. $P<0.05$ was considered significant (*$P<0.05$, **$P<0.01$, ***$P<0.001$).

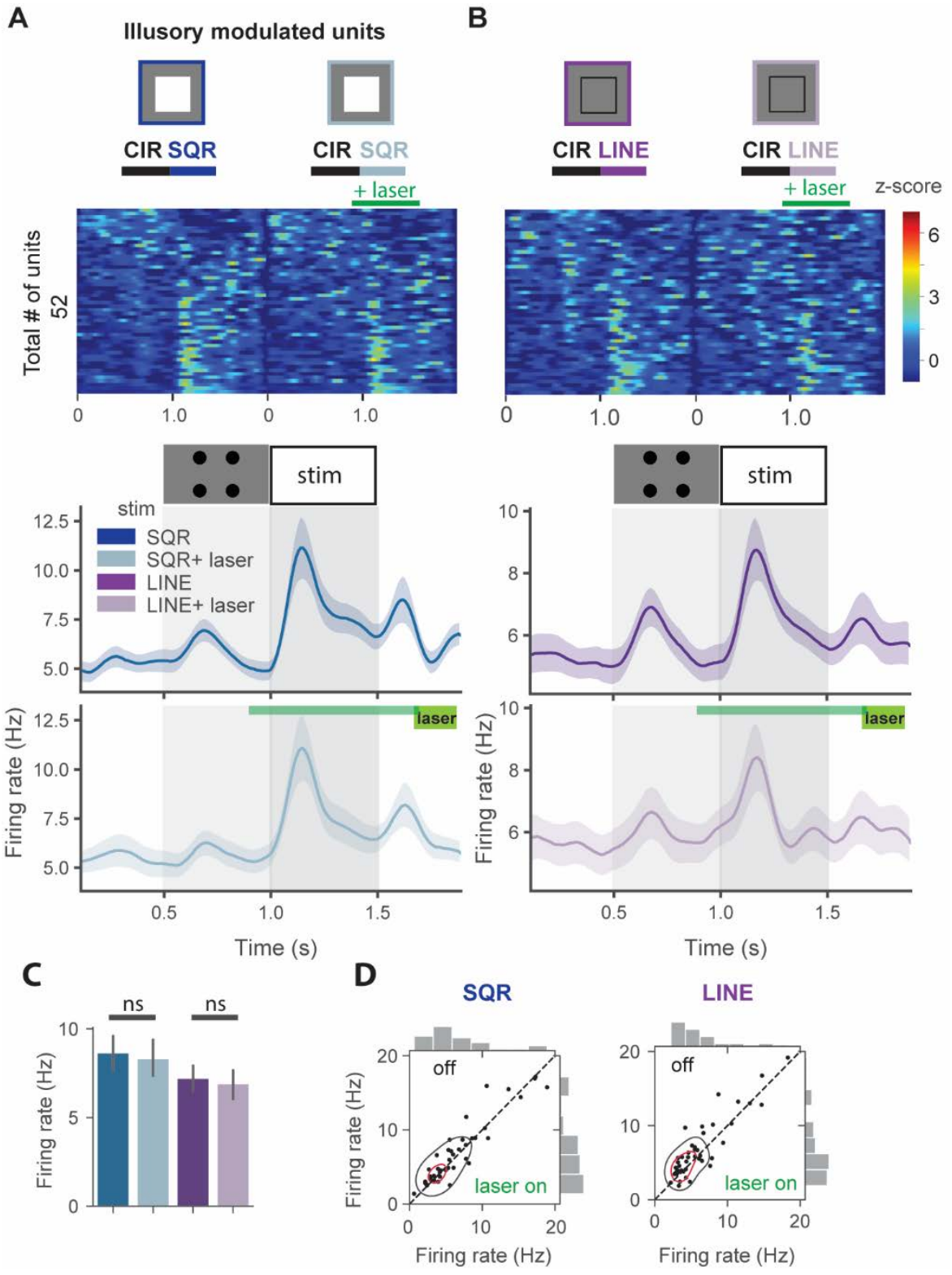
A
Illusory modulated units
CIR SQR
CIR SQR
+ laser
Total # of units
52
0
1.0
0
1.0
stim
stim
SQR
SQR+ laser
LINE
LINE+ laser
12.5
10.0
7.5
5.0
Firing rate (Hz)
laser
0.5
1.0
1.5
Time (s)
B
CIR LINE
CIR LINE
+ laser
z-score
6
3
0
stim
10
8
6
Firing rate (Hz)
laser
0.5
1.0
1.5
Time (s)
C
ns
ns
10
5
0
Firing rate (Hz)
D
SQR
LINE
off
laser on
20
10
0
Firing rate (Hz)
Firing rate (Hz)

Figure 21. Inactivation of top down feedback modulates real contour responses at the population level.

A. Heat maps of unit z-scores to real contours. Each column represents responses to different stimuli. Responses to SQR (blue) and LINE (purple) with (lighter colors) and without (darker colors) green (532 nm) laser light to optogenetically inhibit LM. Circular discs (CIR) were presented at 0.5-1 s and test stimuli at 1-1.5s. Laser stimulation was applied from 0.9 to +1.7s. **B.** Line plots show the time course of mean firing rate to the SQR (top) and LINE (bottom). **C.** Bar plots show the mean ± s.e.m. of firing rate between 1.05-1.5s of across four different conditions: SQR vs SQR+laser (12.00 ± 0.39 vs 11.12 ± 0.36 Hz, P = 2.28E-24), LINE vs LINE+laser (8.39 ± 0.27 vs 8.37 ± 0.26 Hz, P = 0.44), Wilcoxon signed rank test, n = 674 for both comparisons. **D.** Scatter plots show single unit z-score responses with (x-axis) and without (y-axis) LM inactivation. $P<0.05$ was considered significant (*$P<0.05$, **$P<0.01$, ***$P<0.001$).

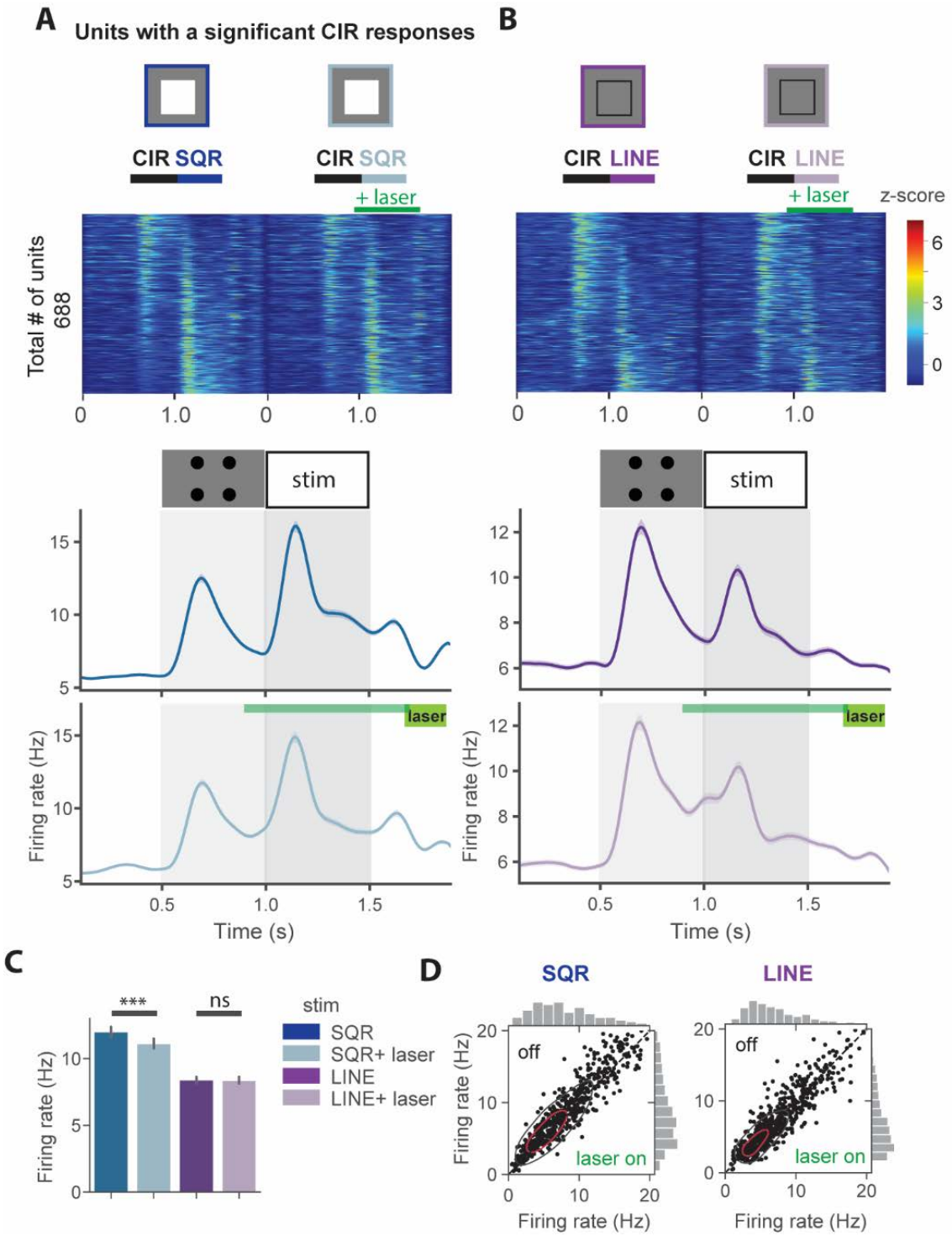
A
Units with a significant CIR responses
CIR SQR
CIR SQR
+ laser
Total # of units
688
0
1.0
0
1.0
stim
15
10
5
laser
Firing rate (Hz)
0.5
1.0
1.5
Time (s)
B
CIR LINE
CIR LINE
+ laser
z-score
6
3
0
12
10
8
6
C
***
ns
stim
SQR
SQR+ laser
LINE
LINE+ laser
Firing rate (Hz)
D
SQR
LINE
off
laser on
Firing rate (Hz)
20
10
0

not LINE in units that had significant responses to CIR (**Figure 21**). These results suggest that optogenetic silencing of LM might differentially modulate responses of different neuronal groups in V1.

3.9 Discussion

Our study suggests that one of the ways top-down feedback influences sensory processing in V1 is by supplying the missing information. We first established that mice can distinguish Kanizsa illusory contours using behavior. Second, we demonstrated that mouse V1 responds to illusory contours. We then showed that the neurons responsive to illusory contours are orientation-selective. Finally, we provided neurophysiological evidence that top-down feedback controls illusory contour responses in mouse V1.

Our behavioral data are consistent with the previous work and strongly suggest that mice can perceive illusory contours (Okuyama-Uchimura & Komai, 2016). Our findings from the transfer stages with luminance-defined bars provide compelling evidence that animals were relying on the global features of the visual stimuli to perform the tasks. Total luminance was different between the illusory bars images containing extra pacmen compared to the images with real bars. Because the mice had not seen the real bars during the training stages, the only strategy to discriminate between the real bars would require learning to discriminate between the illusory bars during training. Not all the mice were able to pass the training stages possibly due to the different strategies they adopt to perform the task. Early stages of training do not require mice to rely on global features to pass the stage. However, mice would not be able to pass a color inversion stage if they relied on a local luminance distribution in the visual stimuli. Consistent with this explanation, all the animals that did not reach the testing stages failed at the color inversion stage. Although this finding does not mean the animals are unable to perceive illusory bars, it suggests that they did not rely on the global features during training.

Our neural data are consistent with the previous single-unit studies describing illusory contour responses in primate V1 (Lee & Nguyen, 2001) and figure-ground modulation in mouse V1 (Schnabel et al., 2018). Consistent with the previous reports of delayed responses to illusory contours compared to real contours, we also observed a 30 ms delay in responses to illusory compared to real contours. Furthermore, we found stronger illusory modulation in the superficial layers, the target of the feedback axonal projections from the secondary visual area LM (Pan et al.,

2012; Wang & Burkhalter, 2007). This observation is also consistent with prior primate work (Lee & Nguyen, 2001) and a more recent human fMRI study (Lawrence, Norris, & de Lange, 2019) investigating laminar modulation by top-down feedback. However, another human fMRI study demonstrated stronger deep layer activation during Kanizsa presentation (Kok, Bains, van Mourik, Norris, & de Lange, 2016). This discrepancy between the mouse and human data could potentially be explained by the differences in the anatomy of mice and humans or by the experimental paradigms. In support of the notion that mice can distinguish illusory contours is the fact that the KIC responses in the mouse V1 are orientation-selective. Orientation selectivity of Kanizsa illusory contours has been demonstrated in primates with high degree of correlation between the tuning curves obtained with real and illusory contours (Peterhans & von der Heydt, 1989; Sheth et al., 1996; von der Heydt & Peterhans, 1989).

Our optogenetic experiments suggest that top-down feedback from LM modulates illusory contour responses in V1. Our data are consistent with the prior primate lesion study and the recurrent processing theories of illusory contours perception (De Weerd et al., 2009; Wyatte et al., 2014). One of the challenges of our study was the proximity of LM to V1. However, our histology and neural data suggest that optogenetic activation was specific to LM. To decrease the likelihood of direct inhibition of V1, we injected a small amount of the construct (50 nL) to minimize the spread of the virus, which resulted in localized injections. Second, optical fiber was painted with the black ink and couplers covered with the foil to restrict light illumination only to LM. Finally, neural responses by illusory modulated neurons to SQR and LINE stimuli were not affected by LM inhibition. Together, these observations suggest that the downregulation of illusory contour responses in V1 was mainly due to LM suppression.

We observed that optogenetic suppression of LM resulted in the downregulation of SQR, but not LINE responses considering all recorded neurons but KIC modulated ones. This observation can be explained by the extensive innervation of V1 by LM and is consistent with the study reporting that top-down feedback modulates feature tuning in V1 (Huh, Peach, Bennett, Vega, & Hestrin, 2018). It is unlikely to be due to the direct V1 inhibition because LINE responses were not affected. It is not clear why SQR responses were not modulated in KIC responsive neurons. This finding could be potentially explained by the distinct LM connectivity and modulation patterns of different neuronal subpopulations in V1.

What is the mechanism of the illusory contour perception? Recurrent processing is required for illusory contour responses (Lee & Nguyen, 2001; Mendola et al., 1999; Pan et al., 2012). Early lesion studies in primates and more recent studies have directly shown the importance of recurrent processing for perception of visual illusions (De Weerd et al., 2009; Luo et al., 2019). The interplay between bottom-up and top-down signals may play a crucial role in illusory shape perception. One plausible mechanism for the illusory responses in early visual cortex might be the top-down feedback modulating effective local connectivity in V1. It has been recently shown that the top-down feedback from V4 to V1 can control the effective connectivity of lateral connections in V1 during a contour detection task in monkeys (Liang et al., 2017). Contour completion that occurs in illusory shapes might be mediated via the above mechanism, similarly oriented edges along one axis would activate units in the higher visual areas that, in turn, could facilitate contour integration by modulating lateral connectivity in V1. Such a mechanism would be robust even in the presence of breaks in the contour continuity.

Recent theories and computational recurrent network models were proposed to explain the illusory contour responses (Lee, 2003; Peterhans & von der Heydt, 1989). One of the proposed models suggests that neurons in V2 might pool orientation selective feedforward inputs from a set of V1 units that were activated by local inducers. Then, activated V2 cells can provide spatially non-specific but feature-specific feedback to those neurons, instructing them about the global context. Feedback signal will thus facilitate contour completion by directly upregulating its V1 targets or modulating them indirectly via recurrent activity (Mignard & Malpeli, 1991). Interestingly, a recent deep convolutional recurrent neural network, PredNet, which represents an implementation of the predictive coding theory, recapitulated dynamics of illusory contour responses as observed in the primate single unit study (Lotter, Kreiman, & Cox, 2018) and in our experiments. Predictive coding postulates that top-down feedback from the higher visual areas conveys expectations about sensory information, while the bottom-up feedforward pathways carry the sensory information. This sensory information is then subtracted from the predictions generated at the higher computational level. According to this framework, the predictions about the illusory shape are sent to V1. Consistent with this theory, human fMRI study showed that V1 responses to the Kanizsa illusion depended on whether the input information was predicted by the bottom-up signals. Authors separately analyzed responses of the regions that corresponded to the illusory shape and inducers that formed the illusion. They compared the responses to the condition

with rotated pacmen that did not produce the illusion and discovered the upregulated resonses to the illusory shape and downregulated responses to the inducers. The authors concluded that the effect could be attributed to the predictions about the stimuli: pacmen induced the bottom-up signals which were predicted while the illusory shape did not. The responses to the unpredicted visual inputs such as the illusory shape, were upregulated, whereas the responses to the inducers that formed the illusion were suppressed (Kok & de Lange, 2014). We did not find similar effects in our study, which might be due to the differences in approach and/or species we used.

In conclusion, our findings suggest that top-down feedback is important for the generation of neural correlates of Kanizsa illusory perception. This feedback is feature-specific, because of the observed orientation selectivity of KIC in mouse V1. Future mechanistic studies of illusory perception in mice, a genetically tractable model system, will greatly facilitate our understanding of perceptual inference in the visual system and help us elucidate the neural computations underlying it.

3.10 References

Bar, M., Kassam, K. S., Ghuman, A. S., Boshyan, J., Schmid, A. M., Dale, A. M., . . . Rosen, B. R. (2006). Top-down facilitation of visual recognition. *Proceedings of the National Academy of Sciences, 103*(2), 449-454.

De Weerd, P., Desimone, R., & Ungerleider, L. G. (2009). Cue-dependent deficits in grating orientation discrimination after V4 lesions in macaques. *Visual neuroscience, 13*(3), 529-538. doi:10.1017/S0952523800008208

Gilbert, C. D., & Li, W. (2013). Top-down influences on visual processing. *Nature Reviews Neuroscience, 14*, 350. doi:10.1038/nrn3476

Grosof, D. H., Shapley, R. M., & Hawken, M. J. (1993). Macaque VI neurons can signal 'illusory'contours. *Nature, 365*(6446), 550.

Han, X., Chow, B. Y., Zhou, H., Klapoetke, N. C., Chuong, A., Rajimehr, R., . . . Boyden, E. S. (2011). A high-light sensitivity optical neural silencer: development and application to optogenetic control of non-human primate cortex. *Front Syst Neurosci, 5*, 18. doi:10.3389/fnsys.2011.00018

Horner, A. E., Heath, C. J., Hvoslef-Eide, M., Kent, B. A., Kim, C. H., Nilsson, S. R., . . . Bussey, T. J. (2013). The touchscreen operant platform for testing learning and memory in rats and mice. *Nat Protoc, 8*(10), 1961-1984. doi:10.1038/nprot.2013.122

Huh, C. Y., Peach, J. P., Bennett, C., Vega, R. M., & Hestrin, S. (2018). Feature-Specific Organization of Feedback Pathways in Mouse Visual Cortex. *Current biology, 28*(1), 114-120. e115.

Kanizsa, G. (1976). Subjective contours. *Scientific American, 234*(4), 48-53.

Kanizsa, G., Renzi, P., Conte, S., Compostela, C., & Guerani, L. (1993). Amodal completion in mouse vision. *Perception, 22*(6), 713-721. doi:10.1068/p220713

Kissinger, S. T., Pak, A., Tang, Y., Masmanidis, S. C., & Chubykin, A. A. (2018). Oscillatory encoding of visual stimulus familiarity. *Journal of Neuroscience, 38*(27), 6223-6240.

Kok, P., Bains, Lauren J., van Mourik, T., Norris, David G., & de Lange, Floris P. (2016). Selective Activation of the Deep Layers of the Human Primary Visual Cortex by Top-Down Feedback. *Current biology, 26*(3), 371-376. doi:10.1016/j.cub.2015.12.038

Kok, P., & de Lange, Floris P. (2014). Shape Perception Simultaneously Up- and Downregulates Neural Activity in the Primary Visual Cortex. *Current biology, 24*(13), 1531-1535. doi:https://doi.org/10.1016/j.cub.2014.05.042

Lawrence, S. J. D., Norris, D. G., & de Lange, F. P. (2019). Dissociable laminar profiles of concurrent bottom-up and top-down modulation in the human visual cortex. *eLife, 8*, e44422. doi:10.7554/eLife.44422

Lee, T. S. (2003). Computations in the early visual cortex. *Journal of Physiology-Paris, 97*(2), 121-139. doi:https://doi.org/10.1016/j.jphysparis.2003.09.015

Lee, T. S., & Nguyen, M. (2001). Dynamics of subjective contour formation in the early visual cortex. *Proceedings of the National Academy of Sciences, 98*(4), 1907-1911. doi:10.1073/pnas.98.4.1907

Li, W., Piëch, V., & Gilbert, C. D. (2004). Perceptual learning and top-down influences in primary visual cortex. *Nature Neuroscience, 7*(6), 651.

Liang, H., Gong, X., Chen, M., Yan, Y., Li, W., & Gilbert, C. D. (2017). Interactions between feedback and lateral connections in the primary visual cortex. *Proc Natl Acad Sci U S A*. doi:10.1073/pnas.1706183114

Lotter, W., Kreiman, G., & Cox, D. (2018). A neural network trained to predict future video frames mimics critical properties of biological neuronal responses and perception. *arXiv preprint arXiv:1805.10734*.

Luo, J., He, K., Andolina, I. M., Li, X., Yin, J., Chen, Z., . . . Wang, W. (2019). Going with the Flow: The Neural Mechanisms Underlying Illusions of Complex-Flow Motion. *The Journal of Neuroscience, 39*(14), 2664-2685. doi:10.1523/jneurosci.2112-18.2019

Maertens, M., Pollmann, S., Hanke, M., Mildner, T., & Möller, H. E. (2008). Retinotopic activation in response to subjective contours in primary visual cortex. *Frontiers in human neuroscience, 2*, 2.

Mendola, J. D., Dale, A. M., Fischl, B., Liu, A. K., & Tootell, R. B. H. (1999). The Representation of Illusory and Real Contours in Human Cortical Visual Areas Revealed by Functional Magnetic Resonance Imaging. *The Journal of Neuroscience, 19*(19), 8560-8572. doi:10.1523/jneurosci.19-19-08560.1999

Mignard, M., & Malpeli, J. (1991). Paths of information flow through visual cortex. *Science, 251*(4998), 1249-1251. doi:10.1126/science.1848727

Murray, M. M., Wylie, G. R., Higgins, B. A., Javitt, D. C., Schroeder, C. E., & Foxe, J. J. (2002). The Spatiotemporal Dynamics of Illusory Contour Processing: Combined High-Density Electrical Mapping, Source Analysis, and Functional Magnetic Resonance Imaging. *The Journal of Neuroscience, 22*(12), 5055-5073. doi:10.1523/jneurosci.22-12-05055.2002

Nieder, A. (2002). Seeing more than meets the eye: processing of illusory contours in animals. *Journal of Comparative Physiology A, 188*(4), 249-260. doi:10.1007/s00359-002-0306-x

Niell, C. M., & Stryker, M. P. (2008). Highly selective receptive fields in mouse visual cortex. *Journal of Neuroscience, 28*(30), 7520-7536.

Okuyama-Uchimura, F., & Komai, S. (2016). Mouse Ability to Perceive Subjective Contours. *Perception, 45*(3), 315-327. doi:10.1177/0301006615614440

Pachitariu, M., Steinmetz, N., Kadir, S., Carandini, M., & Harris, K. D. (2016). Kilosort: realtime spike-sorting for extracellular electrophysiology with hundreds of channels. *bioRxiv*, 061481.

Pan, Y., Chen, M., Yin, J., An, X., Zhang, X., Lu, Y., . . . Wang, W. (2012). Equivalent Representation of Real and Illusory Contours in Macaque V4. *The Journal of Neuroscience, 32*(20), 6760-6770. doi:10.1523/jneurosci.6140-11.2012

Peirce, J. (2009). Generating stimuli for neuroscience using PsychoPy. *Frontiers in Neuroinformatics, 2*(10). doi:10.3389/neuro.11.010.2008

Peterhans, E., & von der Heydt, R. (1989). Mechanisms of contour perception in monkey visual cortex. II. Contours bridging gaps. *Journal of Neuroscience, 9*(5), 1749-1763.

Polley, D. B., Steinberg, E. E., & Merzenich, M. M. (2006). Perceptual learning directs auditory cortical map reorganization through top-down influences. *Journal of Neuroscience, 26*(18), 4970-4982.

Rossant, C., Kadir, S. N., Goodman, D. F. M., Schulman, J., Hunter, M. L. D., Saleem, A. B., . . . Harris, K. D. (2016). Spike sorting for large, dense electrode arrays. *Nature Neuroscience, 19*, 634. doi:10.1038/nn.4268 https://www.nature.com/articles/nn.4268#supplementary-information

Schnabel, U. H., Bossens, C., Lorteije, J. A. M., Self, M. W., Op de Beeck, H., & Roelfsema, P. R. (2018). Figure-ground perception in the awake mouse and neuronal activity elicited by figure-ground stimuli in primary visual cortex. *Scientific Reports, 8*(1), 17800. doi:10.1038/s41598-018-36087-8

Sheth, B. R., Sharma, J., Rao, S. C., & Sur, M. (1996). Orientation maps of subjective contours in visual cortex. *Science, 274*(5295), 2110-2115.

Shobe, J. L., Claar, L. D., Parhami, S., Bakhurin, K. I., & Masmanidis, S. C. (2015). Brain activity mapping at multiple scales with silicon microprobes containing 1,024 electrodes. *Journal of neurophysiology, 114*(3), 2043-2052. doi:10.1152/jn.00464.2015

von der Heydt, R., & Peterhans, E. (1989). Mechanisms of contour perception in monkey visual cortex. I. Lines of pattern discontinuity. *Journal of Neuroscience, 9*(5), 1731-1748.

Wang, Q., & Burkhalter, A. (2007). Area map of mouse visual cortex. *J Comp Neurol, 502*(3), 339-357. doi:10.1002/cne.21286

Wyatte, D., Curran, T., & O'Reilly, R. (2012). The Limits of Feedforward Vision: Recurrent Processing Promotes Robust Object Recognition when Objects Are Degraded. *Journal of cognitive neuroscience, 24*(11), 2248-2261. doi:10.1162/jocn_a_00282

Wyatte, D., Jilk, D. J., & O'Reilly, R. C. (2014). Early recurrent feedback facilitates visual object recognition under challenging conditions. *Frontiers in Psychology, 5*(674). doi:10.3389/fpsyg.2014.00674

Zhuang, J., Ng, L., Williams, D., Valley, M., Li, Y., Garrett, M., & Waters, J. (2017). An extended retinotopic map of mouse cortex. *eLife, 6*, e18372. doi:10.7554/eLife.18372

CHAPTER 4. IMPAIRED ADAPTATION AND LAMINAR PROCESSING OF THE ODDBALL PARADIGM IN THE PRIMARY VISUAL CORTEX OF FMR1 KO MOUSE

4.1 Abstract

Both adaptation and novelty detection are an integral part of sensory processing. Recent animal oddball studies advanced our understanding of circuitry underlying contextual processing in early sensory areas. However, it is unclear how adaptation and mismatch (MM) responses depend on the tuning properties of neurons and their laminar position. Furthermore, given that reduced habituation and sensory overload are among the hallmarks of altered sensory perception in autism, we investigated how oddball processing might be altered in a mouse model of fragile X syndrome (FX). Using silicon probe recordings and a novel spatial frequency (SF) oddball paradigm, we discovered that FX mice show reduced adaptation and enhanced MM responses compared to control animals. Specifically, we found that adaptation is primarily restricted to neurons with preferred oddball SF in FX compared to WT mice. Mismatch responses, on the other hand, are enriched in the superficial layers of WT animals but are present throughout lamina in FX animals. Lastly, we observed altered neural dynamics in FX mice in response to stimulus omissions. Taken together, we demonstrated that reduced feature adaptation coexists with impaired laminar processing of oddball responses, which might contribute to altered sensory perception in FX syndrome and autism.

4.2 Introduction

Fragile X Syndrome (FX) is the most common cause of intellectual disability and of the inherited form of autism. Nearly 1 in 4000 males and half as many females are affected by this condition. It is associated with social communication deficits, hyperactivity, and sensory hypersensitivity (Freund & Reiss, 1991). Given the comorbidity of FX and autism, *Fmr1* KO mice (FX mice) represent a well-defined genetic model that can provide neural circuit-level insights into autism, especially considering the vast diversity of phenotypes and manifestations observed in autism spectrum disorders (ASDs). Such diverse alterations posit a challenge to develop effective diagnostic and treatment tools. FX mice have been shown to exhibit cellular, circuit, and

behavioral alterations that recapitulate some of the manifestations observed in human individuals with FX. Prior autism research has been mostly focused on social-cognitive and behavioral impairments (Robertson & Baron-Cohen, 2017). However, a recent revision of diagnostic criteria for autism recognized sensory processing as an important factor to be considered (American Psychiatric Association, 2013). Previous research in humans suggests that sensory alterations may be predictive of social communication deficits later in life in autism (Boyd et al., 2010; Turner-Brown, Baranek, Reznick, Watson, & Crais, 2012).

Both human and animal studies provide evidence that there is impaired information processing in early sensory areas in both FX and autism (Goel et al., 2018; Rais, Binder, Razak, & Ethell, 2018). Sensory hypersensitivity and reduced adaptation to sensory stimuli are some of the hallmark perceptual impairments in autism. An increase in visual detail processing is often reported in this condition. Visual oddball paradigm studies revealed reduced habituation to repeated stimuli and novel distractors in autistic patients (Sokhadze et al., 2017). Similarly, alterations in the event-related potentials during the auditory and visual oddball tasks were found in FX patients (Van der Molen et al., 2012). Recent work in FX mice found circuit-level impairments in early visual processing, including reduced orientation tuning and functional output from fast-spiking neurons in V1. Reduced orientation tuning of the neurons in the visual cortex correlated with the decreased ability to resolve different orientations of sinusoidal grating stimuli in both mice and human individuals with FX (Goel et al., 2018). Furthermore, altered dendritic spine function and integration were found in layer 4 of the somatosensory cortex in FX mice (Booker et al., 2019). Structural and functional imaging studies of FX mice revealed local hyperconnectivity and long-range hypoconnectivity in V1 (Haberl et al., 2015). Our group has recently shown that there are impaired visual experience-dependent oscillations and altered functional laminar connectivity in V1 of FX mice (S. T. Kissinger et al., 2020). Overall, these studies suggest that there may be circuit-level impairments in early sensory processing in FX.

To shed light on the neural basis of atypical visual perception in FX, we investigated how statistical context influences visual information processing by testing both basic and contextual processing of spatial frequencies (SF) in V1 of FX mice. We measured visually evoked potentials (VEPs) and unit responses in an SF oddball paradigm (Hamm & Yuste, 2016; Ulanovsky, Las, & Nelken, 2003). Two stimuli were presented at different probabilities so that one was a standard stimulus (STD, frequent, redundant), which builds a statistical context. Another one was rare and

violated the expectations of the STD stimulus leading to a mismatch response. This response is hypothesized to reflect a perceptual deviance or change detection. First observed in EEG studies in humans as a delayed negative deflection in event-related potentials, later called mismatch negativity (MMN) (Naatanen, Gaillard, & Mantysalo, 1978), it has been replicated in different species and sensory modalities (Chen, Helmchen, & Lütcke, 2015; Musall, Haiss, Weber, & von der Behrens, 2015; Parras et al., 2017). A decrease in the neural response to the standard stimulus (STD), termed stimulus-specific adaptation (SSA), may be attributed to the predictability of the stimulus because the incoming sensory input matches prediction. Alternatively, it may also be explained by the presynaptic short-term plasticity mechanisms. We computed SSA as the difference between control (CTR) and STD (Hamm & Yuste, 2016; Parras et al., 2017). Given that STD and deviant (DEV) stimuli share the same SF, mismatch (MM) response reports moment-to-moment change detection under the high adaptation level in the local microcircuit, so that any response enhancement can be attributed to change detection. MM, similarly to human MMN, was quantified as the difference between DEV and STD stimuli.

Our SF oddball paradigm is different from the prior oddball studies because both STD and DEV stimuli are of the same low-level feature, spatial frequency so that they only differ in the global pattern. Prior studies used two stimuli that differed in low-level features (e.g., orientation, frequency) and thus needed a reverse sequence (flip-flop), in which low and high probability stimuli switch to control for feature preference of the neurons. Our oddball paradigm allowed us to investigate how contextual processing depended on neuronal tuning. Specifically, we investigated how oddball responses changed as a function of neuron's preferred SF. Furthermore, we investigated how oddball responses are represented by different cortical layers and neuronal types (regular vs. fast spiking) neurons in WT vs. FX mice.

Here, we performed silicon probe recordings in WT and FX mouse V1 during the SF oddball paradigm. First, we report excessive processing of high SF stimuli in late neural responses. Second, we demonstrate that adaptation is mostly confined to neurons preferring the SF within one octave of the oddball SF in FX, but not in WT mice, in which it spreads beyond that range. Third, mismatch responses were differentially modulated by cortical layers in WT but not in FX mice. Lastly, we observed altered neural dynamics during the omission paradigm in FX animals.

4.3 Materials and Methods

4.3.1 Experimental animals

All animal experiments were approved by the Purdue University Animal Care and Use Committee. The following strains were used to generate mice for this study: B6.129P2-Fmr1tm1Cgr/J (Fmr1 KO, JAX Stock No. 003025), B6.Cg-453 Tg(Thy1-COP4/EYFP)18Gfng/J (Thy1-ChR2-YFP, JAX Stock No. 007612), and wild type (WT) C57/BL6. We used 10 male Fmr1 KO and 7 littermate controls. We also bred Thy1-ChR2 with Fmr1 KO mice to generate Thy1-Fmr1 KO mice. We used 4 male Thy1-Fmr1 KO and 4 littermate controls. Additionally, we had 6 male WT mice. In total, we used 14 Fmr1 KO and 17 control animals for physiology experiments. Animals were group-housed on a 12 hr light/dark cycle with full water and food access.

4.3.2 Surgical procedures

Animal surgeries were performed as previously described (Pak, Ryu, Li, & Chubykin, 2020). Briefly, about 2-month-old animals were induced with 5% isoflurane and secured to a motorized stereotaxic apparatus (Neurostar). Their body temperature was controlled using a heating pad, and they were maintained at 1.5-2% isoflurane anesthesia. The scull was exposed to install a small head post and a reference pin. The binocular V1 coordinates (from lambda AP 0.8 mm, LM: ±3.2 mm) were labeled using a Neurostar software with an integrated mouse brain atlas. Medical grade Metabond™ was then used to seal all exposed areas and form a head cap. After surgery, all animals were monitored for 3 days for any signs of distress or infection. Mice were then habituated to a head-fixation apparatus for at least 4 days 90 min per day. They were positioned in front of the monitor that displayed a grey screen. On the recording day, a small craniotomy was made above V1 on one of the hemispheres under 1.5% isoflurane anesthesia. They were then moved to the recording room and head-fixed to the apparatus in front of the monitor screen.

4.3.3 Electrophysiology

All recordings were performed in awake head-fixed mice. After mice were transferred to the recording room, we inserted a 64-channel silicon probe (Justin L. Shobe, Leslie D. Claar, Sepideh Parhami, Konstantin I. Bakhurin, & Sotiris C. Masmanidis, 2015) (channel separation: vertical 25 µm, horizontal 20 µm, 3 columns, 1.05 mm in length) to perform acute extracellular

electrophysiology. 30 min was allowed after insertion for the probe to settle down. Each mouse underwent a maximum of two recording sessions (one per hemisphere). We acquired data at 30 kHz using OpenEphys hardware and software. We used an Arduino board to synchronize recordings and visual stimulus presentations using TTL communication. Custom written Python scripts using PsychoPy and pyserial were used to present visual stimuli and send TTL signals. Trypsin (2.5%) was used to clean the probe after recording sessions.

4.3.4 Histology

Animals were anesthetized with 100 mg/kg ketamine and 16 mg/kg xylazine solution. Mice were then perfused transcardially with a 1x PBS followed by a 4% paraformaldehyde. After decapitation, their brain was extracted and stored in PFA in the fridge. After 24 hours, the brain was sliced in 0.1 mm sections in PBS using a vibratome. Coronal slices were mounted on slides using n-propyl-gallate media and sealed with transparent nail polish. Slices were imaged using light microscopy (VWR) to verify the probe placement in V1.

4.3.5 Visual stimulation

We used a PsychoPy, an open-source Python software, to create and present all visual stimulations (Peirce, 2009). A gamma calibrated LCD monitor (22’ ViewSonic VX2252, 60 Hz) was used to present visual stimuli. The mean luminance of the monitor was 30 cd/m^2. The monitor was placed 17 cm in front of the mouse to binocularly present stimuli. To generate visual stimulations for a spatial frequency tuning and an oddball paradigm, we performed a spatial frequency filtering of random noise. Specifically, we bandpass filtered random noise in different non-overlapping SF bands. This was done by performing the following steps. First, we randomly generated noise and converted it to a frequency domain using FFT (numpy FFT). Second, we created a spatial frequency bandpass filter using Psychopy Butterworth filter with an order of 10. Third, we multiplied the white noise in the frequency domain by our bandpass filter. This step filtered all the frequencies but the desired SF band. Fourth, we took the inverse Fourier transform of our altered frequency domain. The procedure and a Python code for spatial frequency filtering were adapted from http://www.djmannion.net/psych_programming/vision/sf_filt/sf_filt.html. We modified the above code to generate SF filtered noise. Overall, we used 6 different spatial

frequencies for SF tuning: 7.5E-3, 0.015, 0.03, 0.06, 0.12, and 0.24 cycles/degrees. We chose these frequencies based on previous studies and known spatial frequency tuning of mouse V1 neurons. We verified that we could obtain reliable SF tuning similarly to our previous study (Samuel T. Kissinger, Pak, Tang, Masmanidis, & Chubykin, 2018). SF tuning sequence contained 6 different SF stimuli presented in a pseudorandom order at equal probability. We used an inter-trial interval of at least 4s to prevent any adaptation. Furthermore, SF filtered stimuli were randomly generated on each trial to uniformly sample different receptive fields. This was mainly important for lower spatial frequencies. For the oddball paradigm, we used two stimuli of the same SF but the different overall patterns. The first stimulus was a standard (STD) with a probability of 0.875. Its texture did not change across trials. The second one was a deviant (DEV) with a probability of 0.125, its overall pattern changed across trials. This was done to maximize the surprise response. Inter stimulus interval was randomly chosen from the range of 0.5 and 1.2 s. The stimulus was presented for 0.5 s.

4.3.6 LFP analysis

Raw electrophysiology traces were first downsampled to 1 kHz. We then used symmetric linear-phase FIR filter (default parameters) from the mne Python library to remove 60 Hz noise. Next, we identified a Layer 4 by finding a channel with the strongest negative deflection in the first 100 ms after stimulus onset. Time-frequency analysis was done using a complex wavelet convolution. 40 different wavelets were designed across a logarithmic range of 2-80 Hz, with cycles ranging from 3 to 10. This gave us an optimal time-frequency precision tradeoff. We convolved these wavelets with averaged LFP traces and then averaged the resulting power spectra across different conditions. For heatmaps, power was dB baseline normalized. To quantify a mean power within a particular band, we averaged responses within a 0.05-0.5 s time window. We used 6 different frequency bands: theta (4-8 Hz), alpha (8-12 Hz), beta (12-30 Hz), low gamma (30-50 Hz), and high gamma (50-80 Hz).

4.3.7 Single unit analysis

Clustering and manual curation of units were performed as previously described (Pak et al., 2020). Kilosort was used for spike detection and sorting. It uses a template matching algorithm

and allows a GPU acceleration (Pachitariu, Steinmetz, Kadir, Carandini, & Harris, 2016). Default configuration parameters were used for clustering, but a threshold for spike detection was changed from -4 to -6. SD. Templates were initialized from the data. Kilosort was run using MATLAB (Mathworks) on Windows 10 running computer. For clustering purposes, all the different recording blocks were concatenated together. This allowed us to track single neurons across different recording sessions. After clustering, we visualized and verified clustering results using Klusta/Phy GUI. It speeds up the process of manually removing, splitting, and merging units (Rossant et al., 2016). We used several criteria to only include well-isolated units: 1) had more than 10 spikes for each experimental block, 2) less than 5% of spikes violated an absolute refractory period, 3) clean template shape, and 4) templates were localized within a small channel group. To merge and split units, we followed the guidelines available online (https://github.com/kwikteam/phy-contrib/blob/master/docs/template-gui.md).

Peristimulus time histograms (PSTHs) of single units were constructed by binning spike times across trials with 10 ms bins and convolving the obtained histogram with a Gaussian Kernel (width = 100 ms). Z-score was calculated by the following formula:

$$z = \frac{FR - mean(baseFR)}{sd\ (baseFR)}$$

where FR is a firing rate at each time point, and base refers to the baseline activity over 0-0.3s.

For spatial frequency analysis, we averaged the firing rate within 0.05-0.2 s for tuning analysis and 0.2-0.5 s to investigate later responses. Population tuning curves were constructed using baseline-subtracted firing rates across different neurons. We fitted a difference of Gaussian function to SF tuning curves (Hawken & Parker, 1987):

$$R(SF) = \mathrm{R}_0 + K_e e^{\frac{-(SF-\mu_e)^2}{2\sigma_e^2}} - K_i e^{\frac{-(SF-\mu_i)^2}{2\sigma_i^2}}$$

This function has 7 free parameters: baseline firing rate R_0, amplitude K_e and K_i, center μ_e and μ_i, width σ_e and σ_i of the excitatory and inhibitory components, respectively.

$$fit\ error = \frac{\sum(y_i - f_i)^2}{\sum(y_i - \bar{y})^2}$$

where y_i is the observed value, $\bar{y}$ is the mean of observed data, and f_i is the fitted value. The fitting procedure was performed using curve_fit from Python. Initial value for each parameter was set to 0.01. Bounds were set to [0, 1] for width and [0, max firing*2] for other parameters. Tuning sharpness was quantified using the quality factor (Q):

$$Q = \frac{SF_{peak}}{SF_{high} - SF_{low}}$$

where SF_{peak} is the preferred SF of the unit, $SF_{high} and\ SF_{low}$ are the high and low SF cut-offs at which the tuning curve drops below peak/$\sqrt{2}$ (Bredfeldt & Ringach, 2002).

To investigate oddball responses, we focused on neurons that upregulate their firing in response to visual stimuli. We used Wilcoxon signed-rank test to identify these neurons by comparing baseline firing rate -0.25-0.05 s versus stimulus window 0.05-0.35 s. The response to the SF0.03 was used as the control for the oddball paradigm. To equalize the number of trials between STD and DEV stimuli, we only used pre-DEV trials for STD. We computed modulation indices for mismatch response (MM) and stimulus-specific adaptation (SSA) using the following formulas.

$$iSSA = \frac{CTR-STD}{CTR+STD}; \qquad iMM = \frac{DEV_{late}-STD_{late}}{DEV_{late}+STD_{late}}$$

where STD/CTR represent baseline-corrected mean firing rate within 0.05-0.5 s, and STD_{late}/DEV_{late} 0.2-0.5 s relative to the stimulus onset.

To investigate how SSA and MM change as a function of preferred SF of the units, we split neurons into three groups: tuned_in, tuned_out, and untuned units. Tuned_in group included units with preferred SF that lies within 1 octave of oddball SF, 0.03 cpd (0.015 < pref SF < 0.06). The tuned_out group included units with preferred SF that lies outside the 1 octave of the oddball SF (pref SF < 0.015 or pref SF > 0.06). The untuned group included units that did not show any SF tuning properties; the fitting procedure was not successful, or fitting error exceeded 0.9. These units were then further split by the cortical depth. The layer of each neuron was assigned based on the depth of the channel with the strongest negative deflection of the template. We used Kilosort template waveform features to split units into putative regular or fast-spiking (RS vs. FS) neurons. FS units were defined as those with trough-to-peak times less than 0.45 and spike width less than 1.2. RS units, on the other hand, had trough-to-peak times more than 0.45 and spike width larger than 1.2. Units that fall in between were defined as unclassified.

The omission paradigm was analyzed in two different ways. First, we decided to investigate the laminar processing of omission responses. Omission-responsive units were defined as those with significant neural responses during omission (expected stimulus timing vs baseline 0.05-0.35 vs. -0.25-0.05). Neurons with significant responses were further subdivided into omis-excited and omis -inhibited depending on whether their mean response exceeds 0 or not. Overall, 122 WT and

95 FX units were omis-excited, 93 and 92 omis-inhibited, and 230 WT and 134 FX units did not have a significant omission response. The second approach employed an unsupervised clustering algorithm, k-means. The input was omission responses (0.05-0.5s) from both genotypes. We used scikit-learn implementation of k-means and initialized it with PCA for consistency. The number of clusters was determined using an "elbow-method", in which distortion and inertia can be plotted against the number of clusters. It is challenging to find an optimal number of groups for k-means with neurophysiology data; however, we observed that k = 4 is the point at which a slope changes in the inertia and distortion plots. In addition, we qualitatively observed that four groups captured the diversity of omission responses. Given that genotype of units is independent of clustering process, we compared omission responses within each k-means group.

SF neural decoding was performed using Linear Discriminant Analysis in Python scikit-learn package (default parameters) (Virtanen et al., 2020). Population spike counts from different time windows were used to train classifiers. We used 4-fold cross-validation with 5 repeats. The number of folds was chosen so that the test size was not below 30 samples. We also trained logistic regression (multinomial) and SVM (with RBF kernel) classifiers (data not shown), but LDA gave better performance given the number of parameters to specify. The number of units used for training was comparable in both groups. For example, decoding from the 0.35-0.45s interval was performed using 1324 units from WT and 1226 units from FX.

4.3.8 Statistical Analysis

We used scipy.stats Python library to perform statistical analysis. Data were not tested for normality of residuals, and only non-parametric tests were used. Mann-Whitney U test was used to compare two independent populations. It was used to compare a trial-averaged LFP and neuronal firing rate in response. P-values were adjusted using a Benjamini-Hochberg procedure that controls for a false discovery rate. Kolmogorov-Smirnov 2 sample test was used to compare distributions of iSSA and iMM indices between WT and FX mice in different layers.

4.4 Enhanced oddball responses in LFP of FX mice

Using 64 channel silicon probes that span the cortical depth of V1 (J. L. Shobe, L. D. Claar, S. Parhami, K. I. Bakhurin, & S. C. Masmanidis, 2015), we investigated visual processing of

spatial frequencies (SF) during tuning (many standards control) and oddball paradigm in awake head-fixed WT and FX mice (**Figure 22A and B**). For SF tuning, we presented animals with SF filtered visual noise stimuli using six different non-overlapping SF bands (**Figure 22C and D**). Stimuli of the same band have the same spatial frequency but a different overall global pattern. These stimuli have been previously validated for tuning measurements. Furthermore, there was no significant difference between WT and FX mice in neural response variability to the same SF band with different overall patterns (**Figure 23**). Oddball responses were analyzed by comparing responses to standard (STD) and control (CTR) stimuli for SSA and delayed part of STD and deviant (DEV) responses for calculating the mismatch (MM) response (Figure 1F). In contrast to previous animal oddball studies, our STD and DEV have the same low-level features (SF), so that increased delayed part of the DEV response can be attributed to change detection.

We first focused on oddball responses in local field potential (LFP), which represents local population subthreshold activities. We found adaptation and mismatch responses in layer 4 LFP of both genotypes (**Figure 24A and C**). Interestingly, MM responses but not SSA were stronger in FX animals (Figure 2B and D, SSA: STD vs CTR WT ($P = 0.0057$), FX (0.002); WT vs FX STD ($P = 0.440$), CTR ($P = 0.105$); MM: STD vs DEV WT ($P = 0.0016$), FX ($P = 0.0002$), WT vs FX STD (0.075), DEV ($P = 0.015$), n = 17 and 15 recordings, Mann-Whitney U test, p-values were adjusted for multiple comparisons using Benjamini-Hochberg method). Time-frequency analysis was then performed on L4 LFP to investigate whether any frequency bands are modulated by oddball responses (Figure 2E). Entire duration of DEV response was used, so that the window is big enough to quantify low frequency oscillations. We found that only theta oscillations were modulated by the oddball responses in both genotypes (**Figure 24F**, STD vs DEV: theta WT ($P = 0.021$) and FX ($P = 0.0006$); alpha WT ($P = 0.089$) and FX ($P = 0.089$); beta WT ($P = 0.45$) and FX ($P = 0.45$); low gamma WT ($P = 0.21$ and FX ($P = 0.40$), high gamma WT ($P = 0.05$) and FX ($P = 0.05$); WT vs FX STD and DEV all bands ($P > 0.05$), n = 17 WT and 15 FX mice, Mann-Whitney U test, p-values were adjusted for multiple comparisons within each frequency band using Benjamini-Hochberg method).

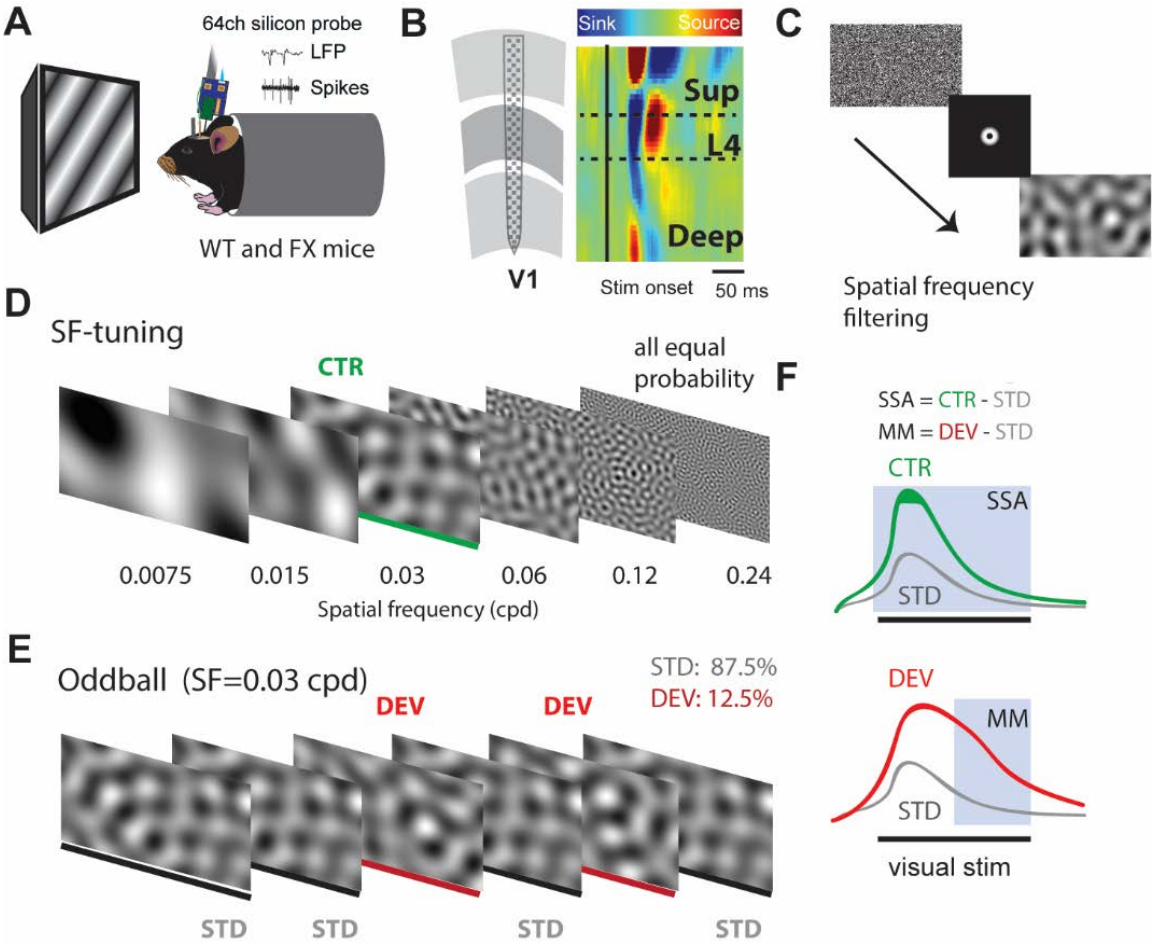

Figure 22. A visual oddball paradigm with all the stimuli containing the same low-level features (spatial frequency) but different global spatial frequency patterns and expectancy.

A. In vivo extracellular silicon probe recordings in V1 of head-fixed mice. **B.** Schematic of a 64-channel silicon probe spanning the whole cortical depth and an example current source density (CSD) heatmap. **C.** To generate visual stimuli, we performed spatial frequency (SF) filtering of white noise. **D.** We used 6 different non-overlapping SF bands from 7.5E-3 to 0.24 cpd for spatial frequency tuning (many standards control). Stimuli were presented in a pseudorandom order and had equal probability. **E.** The oddball sequence contained stimuli of the same SF (0.03 cpd) that only differ in their probability and overall texture. Standard (STD) and deviant (DEV) stimuli were presented with a probability of .875 and 0.125, respectively. **F.** Given that STD and DEV have the same low-level features (SF), we computed a neuronal mismatch (MM) response by comparing late (0.3-0.5s) responses of STD and DEV. Stimulus-specific adaptation (SSA) was obtained by comparing STD and CTR. Since both STD and DEV had the same SF, neural population activity is expected to be adapted during the oddball.

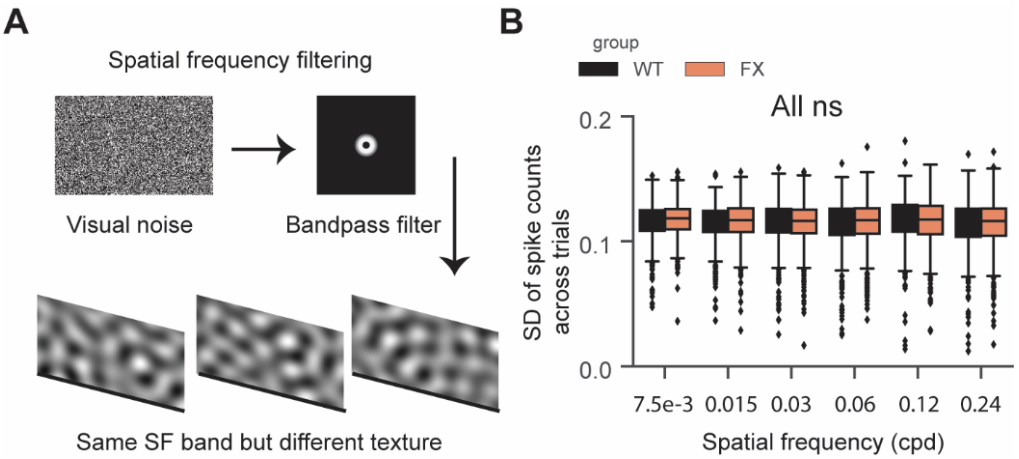

Figure 23. Stimuli of the same SF band but different overall patterns induce similar neural responses.

A. Spatial frequency filtering generates stimuli with the same SF band but different global pattern **B.** Box plots show neural variability (SD of spike counts across trials) for each SF stimulus used in SF tuning experiment (WT vs FX: SF7.5e-3 (P = 0.14), SF0.015 (P = 0.16), SF0.03 (P = 0.29), SF0.06 (P = 0.32), SF0.12 (P = 0.16), and SF0.24 (P = 0.29), n = 594 and 562 units, Mann-Whitney U test, p-values were adjusted for multiple comparisons using Benjamini-Hochberg method).

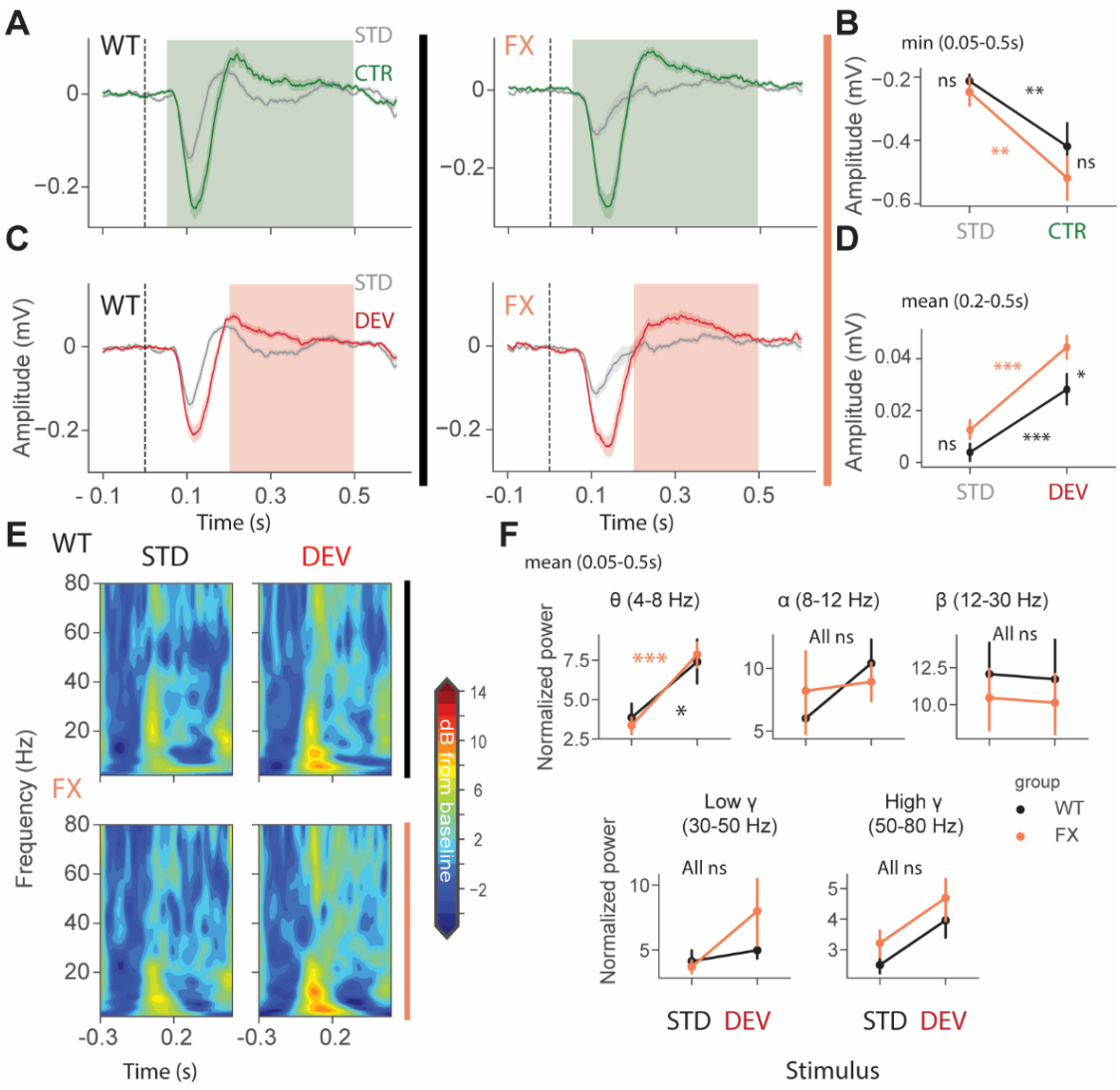

Figure 24. Enhanced late responses in L4 of FX mice during a visual oddball paradigm.

A. Averaged layer 4 LFP traces in response to STD and CTR stimuli for WT (left) and FX (right). **B.** The point plots show the mean and s.e.m. of the strongest negative deflection within 0.05-0.5 s relative to the stimulus onset. **C.** Same as in A but comparing STD vs. DEV. **D.** Same as in B, but responses were averaged within 0.2-0.5s. **E.** Time-frequency spectra of the L4 LFP traces of WT (top) and FX (bottom). **D.** Point plots show the mean power within 0.05-0.5 s relative to the stimulus onset across different frequency bands.

4.5 Excessive processing of high spatial frequencies in V1 of FX mice in late unit responses

We next focused on single-unit activity during tuning (control) and oddball sequence. The time course heatmap of SF tuning revealed enhanced activity in late unit responses in all layers of FX animals, especially at higher SF (**Figure 25A**). To obtain a preferred SF for each unit, we fitted a Difference-of-Gaussian model to tuning curves, which were obtained by averaging the firing rate within 0.05-0.2 s relative to the stimulus onset (**Figure 25B**). We did not observe any differences in the distribution of preferred SF or Q-factor (tuning sharpness) between genotypes (Figure 3C, WT vs FX pref SF ($P = 0.357$), n = 949 and 705 units; Q-factor ($P = 0.404$), n = 192 and 126 units, Kolmogorov-Smirnov 2 sample test). The population mean responses to different SF stimuli revealed enhanced activity in late unit responses at high SF (**Figure 25D**). To quantify these differences, we averaged firing rates within different time windows: 0.05-0.2 s for early and 0.2-0.5 s for late visual responses. We found a significantly stronger response at higher SF (>0.06 cpd) in late visual responses (**Figure 25D** right, WT vs FX 0.05-0.2 s all stimuli ($P > 0.05$), 0.2-0.5 s: SF 7.5e-3 to 0.06 ($P > 0.05$), SF0.12 ($P = 0.014$), and SF0.24 ($P = 0.035$), n = 1057 and 820 units, Mann-Whitney U test, p-values were adjusted for multiple comparisons using Benjamini-Hochberg method).

Next, SF neural decoding was performed using population spike counts (**Figure 25E**). We reasoned that enhanced processing of higher SF might lead to enhanced detection of these stimuli in FX mice. Classifiers were trained on spike counts from different time windows of WT and FX mice using a linear discriminant analysis with 4-fold cross-validation with 5 repeats. Classifiers trained on spike counts from 0.05-0.5 s performed similarly (SF classification mean ± s.e.m. % error WT vs FX: 9.1 ± 0.9 vs 12.0 ± 1). WT classifiers performed slightly better in early time windows (SF classification mean ± s.e.m. % error WT vs FX 0.05-0.15 s: 16.3 ± 1.1 vs 23.1 ± 1.8; 0.15-0.25 s: 6.7 ± 0.9 vs 10.7 ± 1.1). However, classifiers trained on the intervals after 0.25 s show a reduced error in FX vs WT mice (SF classification mean ± s.e.m. % error WT vs FX 0.25-0.35 s: 22.5 ± 1.4 vs 16.3 ± 1.7; 0.35-0.45 s: 26.0 ± 1.6 vs 15.0 ± 1.6), suggesting enhanced processing in late neural responses. Together, these findings suggest an enhancement of processing in late neural responses in FX vs. WT mice, especially at high spatial frequencies.

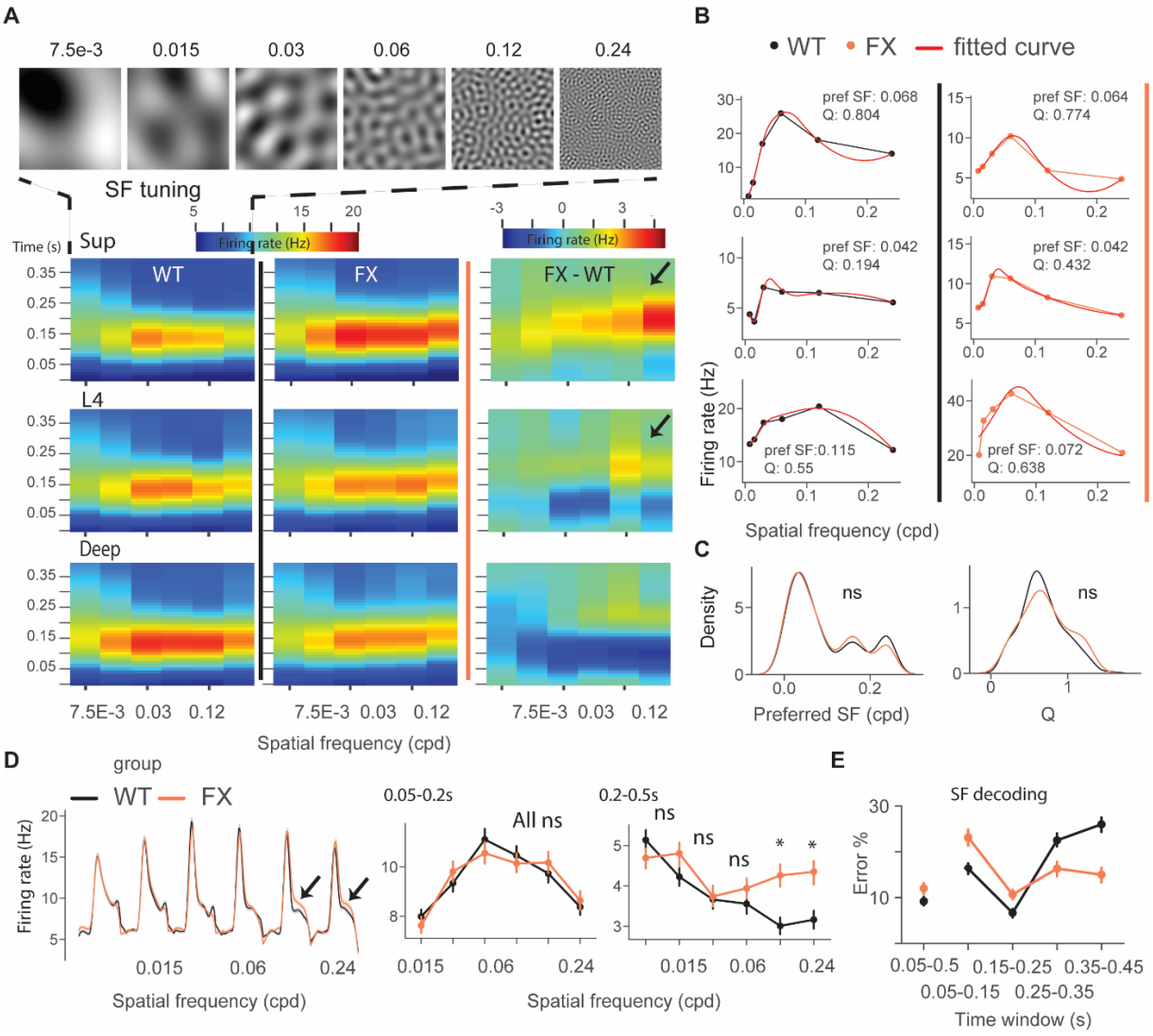

Figure 25. Excessive processing of high SF stimuli in late responses of single units in FX mice.

A. Time-course analysis of SF tuning across the cortical layers. Unit responses for different SF stimuli were plotted for each time step to create the heatmaps for WT (left), FX (middle), and FX-WT (right). **B.** SF tuning curves were computed by averaging responses within 0.05-0.2s relative to the stimulus onset and fitted using Difference-of-Gaussians. Example plots are shown for WT (left) and FX mice (right). **C.** Distribution of preferred SF (left) and Q-factor (right) for both groups. The larger Q values indicate sharper tuning. **D.** Population average firing rates of all units in response to the SF tuning sequence. Note enhanced late part responses at higher SF. The population mean SF tuning responses were averaged for different time intervals. 0.05-0.2 (left) and 0.2-0.5s (right). **E.** Population spike counts from different time windows were used for SF neural decoding. The classifiers that were trained on responses after 0.25 s relative to stimulus onset had a lower error in FX vs. WT mice.

4.6 Both SSA and MM are present in SF tuned units

To investigate whether adaptation and change detection depend on the tuning properties of the units, we split neurons based on their preferred SF. It was defined as a peak (maximum) of the fitted tuning curve of the unit. Based on preferred SF, we then split units into three groups: tuned_in group included neurons with preferred SF that was within ±1 octave of the oddball SF, 0.03 cpd (0.015 < pref SF < 0.06) (**Figure 26A** gray shaded region); tuned_out group included units with preferred SF that was outside the ±1 octave of the oddball SF (pref SF < 0.015 or pref SF > 0.06) (Figure 4G gray shaded region); the untuned group included units that did not show any SF tuning, so that curve fitting was not successful or fitting error was larger than 0.9 (Methods).

We first focused on oddball responses of tuned_in units (Figure 4A-F). iSSA and iMM modulation indices [-1, +1] quantify how strong a given unit is adapted and report MM response correspondingly (positive values indicate stronger modulation). We observed that the majority of tuned_in neurons show both SSA and MM in both genotypes (**Figure 26B**, note marginal distributions). Direct comparison of iSSA and iMM distributions did not reveal any differences between WT and FX mice (**Figure 26C**, WT vs FX iSSA (P = 0.803) and iMM (P = 0.325), n = 201 and 147 units, Kolmogorov-Smirnov 2 sample test). Unit population responses revealed an overall strong adaptation in both genotypes, which is not surprising given that the preferred SF of these units was close to the oddball SF. Interestingly, tuned_in units also show strong MM responses (**Figure 26F**, STD vs CTR WT (P = 1.04e-10) and FX (P = 1.58e-7); STD vs DEV WT (P = 0.0003) and FX (P = 0.0002), n = 249 and 184 units, Mann-Whitney U test). This diverges from theories suggesting that enhancement of DEV response is primarily due to the non-adapted units in the local microcircuit. The proportion of tuned_in units was comparable between genotypes (**Figure 27**). Tuned_out units also showed both SSA and MM at the single-unit level (**Figure 26H**).

Figure 26. SSA and MM are present in single units tuned to various spatial frequencies of both genotypes.

A. Distribution of preferred SF of two different genotypes. Grey shaded area represents tuned_in group, which included units with preferred SF that lies ±1 octave of oddball SF (0.03, red vertical line). **B.** Distribution of iSSA and iMM modulation indices for WT and FX mice (each point is a single unit). **C.** Superimposed distributions of iSSA and iMM with KDE. **D.** The heatmaps show single-unit firing rates in response to STD, DEV, and CTR stimuli across different genotypes. **E**. The line plots show the mean z-scored responses of the units from the heatmaps. **F.** The point plots show the mean ± s.e.m. of the z-scored firing rate between 0.05-0.5s for SSA and 0.2-0.5s for MM relative to the stimulus onset. **J-L.** Same as in A-F but for units which preferred SF was outside 1 octave of the oddball SF.

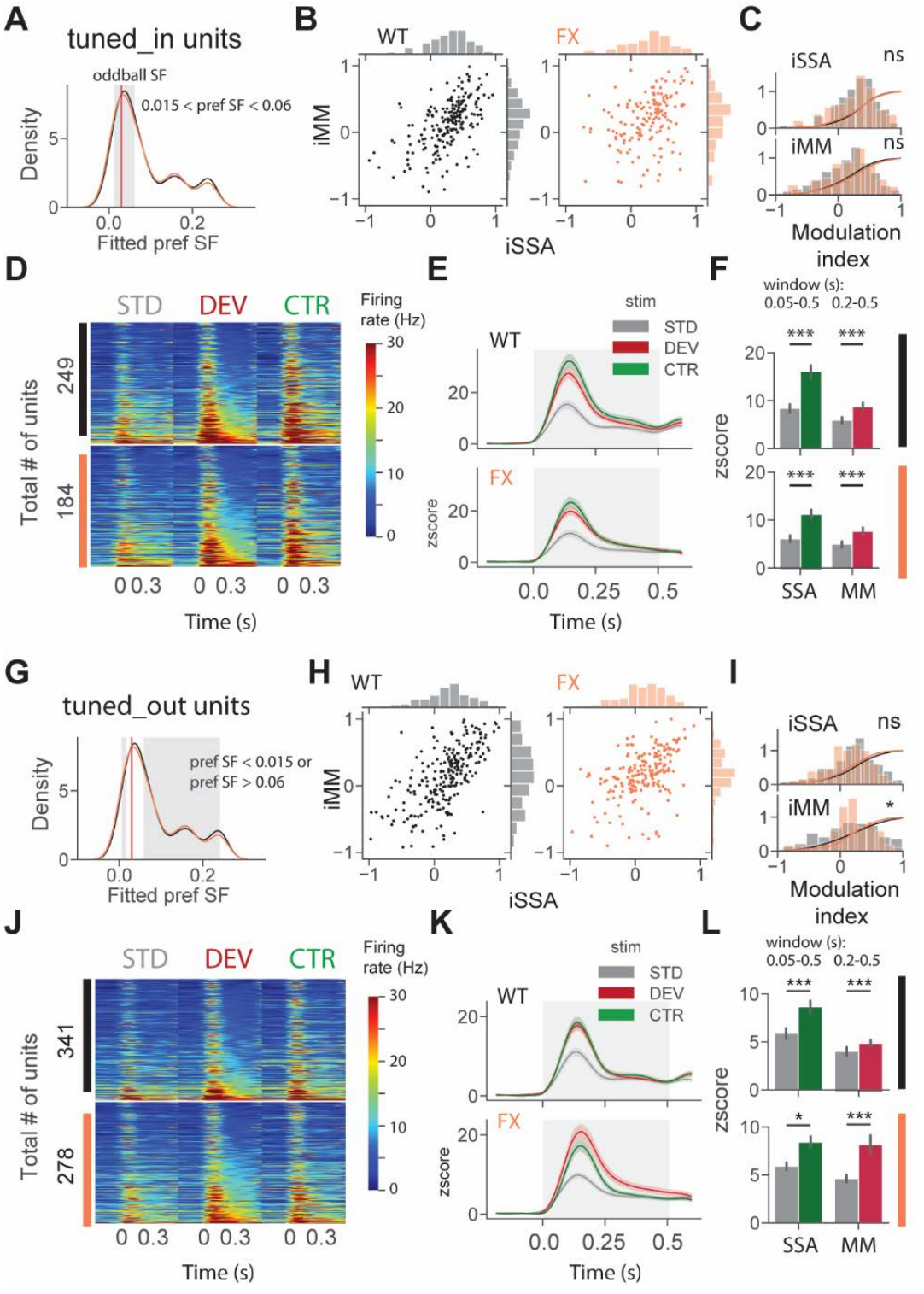
A
tuned_in units
oddball SF
0.015 < pref SF < 0.06
Density
Fitted pref SF
B
WT
FX
iMM
iSSA
C
iSSA
iMM
ns
Modulation index
D
STD
DEV
CTR
Firing rate (Hz)
Total # of units
249
184
Time (s)
E
stim
STD
DEV
CTR
WT
FX
zscore
Time (s)
F
window (s):
0.05-0.5 0.2-0.5
zscore
SSA
MM
G
tuned_out units
pref SF < 0.015 or
pref SF > 0.06
Density
Fitted pref SF
H
WT
FX
iMM
iSSA
I
iSSA
iMM
ns
*
Modulation index
J
STD
DEV
CTR
Firing rate (Hz)
Total # of units
341
278
Time (s)
K
stim
STD
DEV
CTR
WT
FX
zscore
Time (s)
L
window (s):
0.05-0.5 0.2-0.5
zscore
SSA
MM

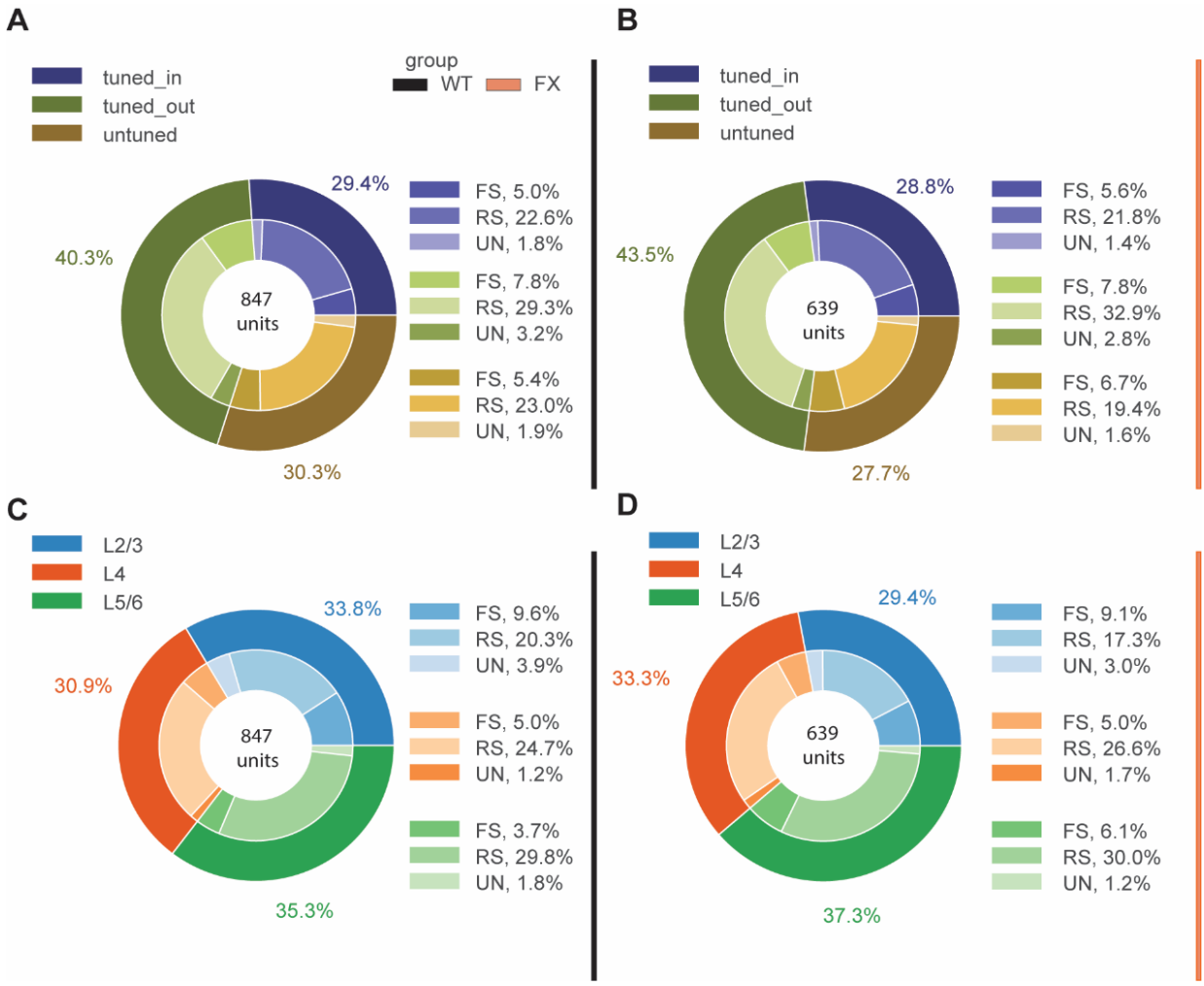

Figure 27. A similar representation of different types and groups of neurons in WT and FX mice.

A. The nested pie chart shows the proportion of units grouped by tuning preference and spiking profile for WT mice. The outer pie chart shows the percentage of units in tuned_in, tuned_out, and untuned group. The inner chart shows the percentage of regular spiking, fast spiking, and unclassified neurons in each subgroup. **B.** Same as in A, but for FX animals. **C.** The nested pie chart shows the proportion of units across the cortical layer for WT mice. The outer pie chart shows the percentage of neurons in layer 2/3, layer 4, and layer 5/6. The inner chart shows the percentage of regular spiking, fast spiking, and unclassified neurons in each subgroup. **D.** Same as in C, but for FX mice.

Distribution of iMM but not iSSA was significantly different between groups (**Figure 26I**, WT vs FX iSSA (P = 0.102) and iMM (P = 0.019), n = 235 and 193 units, Kolmogorov-Smirnov 2 sample test). There was a significant adaptation at the population level in both genotypes, which suggests that adaptation spreads to the units preferring distant SFs. Strong MM responses were also present in both genotypes (Figure 4L, STD vs CTR WT (P = 9.04e-8) and FX (P = 0.014); STD vs DEV WT (P = 2.58e-7) and FX (P = 0.0006), n = 341 and 278 units, Mann-Whitney U test).

4.7 Altered oddball responses in untuned and inhibited units of FX mice

An identical analysis was performed for untuned and inhibited unit oddball responses (**Figure 28**). Untuned units are not tuned to a particular SF (**Figure 28A**), and the inhibited group was suppressed by visual stimuli. Oddball responses in the untuned group were diverse in both genotypes (**Figure 28B**). We found a significant difference in iMM distribution between genotypes (**Figure 28C**, WT vs FX iSSA (P = 0.061) and iMM (P = 0.023), n = 178 and 145 units, Kolmogorov-Smirnov 2 sample test). Unit population responses showed adaptation in both genotypes, whereas MM was not present in WT animals, delayed STD response was slightly stronger than DEV (**Figure 28D-F**, STD vs CTR WT (P = 1.52-5) and FX (P = 0.0011); STD vs DEV WT (P = 0.023) and FX (P = 0.0003), n = 257 and 177 units, Mann-Whitney U test). Interestingly, DEV and CTR evoked significantly stronger inhibition in FX, but not WT mice (**Figure 28G-I**, STD vs CTR WT (P = 0.226) and FX (P = 0.011); STD vs DEV WT (P = 0.065) and FX (P = 0.005), n = 94 and 61 units, Mann-Whitney U test). Contextual modulation of inhibited units in FX but not WT mice might suggest an altered coupling of regular and fast-spiking (RS and FS) neurons.

4.8 Adaptation depends on the spatial frequency tuning of the units and is reduced in FX animals

We next directly compared iSSA and iMM magnitude across different tuning groups and genotypes (**Figure 29A**). First, we observed that iSSA was significantly larger in tuned_in compared to other groups in both genotypes. Interestingly, tuned_out units show stronger adaptation than untuned in WT, but not FX animals. Furthermore, iSSA was significantly larger in WT vs FX tuned_out units (Figure 6A top, iSSA: WT tuned_in vs tuned_out (P = 0.005),

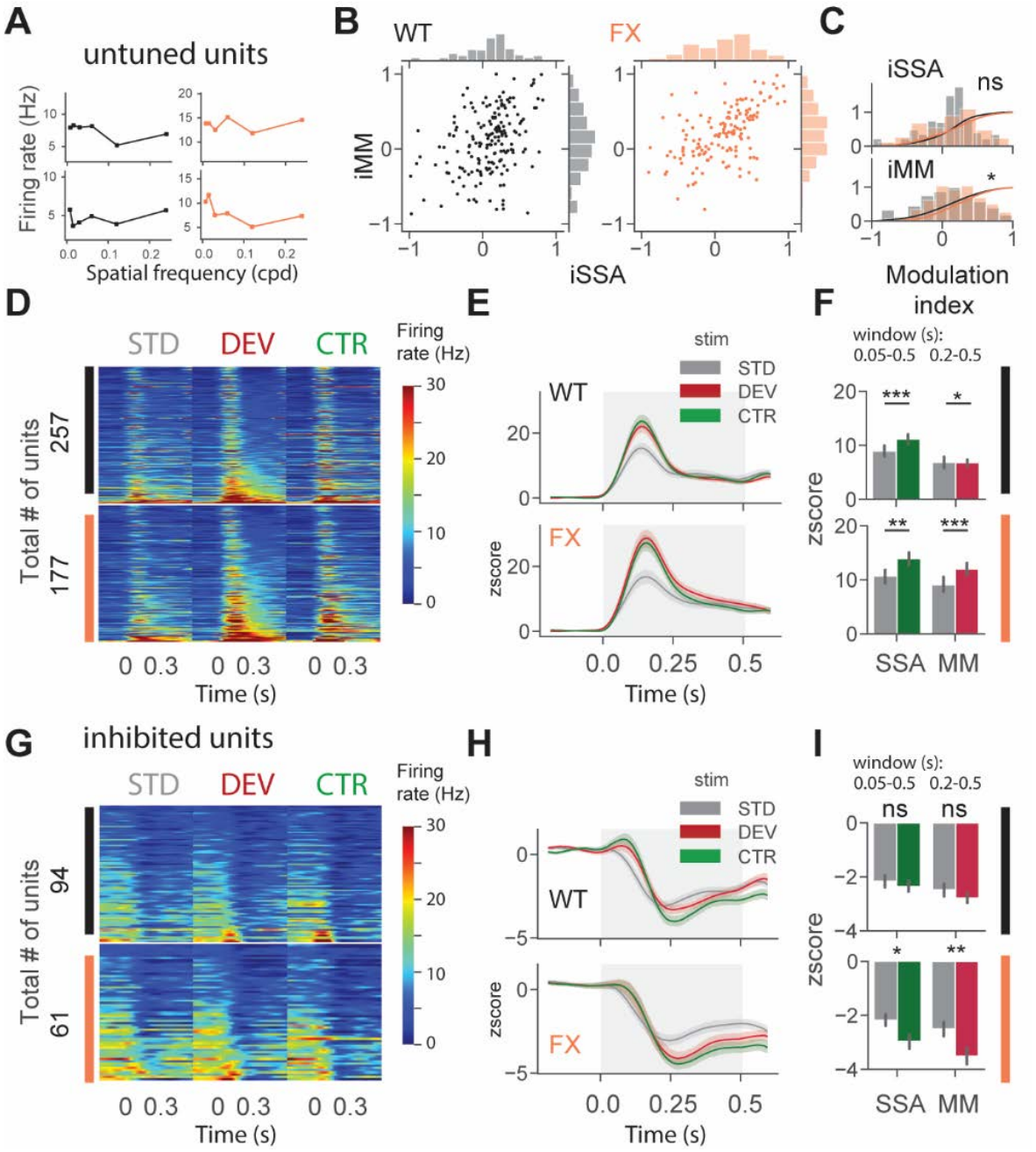

Figure 28. Altered oddball responses in untuned and inhibited units of FX mice.

A. Example SF tuning curves of untuned neurons. Two criteria were used to identify those units: 1) failure of DOG model fitting or 2) high fitting error (>0.9). **B.** Distribution of iSSA and iMM modulation indices for WT and FX mice (each point is a single unit). **C.** Superimposed distributions of iSSA and iMM with KDE. **D.** The heatmaps show single-unit firing rates in response to STD, DEV, and CTR stimuli across different genotypes. **E**. The line plots represent mean z-scored responses of the units from the heatmaps. **F.** The point plots show the mean ± s.e.m. of the z-scored firing rate between 0.05-0.5s for SSA and 0.2-0.5s for MM relative to the stimulus onset. **G-I.** Same as in D-F but for inhibited units.

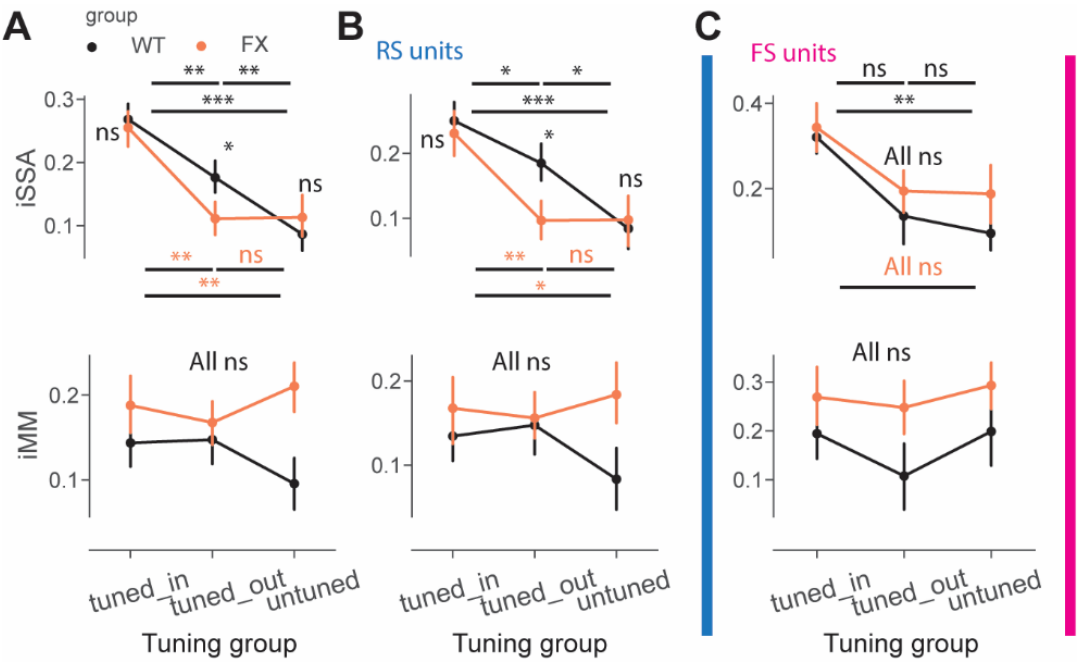

Figure 29. Adaptation depends on the preferred SF of the units.

A. The point plots show iSSA and iMM magnitude for tuned_in, tuned_out, and untuned group for WT and FX for all units. **B.** Same as in A, but for RS units. **C.** Same as in A, but for FS units.

tuned_in vs untuned (P = 1.45e-8), tuned_out vs untuned (P = 0.005); FX tuned_in vs tuned_out (P = 0.0003), tuned_in vs untuned (P = 0.002), tuned_out vs untuned (P =0.465); WT vs FX tuned_in (P = 0.419), tuned_out (P = 0.041), and untuned (P = 0.252), n = 201, 235 and 178 WT units, 147, 193, and 145 FX units, Mann-Whitney U test, p-values were adjusted for multiple comparisons using Benjamini-Hochberg method). MM responses, on the other hand, were not significantly modulated by tuning properties of neurons (**Figure 29A bot**, all comparisons (P > 0.05)). We did not observe any systematic patterns between iSSA/iMM and preferred SF at the single unit level (**Figure 31**).

It has been recently reported that FS neurons are differentially modulated in V1 of FX mice. Thus, we investigated whether oddball processing is altered in FS units (Figure S3). SSA and MM responses were observed in FS of both genotypes (**Figure 30**). We thus decided to investigate how iSSA and iMM represented in RS and FS units. We observed that difference in RS rather than FS units mostly accounted for the differences observed across different tuning groups and genotypes (**Figure 29B and C top**, RS: WT tuned_in vs tuned_out (P = 0.041), tuned_in vs untuned (P = 7.0e-5), tuned_out vs untuned (P = 0.013); FX tuned_in vs tuned_out (P = 0.008), tuned_in vs untuned (P = 0.011), tuned_out vs untuned (P =0.438); WT vs FX tuned_in (P = 0.335), tuned_out (P = 0.036), and untuned (P = 0.461), n = 150, 175, and 141 WT units, 109, 148, and 101 FX units; FS: WT tuned_in vs untuned (P = 0.003), all other comparisons (P > 0.05), Mann-Whitney U test, p-values were adjusted for multiple comparisons using Benjamini-Hochberg method). MM responses were not significantly modulated by tuning properties in RS and FS units (**Figure 29B and C bot**, all comparisons (P > 0.05)). The proportion of units in each subgroup was comparable between genotypes (**Figure 27**). Overall, our results suggest that adaptation depends on the tuning properties of units but not their laminar position along with reduced feature co-adaptation in FX animals.

4.9 Impaired laminar processing of MM responses in FX mice

To gain insight into laminar processing of oddball responses, we quantified population level iSSA and iMM modulation indices across different cortical layers (Figure 7). Adaptation was similarly represented across the cortical column in both genotypes, however, there was a trend towards stronger iSSA in superficial layers of WT mice (**Figure 32A-C top**, all comparisons (P > 0.05)). iMM responses, on other hand, were significantly modulated by cortical layers. They were

significantly stronger in L2/3 vs L4 and L5/6 in WT, however, there was not any laminar preference for MM responses in FX mice Furthermore, L4 MM responses were significantly stronger in FX vs WT mice (**Figure 32A bot**, iMM: WT L2/3 vs L4 (P = 0.0018), L2/3 vs L5/6 (P = 0.04), L4 vs L5/6 (P = 0.242); FX L2/3 vs L4 (P = 0.281), L2/3 vs L5/6 (P = 0.431), L4 vs L5/6 (P = 0.319); WT vs FX L2/3 (P = 0.431), L4 (P = 0.042), and L5/6 (P = 0.068), n = 208, 191 and 215 WT units, 154, 153, and 178 FX units, Mann-Whitney U test, p-values were adjusted for multiple comparisons using Benjamini-Hochberg method).

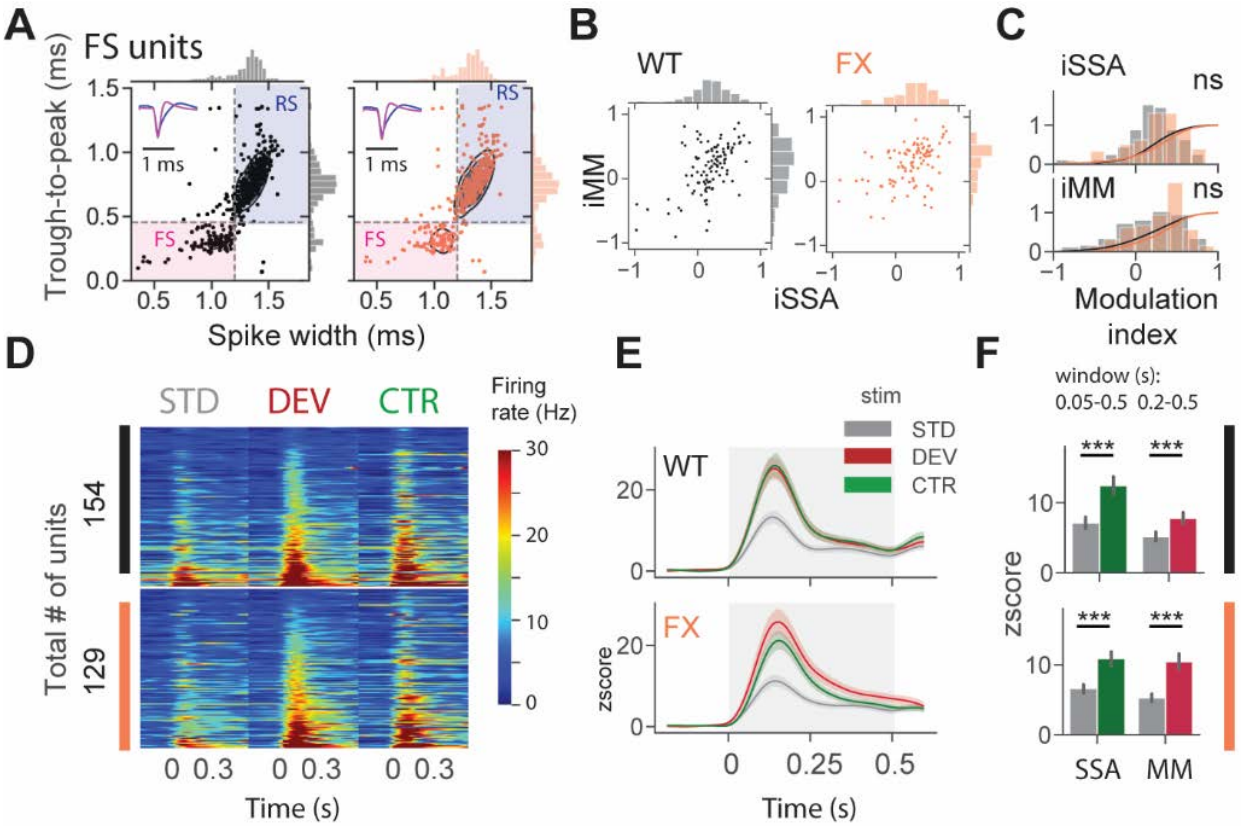

Figure 30. SSA and MM are present in fast spiking units of both genotypes.

A. Units were split into regular, fast spiking, and unclassified based on their template waveform features such as spike width (spw) and trough-to-peak (t-p) time. Fast spiking units had shorter spike width, trough-to-peak time, and narrow waveform (WT and FX spw (0.97 and 1.01 ms), t-p (0.30 and 0.30 ms)). Regular spiking units, on the other hand, had broader waveforms (WT and FX spw (1.36 and 1.37 ms), t-p (0.80 and 0.80 ms)). **B.** Distribution of iSSA and iMM modulation indices for WT and FX mice (each point is a single unit). **C.** Superimposed distributions of iSSA and iMM with KDE (WT vs FX iSSA (P = 0.086) and iMM (P = 0.071), n = 105 and 100 units, Kolmogorov-Smirnov 2 sample test). **D.** The heatmaps show single-unit firing rates in response to STD, DEV, and CTR stimuli across different genotypes. **E**. The line plots represent the mean z-scored responses of the units from the heatmaps. **F.** The point plots show the mean ± s.e.m. of the z-scored firing rate between 0.05-0.5s for SSA and 0.2-0.5s for MM relative to the stimulus onset (STD vs CTR WT (P = 0.0001) and FX (P = 0.0005); STD vs DEV WT (P = 0.0009) and FX (P = 4.31e-5), n = 154 and 129 units, Mann-Whitney U test).

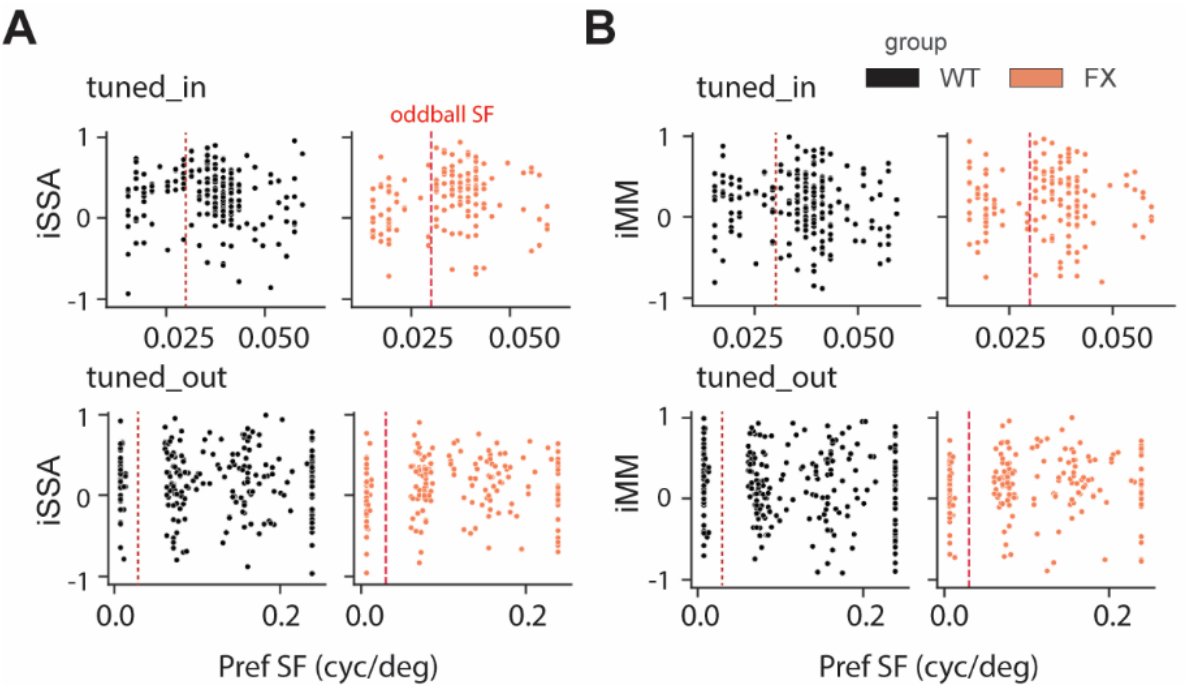

Figure 31. Oddball responses are modulated by the preferred SF of the units.

A. The scatter plots show the relationship between iSSA vs. preferred SF of the units from tuned_in (top) and tuned_out (bot) group for WT and FX mice. Each dot represents a single unit. The vertical dotted line represents the oddball SF. **B.** Same as in A but for iMM vs. preferred SF of the units.

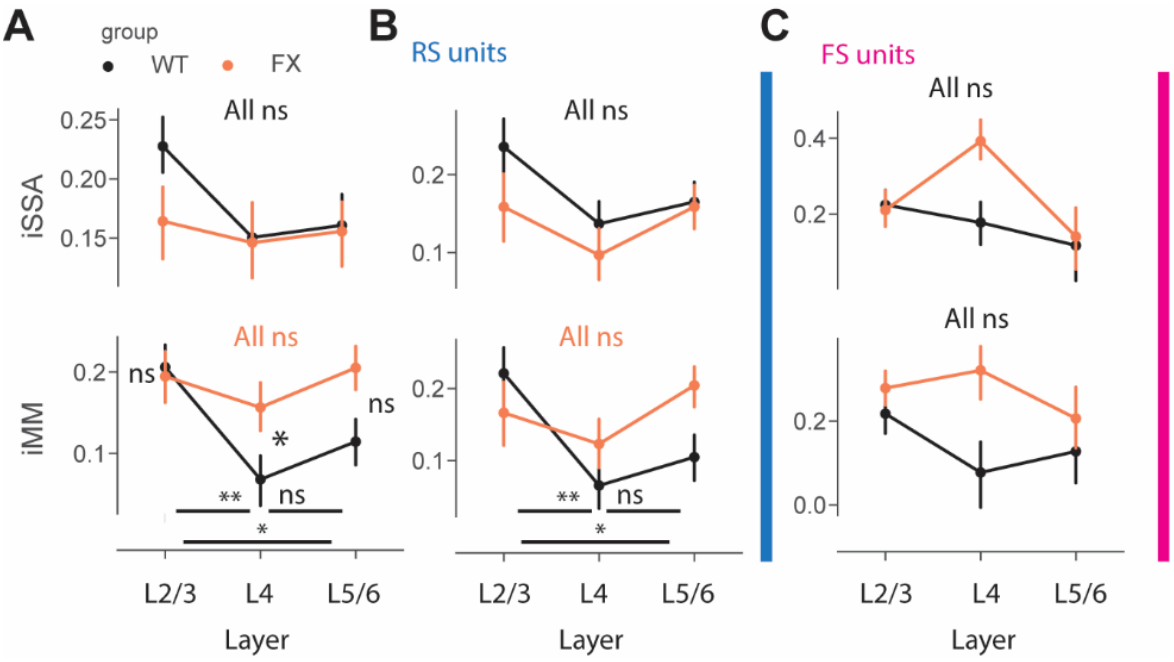

Figure 32. Impaired laminar processing of mismatch responses in FX mice.

A. The point plots show iSSA and iMM magnitude for L2/3, L4, and L5/6 for WT vs. FX for all units. **B.** Same as in A, but for RS units. **C.** Same as in A, but for FS units.

RS units showed similar oddball responses (**Figure 32B,** iMM RS**:** WT L2/3 vs L4 (P = 0.005), L2/3 vs L5/6 (P = 0.04), L4 vs L5/6 (P = 0.237); FX L2/3 vs L4 (P = 0.281), L2/3 vs L5/6 (P = 0.321), L4 vs L5/6 (P = 0.148); WT vs FX L2/3 (P = 0.237), L4 (P = 0.189), and L5/6 (P = 0.085), n = 129, 154 and 183 WT units, 87, 122, and 149 FX units; FS**:** all comparisons (P > 0.05), Mann-Whitney U test, p-values were adjusted for multiple comparisons using Benjamini-Hochberg method). iSSA and iMM responses in FS units were not significantly modulated by cortical layers, though there was a trend towards stronger adaptation in L4 of FX mice (**Figure 32C**). It is unlikely that tuning properties of neurons can explain these observations because there is no difference in cortical distribution of different tuning groups between WT and FX animals (Figure S5). Taken together, these findings suggest that there is a laminar specialization for MM responses in WT but not FX animals.

4.10 Altered representation of omission responses in FX mice

In a subset of animals, we performed local omission experiments, in which every eighth stimulus was omitted (**Figure 33A**). Omission responsive neurons were defined as those with significantly different stimulus (0.05-0.35 s) vs. baseline (-0.25-0.05s) responses (both excited and inhibited see **Figure 34B-D**). Laminar analysis of omission responses did not reveal any differences between WT and FX mice (Figure S6E). We then decided to use an unsupervised clustering algorithm, k-means, to reveal neural dynamics during omissions of the stimulus. Clustering was performed on neural responses within 0.05-0.5 s relative to the stimulus onset from both genotypes. Using an elbow method, we determined that k = 4 was an optimal number of groups (**Figure 33B**). Given that genotype was independent of clustering, we were able to compare responses between WT and FX within each k-means group. Clustering revealed four different

Figure 33. Altered representation of omission responses in FX mice.

A. Local omission paradigm, in which every eighth stimulus is not presented (omission). **B.** The number of groups for k-means was determined using the elbow method. Clustering was performed on omission responses (0.05-0.5s) from units of both genotypes. Given that genotype is independent of clustering, we compared neural responses between WT and FX within each k-means group **C.** The heatmaps of unit firing rate responses across different k-means groups and genotypes (left = STD, right = Omis). The line plots show the mean zscore firing rate responses of units shown in the heatmaps. 1st k-means group shows early, 2nd group mid, and 3rd group late omission responses, and 4th group was inhibited by Omis. **D**. The point plots show the mean ± s.e.m. zscore firing rate for STD (left) and Omis (right) responses for WT and FX.

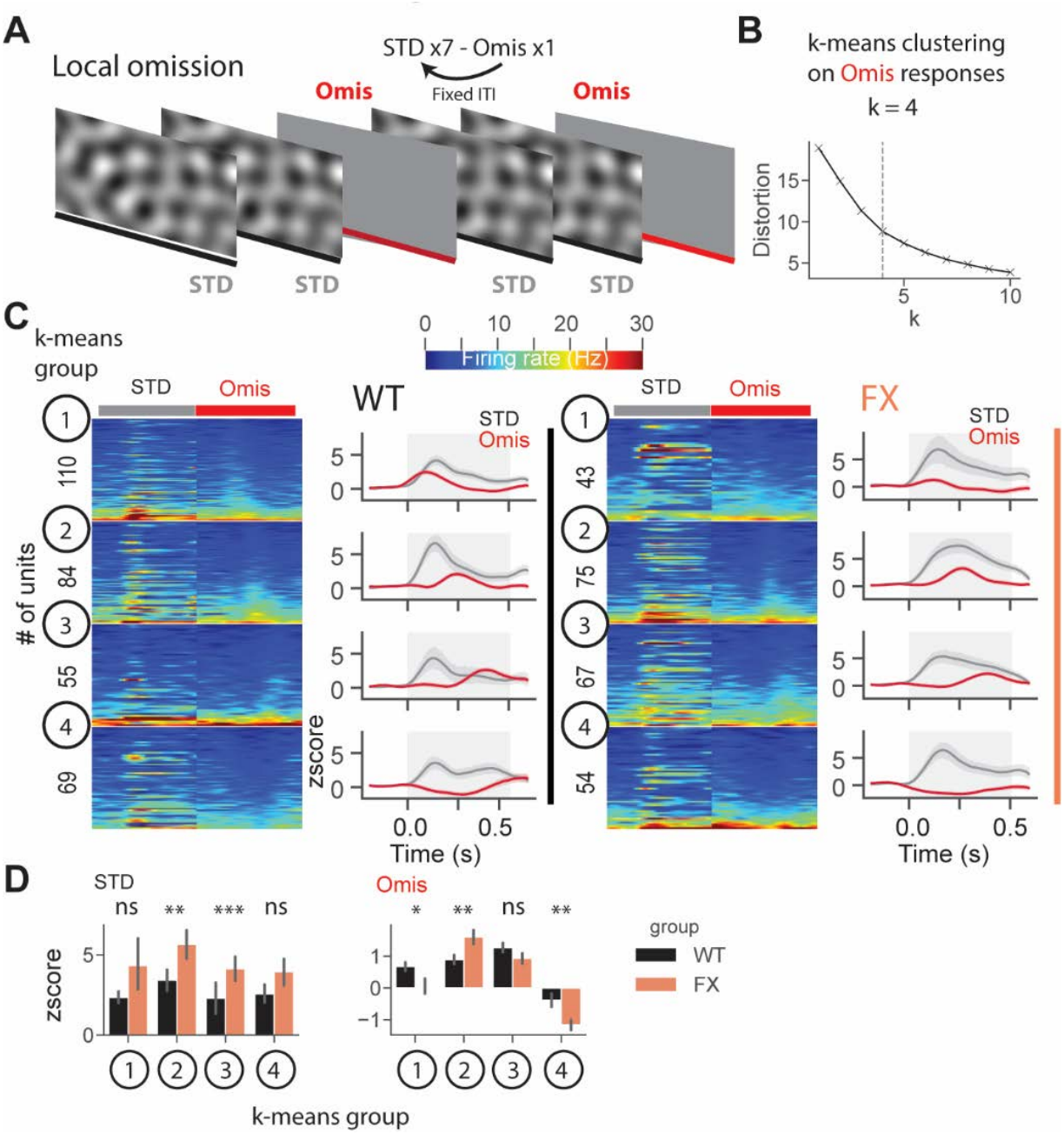
A
Local omission
STD x7 - Omis x1
Fixed ITI
Omis
Omis
STD
STD
STD
STD
B
k-means clustering
on Omis responses
k = 4
Distortion
15
10
5
5
10
k
C
k-means
group
0
10
20
30
Firing rate (Hz)
STD
Omis
WT
FX
# of units
110
84
55
69
43
75
67
54
zscore
5
0
0.0
0.5
Time (s)
D
STD
Omis
ns
**
***
ns
*
**
ns
**
zscore
group
WT
FX
k-means group

types of responses: k-means group 1 - early, group 2 - mid, group 3 late omission responses, and group 4 was inhibited by the omission (**Figure 33C**). Direct comparison of STD between WT and FX revealed stronger responses in FX groups 2 (mid) and 3 (late), which might indicate reduced adaptation during the local omission paradigm. Omission responses were stronger in k-means group 1 (early) in WT, whereas group 2 (mid), and group 4 (inhibited) were stronger in FX mice (**Figure 33D**, WT vs FX k-means group 1 STD ($P = 0.436$), n = 110 and 43 units, Omis ($P = 0.042$), n = 120 and 45 units; group 2 STD ($P = 0.004$), n = 84 and 75 units, Omis ($P = 0.009$), n = 85 and 77 units; group 3 STD ($P = 0.0001$), n = 55 and 67 units, Omis ($P = 0.052$), n = 58 and 70 units, group 4 STD ($P = 0.200$), n = 69 and 54 units, Omis ($P = 0.005$), n = 73 and 59 units, Mann-Whitney U test). Overall, we found the altered processing of omission responses in FX animals.

4.11 Discussion

The lack of a common framework to explain the disparate sensory and social-cognitive deficits in FX and autism is a major roadblock to scientific progress and designing effective diagnostic and intervention tools. Atypical sensory processing has recently been recognized to be an important diagnostic criterion for autism (American Psychiatric Association, 2013). Furthermore, early sensory alterations are predictive of social communication deficits later in life (Robertson & Baron-Cohen, 2017). Investigating the reproducible sensory perception paradigms in well-defined genetic models of autism provides a great opportunity to shed light on the neural basis of atypical sensory experience and its possible interaction with social-cognitive domains in ASD.

Here, we used a novel visual oddball paradigm and silicon probe recordings in V1 to investigate the neural basis of altered sensory perception in FX. Using SF tuning, we first demonstrated that high SF bands are excessively processed in the late stages of visual responses in FX mice. Increased firing rate and lower SF decoding errors at late stages of processing are indicative of over-processing of details. This finding is consistent with previous psychophysical and physiology studies showing altered spatiotemporal processing of high SF information in autism (Caplette, Wicker, & Gosselin, 2016; Kéïta, Guy, Berthiaume, Mottron, & Bertone, 2014). Interestingly, we didn’t observe any difference in SF tuning between genotypes while focusing on peak responses.

Figure 34. Neural responses to stimulus omissions are present across the cortical column in both WT and FX mice.

A. Local omission paradigm, in which every eighth stimulus is not presented (omission). **B.** Example unit responses to the STD and Omis in WT and FX mice. **C.** The heatmaps of unit firing rate responses across different cortical layers, response types, and genotypes (left = STD, right = Omis). The first two columns show units, which were excited by the omission, whereas two columns on the right show units that were inhibited by the omission of the stimuli. **D**. The line plots show the mean z-score firing rate responses of units shown in the heatmaps for excited (left) and inhibited (right) population. **E**. Point plots show the mean ± s.e.m. z-scored firing rate of excited (left two) and inhibited (right two) population across different layers for WT vs FX (**Omis-excited STD:** WT vs FX L2/3 ($P = 0.021$), n = 48 and 29 units, L4 ($P = 0.193$), n = 38 and 29, L5/6 ($P = 0.073$), n = 36 and 40 units; **Omis:** all comparisons ($P > 0.05$); **Omis-inhibited STD:** WT vs FX L2/3 ($P = 0.009$), n = 36 and 19 units, L4 ($P = 0.074$), n = 28 and 33, L5/6 ($P = 0.306$), n = 29 and 40 units; **Omis:** all comparisons ($P > 0.05$); Mann-Whitney U test).

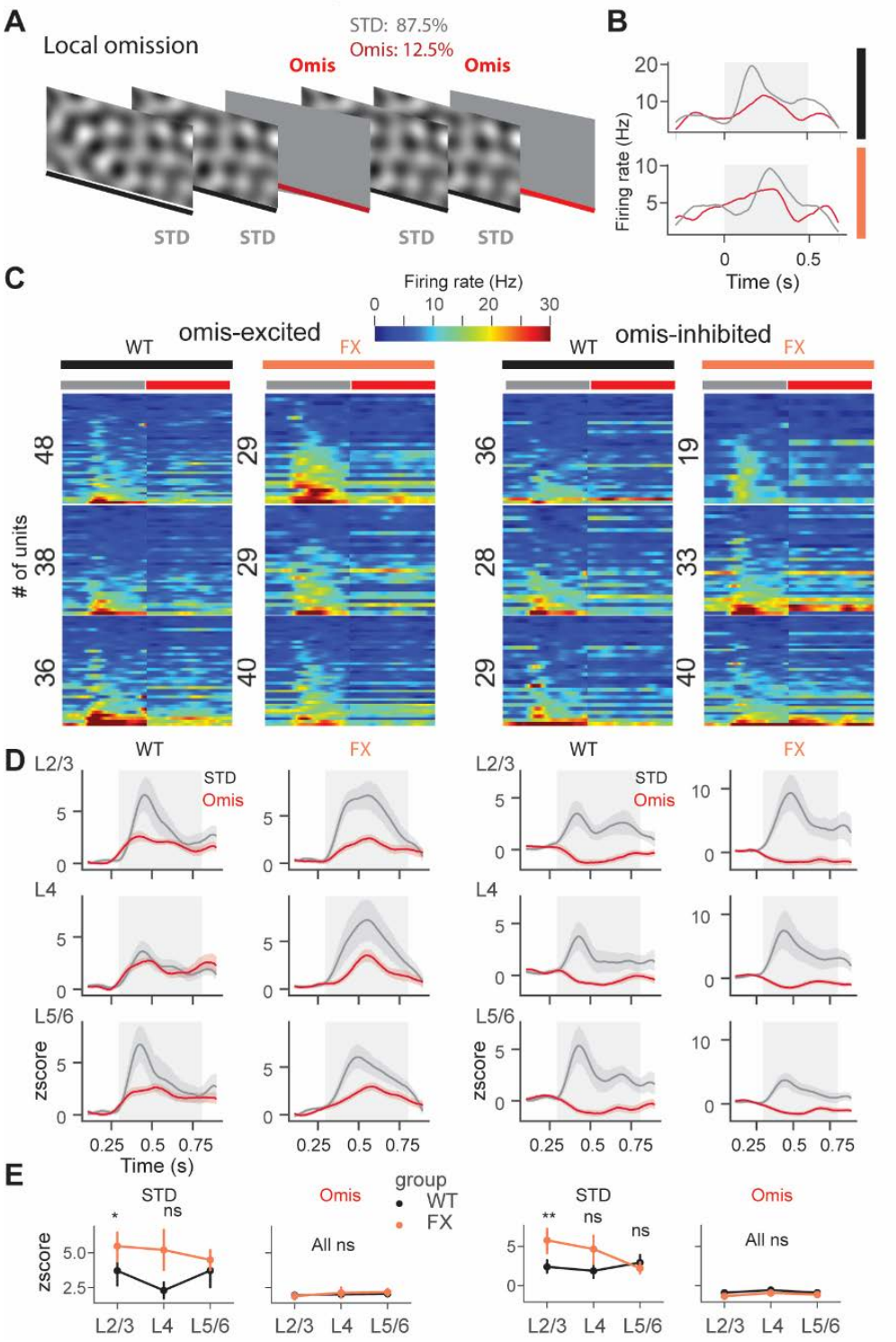
A
Local omission
STD: 87.5%
Omis: 12.5%
Omis
Omis
STD
STD
STD
STD
B
Firing rate (Hz)
Time (s)
C
Firing rate (Hz)
omis-excited
omis-inhibited
WT
FX
WT
FX
# of units
D
L2/3
L4
L5/6
STD
Omis
zscore
Time (s)
E
STD
Omis
group
WT
FX
zscore
All ns
L2/3
L4
L5/6

Using SF oddball paradigm, we then showed that there was a differential contextual processing in V1 of FX mice across different cortical layers and unit types. To investigate the feature specificity of SSA and MM responses, we split neurons into three groups based on their SF preference. We discovered that adaptation was more dependent on the tuning preferences rather than the laminar position of the units. SSA was strongest in tuned_in units in both genotypes, which is not surprising given that their preferred SF was close to the oddball SF (Chen et al., 2015). We observed comparable adaptation levels in tuned_in and tuned_out group in WT but not in FX animals. Interestingly, RS but not FS units were mostly responsible for the observed differences. Analysis of SSA across different cortical layers revealed the strongest adaptation in L2/3 in WT, but it did not reach significance after adjustment for multiple comparisons. Overall, SSA was dependent on the preferred SF of the units and covered a narrower range of spatial frequencies in FX compared to WT animals. This observation might be explained by the reduced spread of adaptation (co-adaptation to neighboring SF) in FX. Our results may provide a mechanism for the reduced habituation and sensory hypersensitivity in FX and autism.

Mismatch responses, on the other hand, were more dependent on the laminar position rather than the tuning preference of units. MM responses were present in the adapted units, suggesting that single units might report mismatch despite strong adaptation levels (Ross & Hamm, 2020). L2/3 had the strongest MM responses in WT, but not in FX, where they were equally represented across the cortical column. Furthermore, L4 MM responses were significantly stronger in FX mice. These observations might be explained by the altered intrinsic properties of L4 neurons similarly to the previously reported observations in the somatosensory cortex (Booker et al., 2019). The lack of laminar specialization for MM in FX might also be linked to the altered information processing in L4 barrel cortex (Domanski, Booker, Wyllie, Isaac, & Kind, 2019). It is important to note that RS units were mostly responsible for the observed differences in MM. This observation is consistent with the previous studies of the reduced excitatory drive onto FS units, which may potentially explain the altered dynamics of FS interneurons (Gibson, Bartley, Hays, & Huber, 2008; Goel et al., 2018) .

Lastly, we observed the altered neural dynamics in FX animals during the local omission paradigm. Interestingly, STD responses were weaker in WT vs. FX animals, which might be indicative of reduced adaptation in FX animals. Our unsupervised clustering revealed four different types of responses to stimulus omissions. Interestingly, these groups had different

temporal patterns covering the whole omission duration with early, mid, late peak responses and inhibition. Early omission responses were stronger in WT, whereas mid and inhibition ones were enhanced in FX animals. We also observed increased delayed responses during SF tuning, oddball, and omission paradigms, which suggest that it might be a common pattern in FX circuits. Given the regularity of omission responses (every eighth stimulus) and fixed inter-trial-interval, we expected the animals to be entrained by the sequence. Overall, reduced STD responses and stimulus timing-locked omission responses suggest that WT but not FX animals were able to learn the regularity of the sequence of stimuli.

In conclusion, we extend prior oddball studies by showing how tuning properties, laminar position, and spiking profile of the neurons influence the contextual processing of visual information. Our discovery of reduced adaptation and altered laminar processing in FX mice provides the mechanistic circuit-level understanding of the impaired sensory perception in FX and might lead to potential diagnostic and therapeutic advances.

4.12 References

American Psychiatric Association. (2013). *Diagnostic and Statistical Manual of Mental Disorders* (5th ed.). Washington, DC.

Booker, S. A., Domanski, A. P. F., Dando, O. R., Jackson, A. D., Isaac, J. T. R., Hardingham, G. E., . . . Kind, P. C. (2019). Altered dendritic spine function and integration in a mouse model of fragile X syndrome. *Nature Communications, 10*(1), 4813. doi:10.1038/s41467-019-11891-6

Boyd, B. A., Baranek, G. T., Sideris, J., Poe, M. D., Watson, L. R., Patten, E., & Miller, H. (2010). Sensory features and repetitive behaviors in children with autism and developmental delays. *Autism Research, 3*(2), 78-87. doi:10.1002/aur.124

Bredfeldt, C. E., & Ringach, D. L. (2002). Dynamics of Spatial Frequency Tuning in Macaque V1. *The Journal of Neuroscience, 22*(5), 1976-1984. doi:10.1523/jneurosci.22-05-01976.2002

Caplette, L., Wicker, B., & Gosselin, F. (2016). Atypical Time Course of Object Recognition in Autism Spectrum Disorder. *Scientific Reports, 6*, 35494. doi:10.1038/srep35494 https://www.nature.com/articles/srep35494#supplementary-information

Chen, I.-W., Helmchen, F., & Lütcke, H. (2015). Specific early and late oddball-evoked responses in excitatory and inhibitory neurons of mouse auditory cortex. *Journal of Neuroscience, 35*(36), 12560-12573.

Domanski, A. P. F., Booker, S. A., Wyllie, D. J. A., Isaac, J. T. R., & Kind, P. C. (2019). Cellular and synaptic phenotypes lead to disrupted information processing in Fmr1-KO mouse layer 4 barrel cortex. *Nature Communications, 10*(1), 4814. doi:10.1038/s41467-019-12736-y

Freund, L. S., & Reiss, A. L. (1991). Cognitive profiles associated with the fra(X) syndrome in males and females. *Am J Med Genet, 38*(4), 542-547. doi:10.1002/ajmg.1320380409

Gibson, J. R., Bartley, A. F., Hays, S. A., & Huber, K. M. (2008). Imbalance of neocortical excitation and inhibition and altered UP states reflect network hyperexcitability in the mouse model of fragile X syndrome. *J Neurophysiol, 100*(5), 2615-2626. doi:90752.2008 [pii] 10.1152/jn.90752.2008

Goel, A., Cantu, D. A., Guilfoyle, J., Chaudhari, G. R., Newadkar, A., Todisco, B., . . . Portera-Cailliau, C. (2018). Impaired perceptual learning in a mouse model of Fragile X syndrome is mediated by parvalbumin neuron dysfunction and is reversible. *Nat Neurosci, 21*(10), 1404-1411. doi:10.1038/s41593-018-0231-0

Haberl, M. G., Zerbi, V., Veltien, A., Ginger, M., Heerschap, A., & Frick, A. (2015). Structural-functional connectivity deficits of neocortical circuits in the Fmr1 (-/y) mouse model of autism. *Sci Adv, 1*(10), e1500775. doi:10.1126/sciadv.1500775

Hamm, J. P., & Yuste, R. (2016). Somatostatin interneurons control a key component of mismatch negativity in mouse visual cortex. *Cell reports, 16*(3), 597-604.

Hawken, M. J., & Parker, A. J. (1987). Spatial properties of neurons in the monkey striate cortex. *Proc R Soc Lond B Biol Sci, 231*(1263), 251-288. doi:10.1098/rspb.1987.0044

Kéïta, L., Guy, J., Berthiaume, C., Mottron, L., & Bertone, A. (2014). An early origin for detailed perception in Autism Spectrum Disorder: biased sensitivity for high-spatial frequency information. *Scientific Reports, 4*, 5475. doi:10.1038/srep05475

Kissinger, S. T., Pak, A., Tang, Y., Masmanidis, S. C., & Chubykin, A. A. (2018). Oscillatory Encoding of Visual Stimulus Familiarity. *The Journal of Neuroscience, 38*(27), 6223-6240. doi:10.1523/jneurosci.3646-17.2018

Kissinger, S. T., Wu, Q., Quinn, C. J., Anderson, A. K., Pak, A., & Chubykin, A. A. (2020). Visual Experience-Dependent Oscillations and Underlying Circuit Connectivity Changes Are Impaired in Fmr1 KO Mice. *Cell Rep, 31*(1), 107486. doi:10.1016/j.celrep.2020.03.050

Musall, S., Haiss, F., Weber, B., & von der Behrens, W. (2015). Deviant processing in the primary somatosensory cortex. *Cerebral Cortex, 27*(1), 863-876.

Naatanen, R., Gaillard, A. W., & Mantysalo, S. (1978). Early selective-attention effect on evoked potential reinterpreted. *Acta Psychol (Amst), 42*(4), 313-329.

Pachitariu, M., Steinmetz, N., Kadir, S., Carandini, M., & Harris, K. D. (2016). Kilosort: realtime spike-sorting for extracellular electrophysiology with hundreds of channels. *bioRxiv*, 061481.

Pak, A., Ryu, E., Li, C., & Chubykin, A. A. (2020). Top-Down Feedback Controls the Cortical Representation of Illusory Contours in Mouse Primary Visual Cortex. *The Journal of Neuroscience, 40*(3), 648-660. doi:10.1523/jneurosci.1998-19.2019

Parras, G. G., Nieto-Diego, J., Carbajal, G. V., Valdés-Baizabal, C., Escera, C., & Malmierca, M. S. (2017). Neurons along the auditory pathway exhibit a hierarchical organization of prediction error. *Nature Communications, 8*(1), 2148.

Peirce, J. (2009). Generating stimuli for neuroscience using PsychoPy. *Frontiers in Neuroinformatics, 2*(10). doi:10.3389/neuro.11.010.2008

Rais, M., Binder, D. K., Razak, K. A., & Ethell, I. M. (2018). Sensory processing phenotypes in fragile X syndrome. *ASN neuro, 10*, 1759091418801092.

Robertson, C. E., & Baron-Cohen, S. (2017). Sensory perception in autism. *Nature Reviews Neuroscience, 18*(11), 671-684.

Ross, J. M., & Hamm, J. P. (2020). Cortical Microcircuit Mechanisms of Mismatch Negativity and Its Underlying Subcomponents. *Frontiers in Neural Circuits, 14*(13). doi:10.3389/fncir.2020.00013

Rossant, C., Kadir, S. N., Goodman, D. F. M., Schulman, J., Hunter, M. L. D., Saleem, A. B., . . . Harris, K. D. (2016). Spike sorting for large, dense electrode arrays. *Nature Neuroscience, 19*, 634. doi:10.1038/nn.4268 https://www.nature.com/articles/nn.4268#supplementary-information

Shobe, J. L., Claar, L. D., Parhami, S., Bakhurin, K. I., & Masmanidis, S. C. (2015). Brain activity mapping at multiple scales with silicon microprobes containing 1,024 electrodes. *Journal of neurophysiology, 114*(3), 2043-2052. doi:10.1152/jn.00464.2015

Shobe, J. L., Claar, L. D., Parhami, S., Bakhurin, K. I., & Masmanidis, S. C. (2015). Brain activity mapping at multiple scales with silicon microprobes containing 1,024 electrodes. *J Neurophysiol, 114*(3), 2043-2052. doi:10.1152/jn.00464.2015

Sokhadze, E., Lamina, E., Casanova, E., Kelly, D., Opris, I., Khachidze, I., & Casanova, M. (2017). Atypical processing of novel distracters in a visual oddball task in autism spectrum disorder. *Behavioral Sciences, 7*(4), 79.

Turner-Brown, L. M., Baranek, G. T., Reznick, J. S., Watson, L. R., & Crais, E. R. (2012). The First Year Inventory: a longitudinal follow-up of 12-month-old to 3-year-old children. *Autism, 17*(5), 527-540. doi:10.1177/1362361312439633

Ulanovsky, N., Las, L., & Nelken, I. (2003). Processing of low-probability sounds by cortical neurons. *Nature Neuroscience, 6*(4), 391-398. doi:10.1038/nn1032

Van der Molen, M. J., Van der Molen, M. W., Ridderinkhof, K. R., Hamel, B. C., Curfs, L. M., & Ramakers, G. J. (2012). Auditory and visual cortical activity during selective attention in fragile X syndrome: a cascade of processing deficiencies. *Clin Neurophysiol, 123*(4), 720-729. doi:10.1016/j.clinph.2011.08.023

Virtanen, P., Gommers, R., Oliphant, T. E., Haberland, M., Reddy, T., Cournapeau, D., . . . SciPy, C. (2020). SciPy 1.0: fundamental algorithms for scientific computing in Python. *Nature Methods*. doi:10.1038/s41592-019-0686-2

CHAPTER 5. DISCUSSION AND CONCLUSION

From light detection in the retina to the precept formation in the cortex, the visual information is processed and transformed by numerous neural circuits in different brain regions. One of the major functions of this process is to extract "meaning" from the incoming visual inputs. It is not a physical stimulation per se but its behavioral significance for the animal that is needed to interpret the current state and guide future actions. To achieve this, contextual information is integrated along with visual inputs to form a percept. Here, context might refer to both visual and non-visual cues, prior experience, and future expectations that might help to interpret visual information. Therefore, the same visual stimulation can be perceived differently by different observers. For example, in the case of visual illusions, different observers may or may not be able to see the same visual illusions. Furthermore, different emotional states also influence visual perception. Finally, the perceptual experience affects how novel or familiar objects are perceived. Leveraging recent advances in neurotechnology and genetic engineering in mice, we aimed to gain a circuit-level understanding of contextual visual processing and how it might be altered in neurodevelopmental disorders.

In the first part of the dissertation, I investigated how perceptual experience alters the neural representation of visual stimuli and how it is altered in SERT KO mice. It has been previously shown that repetitive presentation of the same visual stimulus over the course of several days induces familiarity-evoked low-frequency oscillations in LFP and single units of V1 (Kissinger, Pak, Tang, Masmanidis, & Chubykin, 2018). Importantly, those oscillations were shown to be specific to the spatial frequency content of the familiar stimulus. In this work, we extended those observations by investigating oscillatory activity and tuning properties of single units pre and post perceptual experience in WT and SERT-deficient mice (Pak & Chubykin, 2020). First, we demonstrated longer oscillatory spiking activity in SERT-deficient vs. WT mice after a perceptual experience that might be a consequence of enhanced plasticity in these mice. Second, oscillatory spiking activity was not specific to the spatial frequency of the familiar stimulus in SERT KO mice, suggesting altered fine-tuning of neural circuits in V1 during learning. Third, orientation tuning was impaired after perceptual experience only in SERT KO mice, further supporting impaired refinement of local circuitry after the perceptual experience. Together, these findings suggest that

serotonin signaling might be important for plasticity and fine-tuning of local circuitry during learning.

SERT-deficient mice represent a well-established model to investigate the role of serotonin signaling in physiology and behavior (Murphy & Lesch, 2008). Our work extended prior studies on the effects of serotonin on sensory processing by showing how its dysregulation might affect perceptual learning. Specifically, we did not observe impairments in visual processing in naive SERT-defiant mice but only after the perceptual experience, which supports the role of serotonin in visual learning. However, it is important for future studies to account for the developmental effects of altered serotonin signaling by utilizing control groups that are chronically treated with antidepressant drugs. Furthermore, it will be of great interest to identify specific 5-HT receptors that are responsible for visual learning by using specific 5-HT receptor agonists and/or antagonists (Berthoux, Barre, Bockaert, Marin, & Bécamel, 2019). Optogenetic approaches can also be used to transiently modulate serotonin activity and investigate its role in visual processing and plasticity. Overall, future studies will greatly benefit from using pharmacological, chemogenetic, and/or optogenetic approaches that target specific neural subpopulations or 5-HT receptors to identify the role of serotonin in visual processing and plasticity.

The second part of the dissertation was focused on spatial contextual modulation of visual responses. Visual illusions induce a percept that is not aligned with physical stimulation and therefore represents a great window of opportunity to investigate contextual modulation. It has been previously shown that there are neural correlates of illusory responses in the early visual cortex of primates (Lee & Nguyen, 2001; von der Heydt & Peterhans, 1989). However, it was not clear how different visual areas interplay to produce illusory perception. Leveraging behavioral training, electrophysiology, and optogenetics we showed that top-down feedback from higher-order visual areas is involved in the generation of illusory responses in mouse V1 (Pak, Ryu, Li, & Chubykin, 2020). First, we provided behavioral evidence for illusory perception in mice. Second, we demonstrated orientation-selective illusory and control responses at the population level in mouse V1. Third, we performed perturbation experiments and showed that suppression of the higher-order visual area LM inhibited illusory contour responses in V1. Together, these findings suggest that the interplay of bottom-up and top-down processing might be important for spatial contextual modulation.

Our work was the first to describe the neural correlates of illusory perception in mice and demonstrate that top-down feedback from higher-order visual areas might be important for illusory perception. It is important to note that our findings paved the way for investigating spatial contextual modulation using experimental and genetic tools available in mice. It will be important for future studies to dissect the neural circuity behind the feedback modulation of illusory responses. This can be achieved by investigating genetically defined inhibitory subpopulations and/or directly observing feedback inputs from higher-order areas using imaging approaches (Keller, Roth, & Scanziani, 2020). Another line of research might be focused on computational models that can recapitulate spatial contextual modulation observed in V1 (Lotter, Kreiman, & Cox, 2018). Overall, gaining mechanistic circuit-level insight into illusory processing might shed light on spatial contextual modulation in the visual cortex.

The last part of the dissertation was focused on temporal contextual modulation of neural responses in WT and FX mice. It has been previously shown that recent experience modulates neural responses to amplify novel stimuli (mismatch detection) and suppress redundant ones (adaptation) (Chen, Helmchen, & Lütcke, 2015; Hamm & Yuste, 2016; Ulanovsky, Las, & Nelken, 2003). However, it remains unclear what neural subpopulations contribute to adaptation and mismatch detection along with how it might be altered in neurodevelopmental disorders. Leveraging a novel oddball paradigm and electrophysiology, we demonstrated that tuning properties and laminar position of neurons differentially contribute to adaptation and mismatch detection in WT and are altered in FX mice. First, we showed enhanced processing of high spatial frequency in FX mice, which might reflect detail-oriented visual processing in FX and autism. Second, we showed that adaptation depends on the tuning preferences of neurons in both genotypes. However, it was reduced in FX mice which might be related to hypersensitivity and sensory overload observed in FX and autism. Third, mismatch responses were differentially represented by different cortical layers in WT but not FX mice, suggesting altered laminar processing in V1. Together, our findings suggest that there are a feature specificity and laminar specialization of adaptation and mismatch detection, respectively, and they are impaired in FX mice, which might underlie core sensory deficits observed in FX and autism.

This work advanced the current understanding of the neural implementation of temporal modulation by specifically showing what neural properties contribute to adaptation and mismatch detection. It will be important for future studies to investigate how different inhibitory

subpopulations contribute to the observed properties of temporal contextual modulation and whether those properties hold for more complex visual stimulations (Natan et al., 2015). Furthermore, reported circuit-level impairments of oddball processing in FX mice parallel sensory deficits observed in individuals with FX and autism (Sokhadze et al., 2017). Given that the oddball paradigm has been successfully used in both humans and animal models, there is an opportunity to utilize the strengths of different experimental models to build a framework to guide future research into FX and autism. However, for this endeavor to succeed, it is important to distinguish between conserved and species-specific neural mechanisms; therefore, basic sensory processing represents a good experimental model (Goel et al., 2018). Overall, the FX and autism field would greatly benefit from a circuit-level understanding of conserved mechanisms that can possibly be mapped back to human patients.

5.1 References

Berthoux, C., Barre, A., Bockaert, J., Marin, P., & Bécamel, C. (2019). Sustained Activation of Postsynaptic 5-HT2A Receptors Gates Plasticity at Prefrontal Cortex Synapses. *Cerebral cortex (New York, N.Y. : 1991), 29*(4), 1659-1669. doi:10.1093/cercor/bhy064

Chen, I.-W., Helmchen, F., & Lütcke, H. (2015). Specific early and late oddball-evoked responses in excitatory and inhibitory neurons of mouse auditory cortex. *Journal of Neuroscience, 35*(36), 12560-12573.

Goel, A., Cantu, D. A., Guilfoyle, J., Chaudhari, G. R., Newadkar, A., Todisco, B., . . . Portera-Cailliau, C. (2018). Impaired perceptual learning in a mouse model of Fragile X syndrome is mediated by parvalbumin neuron dysfunction and is reversible. *Nat Neurosci, 21*(10), 1404-1411. doi:10.1038/s41593-018-0231-0

Hamm, J. P., & Yuste, R. (2016). Somatostatin interneurons control a key component of mismatch negativity in mouse visual cortex. *Cell reports, 16*(3), 597-604.

Keller, A. J., Roth, M. M., & Scanziani, M. (2020). Feedback generates a second receptive field in neurons of the visual cortex. *Nature, 582*(7813), 545-549. doi:10.1038/s41586-020-2319-4

Kissinger, S. T., Pak, A., Tang, Y., Masmanidis, S. C., & Chubykin, A. A. (2018). Oscillatory Encoding of Visual Stimulus Familiarity. *The Journal of Neuroscience, 38*(27), 6223-6240. doi:10.1523/jneurosci.3646-17.2018

Lee, T. S., & Nguyen, M. (2001). Dynamics of subjective contour formation in the early visual cortex. *Proceedings of the National Academy of Sciences, 98*(4), 1907-1911. doi:10.1073/pnas.98.4.1907

Lotter, W., Kreiman, G., & Cox, D. (2018). A neural network trained to predict future video frames mimics critical properties of biological neuronal responses and perception. *arXiv preprint arXiv:1805.10734*.

Murphy, D. L., & Lesch, K.-P. (2008). Targeting the murine serotonin transporter: insights into human neurobiology. *Nature reviews. Neuroscience, 9*(2), 85-96. doi:10.1038/nrn2284

Natan, R. G., Briguglio, J. J., Mwilambwe-Tshilobo, L., Jones, S. I., Aizenberg, M., Goldberg, E. M., & Geffen, M. N. (2015). Complementary control of sensory adaptation by two types of cortical interneurons. *eLife, 4*, e09868.

Pak, A., & Chubykin, A. A. (2020). Cortical Tuning is Impaired After Perceptual Experience in Primary Visual Cortex of Serotonin Transporter-Deficient Mice. *Cerebral Cortex Communications, 1*(1). doi:10.1093/texcom/tgaa066

Pak, A., Ryu, E., Li, C., & Chubykin, A. A. (2020). Top-Down Feedback Controls the Cortical Representation of Illusory Contours in Mouse Primary Visual Cortex. *The Journal of Neuroscience, 40*(3), 648-660. doi:10.1523/jneurosci.1998-19.2019

Sokhadze, E. M., Lamina, E. V., Casanova, E. L., Kelly, D. P., Opris, I., Khachidze, I., & Casanova, M. F. (2017). Atypical Processing of Novel Distracters in a Visual Oddball Task in Autism Spectrum Disorder. *Behavioral sciences (Basel, Switzerland), 7*(4), 79. doi:10.3390/bs7040079

Ulanovsky, N., Las, L., & Nelken, I. (2003). Processing of low-probability sounds by cortical neurons. *Nature Neuroscience, 6*(4), 391-398. doi:10.1038/nn1032

von der Heydt, R., & Peterhans, E. (1989). Mechanisms of contour perception in monkey visual cortex. I. Lines of pattern discontinuity. *Journal of Neuroscience, 9*(5), 1731-1748.

VITA

Alex Pak

DATA ANALYSIS

Signal processing
- spatiotemporal filtering
- spectral analysis

Time-series analysis
Machine learning
- GLM • k-means
- PCA • SVM

Computer vision
- OpenCV

Deep learning
- convnets

PROGRAMMING

Python (4+ years)
- numpy • matplotlib
- pandas • scikit-learn

MATLAB (2+ years)
R (1+ years)
- bioinformatics
- statistical inference

Java (intermediate)

LABORATORY SKILLS

Stereotaxic animal surgery and viral injections
Extracellular electrophysiology and optogenetics in awake mice
Behavioral training
Molecular biology, cell culture
ELISA, Western blot

LANGUAGE SKILLS

• English • Russian
• Kazakh • Turkish

CURRENT POSITION

Purdue University
Graduate Researcher | 2016 - present

EDUCATION

Purdue University, West Lafayette, IN
Ph.D. candidate, Systems Neuroscience
Expected Graduation: Fall 2020

Nazarbayev University, Nur-Sultan, Kazakhstan
B.S. Biomedicine | 2015 | GPA 3.9/4.0
Thesis: Bioinformatic analysis of HIV-1 protease plasticity in treatment-naïve Japanese patients
Advisor: Christian Schönbach, Ph.D.

RESEARCH EXPERIENCE

Purdue University, West Lafayette, IN | 2016 - present
Graduate Researcher; Advisor: Alexander A. Chubykin, Ph.D.
Computational (https://github.com/apaks/ena)

• Developed a data analysis pipeline for LFP (preprocessing, filtering, wavelet analysis, phase-amplitude coupling) and units (quality control after spike sorting, waveform analysis, PSTH, tuning, correlation, spike-filed coherence)

• Developed computer vision software for object tracking using OpenCV

• Performed unsupervised clustering of neural population data based on temporal response profile using k-means

• Performed neural decoding using LDA, GLM, and SVM

Experimental

• Performed in-vivo extracellular silicon probe recordings in awake mice

• Performed optogenetics in freely moving and head-fixed mice

• Designed novel behavioral tasks

• Trained animals in classical and operant conditioning tasks

PUBLICATIONS

• Kissinger, S. T.*, **Pak, A.***, Tang, Y., Masmanidis, S. C., & Chubykin, A. A. (2018) Oscillatory encoding of visual stimulus familiarity. Journal of Neuroscience
doi: https://doi.org/10.1523/JNEUROSCI.3646-17.2018
(* authors equally contributed to the work)

• **Pak, A**., Ryu, E., Li, C., & Chubykin, A. A. (2020) Top-down feedback controls the cortical representation of illusory contours in mouse primary visual cortex. Journal of Neuroscience
doi: https://doi.org/10.1523/JNEUROSCI.1998-19.2019

• Kissinger, S. T., Wu, Q., Quinn, C.J., Anderson, A.K., **Pak, A**., & Chubykin, A. A (2020) Visual Experience-Dependent Oscillations and Underlying Circuit Connectivity Changes Are Impaired in Fmr1 KO Mice. Cell Reports
doi: https://doi.org/10.1016/j.celrep.2020.03.050

• **Pak, A** and Chubykin, A. A. (2020) Cortical tuning is impaired after perceptual experience in primary visual cortex of serotonin transporter-deficient mice. Cerebral Cortex Communications
doi: https://doi.org/10.1093/texcom/tgaa066

Preprints

• **Pak, A**., Kissinger, S. T., & Chubykin, A. A. (2020) Differential processing and habituation in distinct spatial frequency channels in V1 of a mouse model of fragile X syndrome, bioRxiv
doi: https://doi.org/10.1101/2020.01.24.919035

FUNDING AND AWARDS

• Purdue Research Foundation Fellowship | 2019-20
• Yeunkyung Woo Achieve Excellence Travel Award | 2019
• Purdue Graduate Student Government Travel Grant | 2018
• PULSe Five Minute Thesis Competition (winner) | 2018
• Purdue Institute for Integrative Neuroscience Travel Grant | 2018
• Taiburyl Scholarship | 2014-2015
• Vanderbilt International Summer Research Academy | Summer 2014
• Dean's List | 2011-2015
• Overseas Korean Foundation Scholarship | 2013

PROFESSIONAL TRAINING

• Git, SQL, and C++
• Neuromatch Academy (GLM, MDP, Kalman filtering, causal inference, reinforcement learning)
• Fast.ai (Practical Deep Learning for Coders using fastai and PyTorch)
• Coursera (Deeplearning.ai CNN, RNN with Tensorflow/Keras (5 courses), Computational Neuroscience)

TEACHING EXPERIENCE

Graduate Teaching Assistant, Purdue University | spring 2018
BIOL 595: Data Analysis for Neuroscience
• Python for data analysis (numpy, pandas, matplotlib)

CONFERENCE PRESENTATIONS

• Pak, A., Kissinger, S. T., & Chubykin, A. A., Visual Oddball Paradigm Reveals Feature Non specific Prediction Errors in V1 of a Mouse Model of Fragile X Syndrome. Poster at Society for Neuroscience meeting, Chicago, IL, USA | October 2019

• Pak, A., Ryu, E., & Chubykin, A. A. The cortical representation of illusory contours requires higher-order input. Poster at Cosyne19, Lisbon, Portugal | March 2019

• Pak, A., Ryu, E., & Chubykin, A. A. The cortical representation of illusory contours requires higher-order input. Poster at Sigma Xi, Purdue University, West Lafayette, IN | February 2019

• Pak, A., Kissinger, S. T., & Chubykin, A. A., Spatial frequency-specific entrainment of slow oscillatory activity in primary visual cortex (V1). Poster at Neuronal Circuits Meeting. Cold Spring Harbor Laboratory, New York, NY | April 2018

• Pak, A., Kissinger, S. T., & Chubykin, A. A., Spatial frequency-specific entrainment of slow oscillatory activity in visual cortex. Poster at Sensorium. University of Cincinnati, Cincinnati, OH | September 2017

• Pak, A., Kissinger, S. T., & Chubykin, A. A., Spatial frequency-specific entrainment of slow oscillatory activity in visual cortex. Poster at Purdue Institute for Integrative Neuroscience retreat | May 2017

• Pak, A., Wang, B, & Low, S. P., Ex Vivo Tumor models for MDSCs-targeted Drug Screening. Poster at PULSe Spring reception, Purdue University, West Lafayette, IN | May 2016

INVITED TALKS

• Pak, A., & Chubykin, A. A. How visual experience reshapes neural population activity. Purdue University Interdisciplinary Life Science Seminar Series, Purdue University, West Lafayette, IN | March 2018